

Neutrino Oscillation Physics with a Fermilab Proton Driver

December 3, 2004

Entire Author list goes here

¹*First institution*

²*Second institution*

A Note to Readers of the 1st Draft

This first draft has key components that are complete, but much else that still needs work. The main arguments are described in pretty much complete form in the Executive Summary, the Table of Contents, the Introduction, and the paragraphs that start each chapter. The bulk of the material is in place, but in many cases it is completely unedited and in the form that it was received from the contributing authors. The document is also quite long in its current form and the editors would welcome guidance on how long/detailed the final version should be.

Executive Summary

Neutrinos are the most ubiquitous matter particles in the universe. In number, they exceed the constituents of ordinary matter (electrons, protons, neutrons) by a factor of ten billion. They account for at least as much energy in the universe as all the stars combined and, depending on their exact masses, might account for a sizable fraction of the so-called "dark matter". Neutrinos are also important in stellar dynamics. There are about $7 \times 10^9 \text{ cm}^{-2} \text{ sec}^{-1}$ streaming through the Earth from the Sun. Neutrinos govern the dynamics of supernovae, and hence the production of heavy elements in the universe. Furthermore, if there is CP Violation in the neutrino sector, the physics of neutrinos in the early universe might ultimately be responsible for Baryogenesis.

If we are to understand "why we are here" and the basic nature of the universe in which we live, we must understand the basics properties of the neutrino.

In the last few years solar, atmospheric, and reactor neutrino experiments have revolutionized our understanding of the nature of neutrinos. We now know that neutrinos produced in a given flavor eigenstate can transform themselves into neutrinos of a different flavor eigenstate as they propagate over macroscopic distances. This means that, like quarks, neutrinos have a finite mass, the flavor eigenstates are different from the mass eigenstates, and hence neutrinos mix. However, we have incomplete knowledge of the properties of neutrinos since **we do not know the spectrum of neutrino masses, and we have only partial knowledge of the matrix that describes the mixing between the three known neutrino flavor eigenstates.** Furthermore, it is possible that the simplest three-flavor mixing scheme is not the whole story, and that a complete understanding of neutrino properties will require a more complicated framework. In addition to determining the parameters that describe the neutrino sector, the three-flavor mixing framework must also be tested.

The Standard Model cannot accommodate finite neutrino mass terms without some modification. We must either introduce right-handed neutrinos (to generate Dirac mass terms) or allow neutrinos to be their own antiparticle (violating lepton number conservation, and allowing Majorana mass terms). Hence **the physics of neutrino masses is physics beyond the Standard Model.**

Although we do not know the neutrino mass spectrum, we do know that the masses, and the associated mass-splittings, are tiny compared to the masses of any other fundamental fermion. This suggests that the physics responsible for neutrino masses will include new components radically different from those of the Standard Model. Furthermore, although we do not have complete knowledge of the neutrino

mixing matrix, we do know that it is qualitatively very different from the corresponding quark mixing matrix. The observed difference necessarily constrains our ideas about the underlying relationship between quarks and leptons, and hence models of quark and lepton unification in general, and Grand Unified Theories (GUTs) in particular. Note that in neutrino mass models the seesaw mechanism provides a quantitative explanation for the observed small neutrino masses, which arise as a consequence of the existence of right-handed neutral leptons at the GUT-scale. Over the last few years, as our knowledge of the neutrino oscillation parameters has improved, a previous generation of neutrino mass models has already been ruled out, and a new set of models has emerged specifically designed to accommodate the neutrino parameters. Further improvement in our knowledge of the oscillation parameters will necessarily reject many of these models, and presumably encourage the emergence of new ideas. Hence **neutrino physics is experimentally driven, and the experiments are already directing our ideas about what lies beyond the Standard Model.**

Our desire to understand both the universe in which we live and physics beyond the Standard Model provides a compelling case for an experimental program that can elucidate the neutrino mass spectrum and mixing matrix, and test the three-flavor mixing framework. It seems likely that complete knowledge of the neutrino mass splittings and of the mixing matrix is accessible to accelerator-based neutrino oscillation experiments. This will certainly be the case if the unknown mixing angle θ_{13} is not too small. Even if θ_{13} does turn out to be very small, stringent upper limits will provide invaluable guidance to model builders, may indicate the existence of a new symmetry associated with the physics of neutrino mass, and would hopefully lead to new ideas about physics beyond the Standard Model.

In the long-term the route that must be followed to determine all of the neutrino properties accessible to accelerator-based experiments will depend on the value of θ_{13} and whether there are any surprises along the way. However, the next big step towards an accelerator-based program beyond the MiniBooNE, MINOS, K2K, and the CNGS program is independent of these uncertainties, and is determined by two things:

- (i) To probe θ_{13} we need to search for transitions between muon neutrinos ν_μ and electron neutrinos ν_e . These transitions also provide the key to understanding the pattern of neutrino masses and whether there is CP violation in the lepton sector.
- (ii) The crucial neutrino oscillation experiments must confront the smallness of the neutrino cross-section, the small $\nu_e \leftrightarrow \nu_\mu$ oscillation amplitude (at most $O(0.01)$), and the need for long baselines, at the cost of small neutrino fluxes. If precise values for all the neutrino parameters are required, the needed sensitivity can only be accomplished with a combination of the largest detectors affordable, the most intense neutrino sources affordable, and the longest running times that are reasonable. A MW-scale proton source is necessarily a part of this recipe.

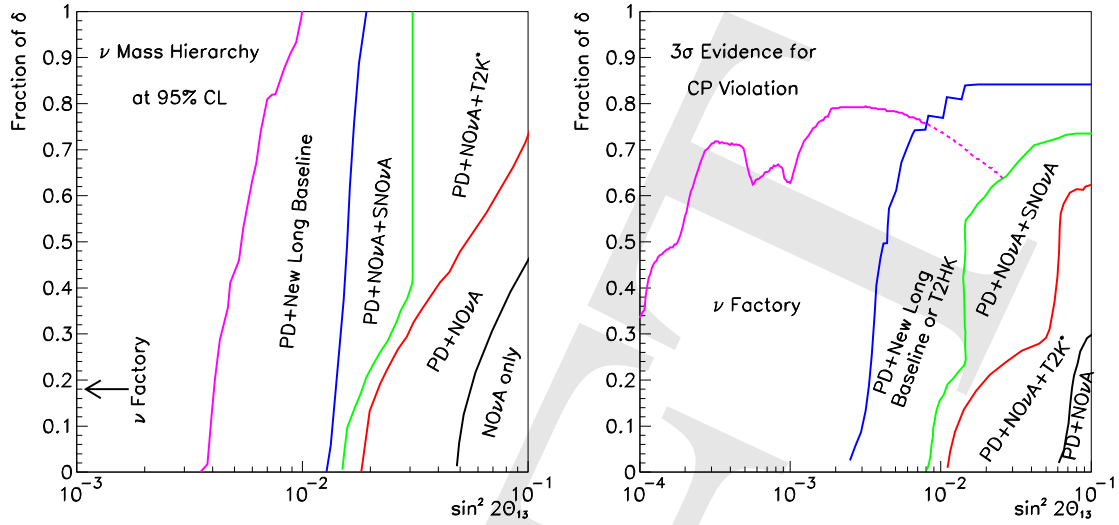


Figure 1: Possible evolution of the experimental sensitivity to the neutrino mass hierarchy (left plot) and CP violation in the lepton sector (right plot). The sensitivity is characterized by, for each value of $\sin^2 2\theta_{13}$, the fraction of the δ parameter space for which the mass hierarchy could be determined at 2σ or CP violation observed at 3σ . Note that δ is the unknown CP phase in the mixing matrix. The curves correspond to various stages of the global neutrino oscillation program. “NO ν A alone” corresponds to a 50kton NO ν A detector at 15 mrad from the NuMI beamline axis running 3 years neutrino mode, 3 years antineutrino mode, with a 0.4 MW proton source. “PD+NO ν A” corresponds to the same running time and detector but with 2 MW proton driver. PD+NO ν A+T2K* corresponds to the addition of T2K with an upgraded proton source (4 MW), with the same 3+3 year run. “PD+NO ν A+ SNO ν A” corresponds to the addition of a 50kton detector at 42mrad, where the new (later) detector runs for 3+3 years, and the 15 mrad detector takes data for 6+6 years. PD+new long baseline or T2HK corresponds to either a new long baseline (> 1000 km) experiment combined with a Megaton class detector (at a National Underground Lab), or combining PD+NO ν A+ T2K with the Hyper-Kamiokande detector. The Neutrino Factory consists of a 50GeV muon storage ring with 5×10^{20} muon decays per year, fed by a 4MW proton source, with $4\nu+4\bar{\nu}$ years of running time and a 50 kton MINOS-like detector.

The conclusions presented in this report are based on studying a number of different scenarios, chosen to help us consider the different outcomes that are possible from the experiments we expect to be conducted before the Proton Driver era:

Scenario 1: $\sin^2 2\theta_{13}$ is just below the present limit. Specifically, $\sin^2 2\theta_{13} > 0.04$. If this is the case the presently approved generation of experiments are expected to provide the first measurements of θ_{13} in the next few years.

Scenario 2: $\sin^2 2\theta_{13}$ is small, but is large enough for $\nu_\mu \rightarrow \nu_e$ transitions to be observable and the neutrino mass hierarchy to be determined (at the level of a few standard deviations) without a Proton Driver. Specifically, $0.04 < \sin^2 2\theta_{13} < 0.01$.

Scenario 3: $\sin^2 2\theta_{13}$ is too small for $\nu_\mu \rightarrow \nu_e$ transitions to be observable in accelerator-based experiments without a Proton Driver. Specifically, $\sin^2 2\theta_{13} < 0.01$.

Independent of which of the three θ_{13} scenarios nature has chosen, there are three special cases that must also be considered:

Special Case 1: The atmospheric neutrino mixing angle θ_{23} is maximal or very close to it.

Special Case 2: LSND Oscillations are confirmed by MiniBooNE.

Special Case 3: Something else unexpected is discovered.

The main conclusions described in this report are:

1. In all scenarios, a long-baseline program at Fermilab based upon one or more very massive detectors and a 2 MW Main Injector beam (available in about a decade) would provide a unique, World class, cutting edge neutrino oscillation program, and provide a logical step towards a Neutrino Factory, if needed.
2. In θ_{13} **Scenario 1** the unique contribution of the Fermilab Proton Driver based experiments to the global neutrino oscillation program would be to:
 - (a) Greatly improve our knowledge of the neutrino mass spectrum. Depending on the oscillation parameters and on the sensitivity that might be achieved by a NuMI based experiment in the pre Proton Driver era, the Proton Driver era experiment(s) would either make the first determination of the neutrino mass hierarchy by distinguishing between the so called "normal" or "inverted" patterns of masses that are presently viable, or would increase the significance of an existing observation from the "first evidence" level to a high degree of confidence. Depending on the oscillation parameters, to achieve this goal might require a multi-step program, and might require combining Fermilab Proton Driver results with results from shorter baseline experiments (for example, an *upgraded* T2K experiment in Japan). The possible evolution of the sensitivity to the neutrino mass hierarchy, characterized by, for any given value of $\sin^2 2\theta_{13}$, the fraction of the parameter space within which the mass hierarchy would be determined, is shown on the left of Fig. 1. In all cases the Proton Driver program will provide the crucial measurements needed to determine the pattern of neutrino masses.
 - (b) Enable the first sensitive searches for CP violation in the lepton sector. This would be part of a global program, beginning with a search based on the Fermilab Proton Driver experiment(s) alone, but gaining much greater sensitivity when combined with shorter baseline experiments, for example an *upgraded* T2K experiment in Japan. The possible evolution of the sensitivity to CP violation, characterized by, for any given value of $\sin^2 2\theta_{13}$, the fraction of the parameter space within which CP violation would be observed, is shown on the right of Fig. 1. Note that a Fermilab Proton Driver program would play a unique and critical role in the global search for CP violation and in the precision measurements that would be required following discovery.

3. In θ_{13} **Scenario 2** the unique contribution of the Fermilab Proton Driver based experiments to the global neutrino oscillation program would be to:
 - (a) Greatly improve our knowledge of the neutrino mass spectrum by making the first determination of the neutrino mass hierarchy. Depending on the oscillation parameters, to achieve this goal might require a multi-step program, and might require combining Fermilab Proton Driver results with results from shorter baseline experiments (for example, an *upgraded* T2K experiment in Japan). However, in all cases the Proton Driver program will provide the crucial measurements needed to determine the pattern of neutrino masses (see Fig. 1).
 - (b) Enable the first sensitive searches for CP violation in the lepton sector. This would be part of a global program, and will require a Proton Driver program with multiple detectors and/or additional results from shorter baseline experiments, for example from an *upgraded* T2K experiment in Japan (see Fig. 1). Note that a Fermilab Proton Driver program would play a unique and critical role in the global search for CP violation and in the precision measurements that would be required following discovery.
4. In θ_{13} **Scenario 3** the unique contribution of the Fermilab Proton Driver based experiments to the global neutrino oscillation program would be to:
 - (a) Significantly improve our knowledge of θ_{13} by improving the sensitivity by a factor of a few. This will push the θ_{13} sensitivity as far as seems possible using conventional neutrino beams, and will give experience with a Neutrino Factory class Proton Driver (and perhaps an associated muon source) should it be necessary to go further by building a Neutrino Factory.
 - (b) Enable the neutrino mass hierarchy to be determined within a significantly extended region of parameter space (see Fig. 1). This will require a very long baseline experiment and hence a new beamline. However, this beamline could be built as a second phase, after θ_{13} has been determined to be finite, or alternatively the Proton Driver complex could then evolve into a Neutrino Factory which would enable the neutrino oscillation physics program to be completed with high precision.
 - (c) Enable a search for CP violation in the lepton sector over a significantly extended region of parameter space (see Fig. 1). This will require a very long baseline experiment and hence a new beamline, and will also require a *greatly upgraded* T2K experiment (or equivalent). However, the additional investment could be made as a second phase, after θ_{13} has been determined to be finite, or alternatively the Proton Driver complex could then evolve into a Neutrino Factory which would enable the neutrino oscillation physics program to be completed with high precision.

In summary, for all three θ_{13} scenarios there is a strong physics case for a long-baseline neutrino oscillation program at a new 2MW Fermilab Proton Driver. In scenarios (1) and (2) the main contributions of the Proton Driver program to the global

neutrino program are qualitatively similar and the experimental programs share a common first step. In scenario (3) the Proton Driver would provide the last significant step that can be made with conventional neutrino beams, and prepare the way (or perhaps evolve into) a Neutrino Factory program.

Contents

1	Introduction	11
2	Neutrino Oscillations	13
2.1	Introduction	13
2.2	Three-flavor neutrino oscillations	14
2.3	Muon neutrino disappearance measurements	16
2.4	Electron neutrino appearance measurements	16
2.4.1	The measurement of θ_{13}	16
2.4.2	Matter effects and the mass hierarchy determination	17
2.4.3	The sensitivity to δ_{CP}	18
2.5	Complementarity of reactor experiments	21
2.6	The LSND anomaly and “new” physics	22
3	Theoretical Motivations for Neutrino Oscillation Measurements	27
3.1	Neutrino Masses and Physics beyond the SM	27
3.2	Model Predictions	28
3.2.1	Motivation for Non-Zero θ_{13}	28
3.2.2	Deviations from Maximal θ_{23}	29
3.2.3	Mass Schemes	30
3.2.4	Dirac and Majorana CP Phases	31
3.3	Implications of Quantum Corrections	31
3.4	Impact of Future Measurements on Theory	33
4	Scenarios for Neutrino Oscillations at Proton Driver Startup	35
4.1	Oscillation Measuremnets Before Proton Driver Startup	35
4.1.1	Conventional beam experiments	36
4.1.2	The first-generation superbeams T2K and NOvA	36
4.1.3	The reactor experiments Double-Chooz and Reactor-II	38
4.1.4	The Short Baseline Experiment MiniBooNE	38
4.2	The $\sin^2 2\theta_{13}$ bound from different experiments at Proton Driver Startup	39
4.3	The measurements of Δm_{31}^2 and θ_{23}	39
4.4	The MiniBooNE Measurement	42
4.5	The Scenarios	42

5	Scenario 1: $\sin^2 2\theta_{13}$ Greater Than ~ 0.04	43
5.1	The NOvA experiment	43
5.2	Synergy with T2K Measurements	46
6	Scenario 2: $\sin^2 2\theta_{13}$ Between ~ 0.01 and ~ 0.04	49
6.1	Use Other or New Detectors with NOvA	50
6.2	Narrow Band Beams from Fermilab to Homestake	51
6.3	Broadband Beam to Homestake or WIPP	52
6.4	Very Long Baselines	55
7	Scenario 3: $\sin^2 2\theta_{13}$ Less Than ~ 0.01	59
7.1	Neutrino Factory	59
7.1.1	Neutrino Factory Physics Reach	60
7.2	BetaBeam	61
7.2.1	Background	61
7.2.2	Physics with a beta beam	62
8	The Special Cases	65
8.1	Special Case 1: $\sin^2 2\theta_{23}$ Still Consistent with 1	65
8.1.1	NOvA Measurement	65
8.1.2	Broadband Beam Measurement	66
8.1.3	FeHo Measurement	70
8.2	Special Case 2: LSND Oscillations Confirmed by MiniBooNE	71
8.2.1	Decay at Rest Source	71
8.2.2	NuMI ν_μ to ν_τ	75
8.2.3	Effect on LBL Measurements	77
8.3	Special Case 3: Something Else Unexpected	78
9	Summary	83
A	Experiment descriptions	85
A.1	The NOvA Experiment	85
A.2	Broadband Beam to Homestake or WIPP	89
A.3	Several Narrow Band Beams to Homestake	91
A.4	Beta Beams using the TeVatron	92
A.5	Neutrino Factory at Fermilab	94
A.5.1	Evolution towards a Neutrino Factory	94

Chapter 1

Introduction

Neutrinos are the most ubiquitous matter particles in the universe. In number, they exceed the constituents of ordinary matter (electrons, protons, neutrons) by a factor of ten billion. They account for at least as much energy in the universe as all the stars combined and, depending on their exact masses, might account for a sizable fraction of the so-called "dark matter". Neutrinos are also important in stellar dynamics. There are about $7 \times 10^9 \text{ cm}^{-2} \text{ sec}^{-1}$ streaming through the Earth from the Sun. Neutrinos govern the dynamics of supernovae, and hence the production of heavy elements in the universe. Furthermore, if there is CP Violation in the neutrino sector, the physics of neutrinos in the early universe might ultimately be responsible for Baryogenesis.

If we are to understand "why we are here" and the basic nature of the universe in which we live, we must understand the basics properties of the neutrino.

Our desire to understand both the universe in which we live and physics beyond the Standard Model provides a compelling case for an experimental program that can elucidate the neutrino mass spectrum and mixing matrix, and test the three-flavor mixing framework. It seems likely that complete knowledge of the neutrino mass splittings and of the mixing matrix is accessible to accelerator-based neutrino oscillation experiments. This will certainly be the case if the unknown mixing angle θ_{13} is not too small. Even if θ_{13} does turn out to be very small, stringent upper limits will provide invaluable guidance to model builders, may indicate the existence of a new conservation law associated with the physics of neutrino mass, and would hopefully lead to new ideas about physics beyond the Standard Model.

This study contains several levels of details, which are targeted towards different readers. At the top level, the general line of argumentation is outlined in the short executive summary on page 3, and is intended for anyone interested in this study. At the next level of detail are the summary paragraphs that start each chapter. They are targeted to any reader who wants to quickly get an overview and understand the argumentation without being bothered with too many details. Together with the summary in Chapter 9, they should give a self-consistent picture of this study. The reader familiar with the subject may want to continue on to the level of individual chapters, where reading the summary paragraphs enables one to easily jump some chapters. Technical details can finally be found in the Appendices.

The document is organised in the following way. We first give an introduction to the phenomenology of neutrino oscillations in Chapter 2, which is followed by a theoretical discussion of why one should do these measurements in Chapter 3. Chapter 4 then lays out the different scenarios for neutrino oscillation physics at the time of Proton Driver startup. In the following chapters the three cases of very large $\sin^2 2\theta_{13} \gtrsim 0.04$ (in Chapter 5), medium $0.01 \lesssim \sin^2 2\theta_{13} \lesssim 0.04$ (in Chapter 6), and small $\sin^2 2\theta_{13} \lesssim 0.01$ (in Chapter 7) are discussed. Since $\sin^2 2\theta_{13}$ sets the scale of the measurements one would like to make, these three scenarios place quite different requirements on subsequent experiments. There may be other interesting physics special cases established within that same time period and these are discussed in greater detail in Chapter 8. Finally, we give a summary in Chapter 9.

Chapter 2

Neutrino Oscillations

From the atmospheric and solar neutrino observations, we know that neutrinos change flavor. Currently, the leading mechanism for these flavor changes is established to be three-flavor neutrino oscillations, where the atmospheric and solar neutrino oscillations decouple in the limit of $\theta_{13} \rightarrow 0$. So far, only upper bounds for θ_{13} have been obtained from solar and reactor neutrino experiments. It is therefore a major objective for future long-baseline neutrino oscillation experiments to establish $\theta_{13} > 0$ by observing $\nu_\mu \rightarrow \nu_e$ flavor transitions. This would open the search for sub-leading effects, such as mass hierarchy and CP violation measurements. The only inconsistency in this picture has been the LSND experiment, which will be further tested by MiniBOONE. If MiniBOONE finds a signal, the number of possibilities will increase, which means that new short- and long-baseline experiments will have to test this “new physics”. In either case, one of the important constraints will be the number of available protons limiting the statistics of these experiments.

2.1 Introduction

Recently, the Super-Kamiokande [1–3] and K2K [4, 5] experiments have provided very strong evidence that the muon neutrino undergoes flavor changing transitions. These transitions have been observed for neutrinos with a path length divided by energy (L/E) of the order of $\sim 500 \text{ km/GeV}$. The Super-Kamiokande experiment also has some supporting evidence that these muon neutrinos are primarily transformed into tau neutrinos: Although the Super-Kamiokande detector has some sensitivity to flavor transitions into electron neutrinos, their data has shown no involvement of electron neutrinos in these transitions. In fact, the CHOOZ [6] reactor experiment has even provided a tighter constraint on the upper limit on the probability of transitions of the electron neutrino flavor of the order of $\sim 5 - 10\%$, which has been observed at a

similar L/E to the one of Super-Kamiokande. This leaves the following interesting and important question open: What is the role of the electron neutrino in flavor transitions at these values of L/E ? A measurement (or stringent limit) on the probability of $\nu_\mu \rightarrow \nu_e$ for $L/E \sim 500\text{km/GeV}$ is an important step in understand these neutrino flavor transitions in atmospheric neutrinos. As the NuMI beam is primarily a ν_μ beam, the observation of ν_e appearance would address this question directly. This would be the primary goal of any new long baseline experiment using neutrinos from the NuMI beam line.

The SNO [7, 8] experiment has recently reported large transitions of solar electron neutrinos into muon or tau neutrinos both with and without salt added to the heavy water. In addition, Super-Kamiokande [9] studying solar neutrinos and KamLAND [10] studying reactor neutrinos have also observed large electron neutrino flavor transitions. From a combined analysis, the L/E for these flavor transitions is a factor of ~ 30 times larger than the L/E for flavor transitions in atmospheric muon neutrinos. These transitions occur for an L/E such that the transition probability $\nu_\mu \rightarrow \nu_e$ measured by an experiment in the NuMI beam will also have some sensitivity to the flavor transitions associated with solar neutrinos through interference effects.

The LSND [11] experiment has reported small muon anti-neutrino to electron anti-neutrino transitions for values of L/E which are less than two orders of magnitude smaller than the transitions seen in atmospheric neutrinos. However this transition probability is very small compared to the one observed in atmospheric and solar neutrinos, it is of the order of 0.3%. If this result is confirmed by the up coming MiniBoone [12] experiment, it will be an important background for a measurement of $\nu_\mu \rightarrow \nu_e$ transitions at the larger values of L/E associated with atmospheric neutrinos.

To explain the above phenomena, extensions to the Standard Model are required. The simplest and most widely accepted extension is to allow the neutrinos to have masses and mixings such that the above phenomena are explained by neutrino oscillations. The masses and mixing of the neutrinos in these extensions would be the low energy remnant of some yet to be determined high energy physics. Thus, neutrino masses and mixing provide a unique window on physics that is inaccessible to current or near future collider experiments. One popular theory is the so-called “seesaw” mechanism [13–17], where the active left handed neutrinos “seesaw” off their heavier right handed (sterile) partners leaving three very light Majorana neutrinos. It is already clear that the masses and mixings in the neutrino sector are very different than the masses and mixing in the quark sector and that a detailed understanding of the neutrino masses and mixings will be important in differentiating fermion mass theories. Also, they may provide the key to advancing our theoretical understanding of this fundamental question.

2.2 Three-flavor neutrino oscillations

If the neutrinos have masses and mixings then the neutrino mass eigenstates, $\nu_i = (\nu_1, \nu_2, \nu_3, \dots)$ with masses $m_i = (m_1, m_2, m_3, \dots)$ are related to the flavor

eigenstates, $\nu_\alpha = (\nu_e, \nu_\mu, \nu_\tau, \dots)$ by a mixing matrix U^ν ,

$$|\nu_\alpha\rangle = \sum_i U_{\alpha i}^\nu |\nu_i\rangle \quad (2.1)$$

The charged weak current, for the neutrino flavor states, is given by $J_\lambda = \bar{\nu}_L \gamma_\lambda \ell_L$ where $\ell = (e, \mu, \tau)$ is the vector of charged lepton mass eigenstates. In the absence of light sterile neutrinos, the 3×3 lepton mixing matrix U is unitary. Lepton flavor mixing was first discussed (for the 2×2 case) by Maki, Nakagawa, and Sakata.

If we restrict the light neutrino sector to the three known active flavors and set aside the LSND results¹ then the unitary matrix MNS matrix, U , can be written as

$$U_{\alpha i} = \begin{pmatrix} c_{13}c_{12} & c_{13}s_{12} & s_{13}e^{-i\delta} \\ -c_{23}s_{12} - s_{13}s_{23}c_{12}e^{i\delta} & c_{23}c_{12} - s_{13}s_{23}s_{12}e^{i\delta} & c_{13}s_{23} \\ s_{23}s_{12} - s_{13}c_{23}c_{12}e^{i\delta} & -s_{23}c_{12} - s_{13}c_{23}s_{12}e^{i\delta} & c_{13}c_{23} \end{pmatrix} \quad (2.2)$$

where $c_{jk} \equiv \cos \theta_{jk}$ and $s_{jk} \equiv \sin \theta_{jk}$.

With this labeling, the atmospheric neutrinos oscillations are primarily determined by θ_{23} and Δm_{32}^2 , whereas the solar neutrino oscillations depend on θ_{12} and Δm_{21}^2 , where $\Delta m_{ij}^2 = m_i^2 - m_j^2$. From Super-Kamiokande, we already have some knowledge of $|\Delta m_{32}^2| = (1.5 - 3.5) \times 10^{-3} \text{ eV}^2$ and $0.35 < \sin^2 \theta_{23} < 0.65$ (i.e., $\sin^2 2\theta_{23} > 0.91$). Note the substantial uncertainty in these atmospheric measurements. A combined analysis of the SNO, Super-Kamiokande, and KamLAND experiments gives $\Delta m_{21}^2 = +7.1 \pm 2.0 \times 10^{-5} \text{ eV}^2$ and $0.23 < \sin^2 \theta_{12} < 0.35$ with $\sin^2 \theta_{12} = 0.5$ excluded at more than 5σ .² This corresponds to $0.71 < \sin^2 2\theta_{12} < 0.91$. For the purpose of these long baseline experiments, our knowledge of the solar parameters is already in very good shape and is even expected to improve with time.

The CHOOZ (and Super-Kamiokande) experiments have provided a limit on $\sin^2(2\theta_{13})$. The CHOOZ limit is dependent on the input value used for $|\Delta m_{31}^2| \approx |\Delta m_{32}^2|$. For the current central value $2.5 \times 10^{-3} \text{ eV}^2$, the bound is $\sin^2(2\theta_{13}) < 0.11$, while for $|\Delta m_{31}^2| = 2.0 \times 10^{-3} \text{ eV}^2$, it is $\sin^2(2\theta_{13}) < 0.18$ [6]. Thus, any new long-baseline neutrino oscillation experiment sensitive to $\nu_\mu \rightarrow \nu_e$ must be able to search a substantial range below this upper bound.

The MINOS experiment [21] will provide a 10% measurement of the atmospheric $|\Delta m_{32}^2|$, but not improve our knowledge of θ_{23} . This experiment has sensitivity to $\sin^2(2\theta_{13})$ only about a factor of two below the CHOOZ bound. Any future reactor experiment to measure $\sin^2 2\theta_{13}$ [22,23] could improve our knowledge of this important parameter, but such an experiment has no sensitivity to θ_{23} , the sign of Δm_{32}^2 or the CP violating phase δ_{CP} . Therefore, such a reactor experiment would be truly complimentary to long-baseline experiment to observe $\nu_\mu \rightarrow \nu_e$.

¹In the 3+1 neutrino mass hierarchy the LSND result can be accommodated as a perturbation on the pure active 3 neutrino hierarchy. The 2+2 mass hierarchy would require major modifications.

²In fact, more recent global analyses [18–20] favor a somewhat larger value of $\Delta m_{21}^2 = 8.2_{-0.8}^{+1.0} \cdot 10^{-5} \text{ eV}^2$ (3σ) with much smaller errors. These results favor the general results of this study, such as the accessibility of CP effects.

2.3 Muon neutrino disappearance measurements

One important oscillation channel for long baseline experiments is the $\nu_\mu \rightarrow \nu_\mu$ disappearance channel. Its oscillation probability in vacuum is given by

$$P(\nu_\mu \rightarrow \nu_\mu) = \left| \sum_{j=1}^3 U_{\mu j}^* U_{\mu j} e^{-i(m_j^2 L/2E)} \right|^2 \simeq 1 - 4|U_{\mu 3}|^2(1 - |U_{\mu 3}|^2) \sin^2 \Delta_{32}, \quad (2.3)$$

where $\Delta_{32} \approx 1.27 \left(\frac{\Delta m_{32}^2 L}{E} \right)$ and the approximation that the splitting between solar mass eigenstates is small has been used. The amplitude of the oscillation is, for small θ_{13} ,

$$4|U_{\mu 3}|^2(1 - |U_{\mu 3}|^2) = 4 \cos^2 \theta_{13} \sin^2 \theta_{23} (1 - \cos^2 \theta_{13} \sin^2 \theta_{23}) \simeq \sin^2 2\theta_{23} + \mathcal{O}(\sin^2 \theta_{13}). \quad (2.4)$$

This probability does not depend on matter effects to zeroth and first order in θ_{13} and $\alpha \equiv \Delta m_{21}^2 / \Delta m_{31}^2$ [24]. This means that for baselines of less than about 1 000 km matter effects are small in this channel and can be ignored for this discussion.

A high precision measurement of $\nu_\mu \rightarrow \nu_\mu$ can be used to determine the atmospheric Δm^2 to the 10^{-4} eV^2 level. If in addition $\sin^2 2\theta_{23}$ can be determined to better than 1%, such a measurement will determine how much θ_{23} deviates from maximal mixing $\pi/4$. However, it cannot determine the sign of this deviation since $\sin^2 2\theta_{23}$ is symmetric about $\theta_{23} = \pi/4$. For example, if

$$\sin^2 2\theta_{23} = 1 - \epsilon^2 \Rightarrow \sin^2 \theta_{23} = \frac{1 \mp |\epsilon|}{2}. \quad (2.5)$$

Thus, there are two solutions for θ_{23} unless $\sin^2 2\theta_{23} \equiv 1$. Currently, we have $|\epsilon| < 0.3$ at the 90% CL. Note that the value of $\pi/4 - \theta_{23}$ is a measure of the breaking of a $\nu_\mu \leftrightarrow \nu_\tau$ symmetry at some high energy scale, as we will discuss in greater detail in the next chapter.

2.4 Electron neutrino appearance measurements

The most important oscillation channel for future long baseline experiments is the appearance probability $\nu_\mu \rightarrow \nu_e$, which we will discuss in several steps.

2.4.1 The measurement of θ_{13}

The appearance probability in vacuum is to leading order in $\alpha \equiv \Delta m_{21}^2 / \Delta m_{31}^2$ given by

$$P_{\text{vac}}(\nu_\mu \rightarrow \nu_e) = \sin^2 \theta_{23} \sin^2 2\theta_{13} \sin^2 \Delta_{31} \quad (2.6)$$

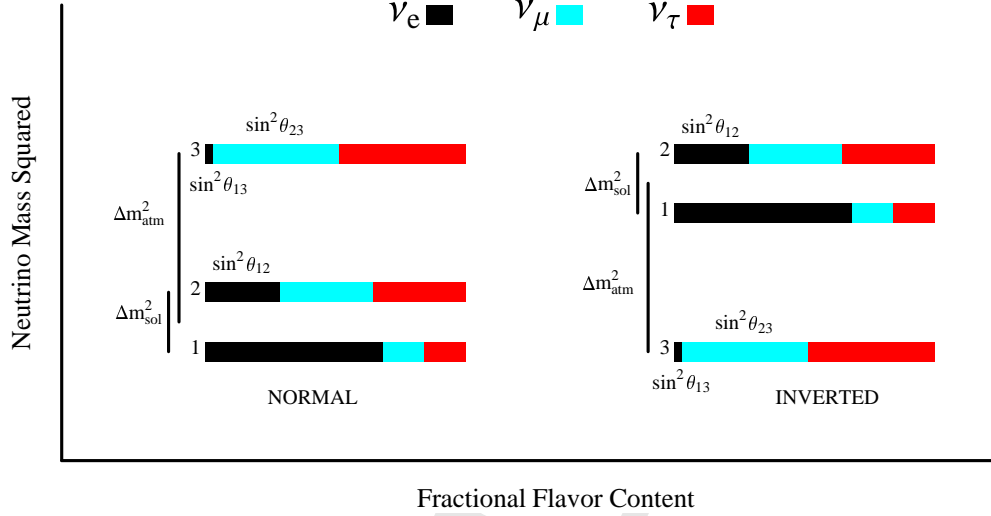


Figure 2.1: The two allowed three-neutrino mass squared spectrums that account for the oscillations of solar and atmospheric neutrinos. The normal spectrum has $\Delta m_{32}^2 > 0$ and the inverted has $\Delta m_{32}^2 < 0$. The ν_e fraction of each mass eigenstate is indicated by the black solid region whereas the ν_μ (ν_τ) fraction is indicated by the blue (red) regions. The ν_e fraction in the mass eigenstate labeled “3” has been set to the CHOOZ bound.

where $\Delta_{31} \approx 1.27 \left(\frac{\Delta m_{31}^2 L}{E} \right)$. If the experiment is performed at one the peaks of this probability, that is, when $\Delta_{31} = \frac{\pi}{2} + n\pi$, then we will have

$$P_{\text{vac}}(\nu_\mu \rightarrow \nu_e) = \frac{1}{2} \sin^2 2\theta_{13} = 2.5\% \left(\frac{\sin^2 2\theta_{13}}{0.05} \right). \quad (2.7)$$

The first peak occurs at the neutrino energy

$$E = 1.7 \text{ GeV} \left(\frac{\Delta m_{31}^2}{2.5 \times 10^{-3} \text{eV}^2} \right) \left(\frac{L}{820 \text{km}} \right). \quad (2.8)$$

Since the limit on $\sin^2 2\theta_{13}$ from the CHOOZ experiment varies from 0.11 to 0.18 depending on the atmospheric Δm_{31}^2 , the maximum appearance probability will range from $\sim 5 - 10\%$. To provide useful information on θ_{13} , any ν_e appearance experiment has to aim to exclude or convincingly observe a signal at least one order of magnitude below this 5% limit.

2.4.2 Matter effects and the mass hierarchy determination

The neutrinos in the NuMI beam propagate through the Earth and matter induced contributions to the appearance propagation amplitude are non-negligible. These matter effects have opposite sign for neutrinos and anti-neutrinos and for the normal versus inverted neutrino mass hierarchies. The matter effects can be thus used to distinguish the two possible three neutrino mass hierarchies (*cf.*, Figure 2.1). If the

experiment is performed at the first peak in the oscillations, as above, the matter effects are primarily a function of the energy of the neutrino beam and the transition probability in matter can be approximated by

$$P_{\text{mat}}(\nu_\mu \rightarrow \nu_e) \approx \left(1 \pm 2 \frac{E}{E_R}\right) P_{\text{vac}}(\nu_\mu \rightarrow \nu_e). \quad (2.9)$$

Here E_R is the matter resonance energy associated with the atmospheric Δm^2 :

$$E_R = \frac{\Delta m_{31}^2}{2\sqrt{2}G_F N_e} = 12 \text{ GeV} \left(\frac{\Delta m_{31}^2}{2.5 \times 10^{-3} \text{eV}^2} \right) \left(\frac{1.4 \text{ g} \cdot \text{cm}^{-3}}{Y_e \rho} \right) \quad (2.10)$$

with N_e the electron number density in the earth, ρ the matter density ($\sim 2.8 \text{ g} \cdot \text{cm}^{-3}$) and $Y_e = \frac{1}{2}$ the electron fraction.

For the normal hierarchy, matter effects enhance (suppress) the transition probability for neutrinos (anti-neutrinos) and vice versa for the inverted hierarchy. For a neutrino energy of 2 GeV, matter effects give a 30 % enhancement or suppression in the transition probability. Therefore, they can help to determined the mass hierarchy. In particular, the normal and inverted hierarchies could very well be distinguished by a comparison of the probability of $\nu_\mu \rightarrow \nu_e$ between two different experiments at different baselines [25–27], such as NO ν A and T2K [28]. If both experiments operated at the first oscillation and both run neutrinos, then

$$P_{\text{mat}}^N(\nu_\mu \rightarrow \nu_e) \cong \left(1 \pm 2 \frac{(E^N - E^T)}{E_R}\right) P_{\text{mat}}^T(\nu_\mu \rightarrow \nu_e), \quad (2.11)$$

where (P^N, E^N) and (P^T, E^T) are the neutrino transition probabilities and energies for NO ν A and T2K, respectively. In addition, E_R is the matter resonance energy associated with the atmospheric Δm^2 , which is about 12 GeV as given by Eq. (2.10). The plus sign is for the normal hierarchy, and the minus sign for the inverted hierarchy. For anti-neutrinos, these signs are reversed. If either experiment is significantly away from oscillation maximum, the relationship between the two probabilities is more complicated (*cf.*, Ref. [27]).

2.4.3 The sensitivity to δ_{CP}

Now that the solution to the solar neutrino puzzle consistent with neutrino oscillations is the “Large Mixing Angle” (LMA) region, we now that (provided that $\sin^2 2\theta_{13}$ is large enough) the $\nu_\mu \rightarrow \nu_e$ transition probability will be sensitive to sub-leading effects and in particular to the CP violating phase δ_{CP} . In vacuum, the shift in the transition probability associated with the CP violating phase is given by

$$\Delta P_\delta(\nu_\mu \rightarrow \nu_e) \approx J_r \sin \Delta_{21} \sin \Delta_{31} (\cos \delta \cos \Delta_{32} \mp \sin \delta \sin \Delta_{32}), \quad (2.12)$$

where the minus (plus) sign is for neutrinos (anti-neutrinos),

$$J_r = \sin 2\theta_{12} \sin 2\theta_{23} \sin 2\theta_{13} \cos \theta_{13} \simeq 0.9 \sin 2\theta_{13}, \quad (2.13)$$

$$\text{and } \Delta_\odot = 1.27 \frac{\Delta m_{21}^2 L}{E} = \frac{\Delta m_{21}^2}{\Delta m_{31}^2} \Delta_{32} \simeq \frac{1}{36} \Delta_{32}. \quad (2.14)$$

At the first oscillation maximum of the atmospheric Δm^2 scale, the shift in the transition probability (depending on δ) is of the order

$$|\Delta P_\delta(\nu_\mu \rightarrow \nu_e)| \sim 0.6\% \sqrt{\frac{\sin^2 2\theta_{13}}{0.05}}. \quad (2.15)$$

Note that this shift is proportional to $\sqrt{\sin^2 2\theta_{13}}$, whereas the leading term is proportional to $\sin^2 2\theta_{13}$. Thus, the relative importance of the sub-leading terms grows as $\sin^2 2\theta_{13}$ becomes smaller.

The full vacuum transition probability is given by

$$\begin{aligned} P(\nu_\mu \rightarrow \nu_e) &= \left| \sum_{j=1}^3 U_{\mu j}^* U_{e j} e^{-i(m_j^2 L/2E)} \right|^2 \\ &= |2U_{\mu 3}^* U_{e 3} e^{-i\Delta_{32}} \sin \Delta_{31} + 2U_{\mu 2}^* U_{e 2} \sin \Delta_{21}|^2. \end{aligned} \quad (2.16)$$

The second form of this probability is especially illuminating as the first term is the amplitude for $\nu_\mu \rightarrow \nu_e$ associated with the atmospheric Δm^2 , and the second term the amplitude associated with the solar Δm^2 . The interference between these two amplitudes differs for neutrinos and anti-neutrinos, because for anti-neutrinos the U matrix is replaced with U^* . This difference in the interference term leads to the difference in the transition probabilities $\nu_\mu \rightarrow \nu_e$ between neutrino and anti-neutrinos, which is the CP violation.

Using the MNS mixing matrix given in Eq. (2.2), we evaluate

$$\begin{aligned} 2U_{\mu 3}^* U_{e 3} &= e^{-i\delta} \sin 2\theta_{13} \sin \theta_{23} \\ 2U_{\mu 2}^* U_{e 2} &= \sin 2\theta_{12} \cos \theta_{23} \cos \theta_{13} + \mathcal{O}(\sin \theta_{13}). \end{aligned} \quad (2.17)$$

Since the $\mathcal{O}(\sin \theta_{13})$ term is multiplied by $\sin(\Delta_{21})$ in the amplitude, it is quadratic in the small quantities $\sin \theta_{13}$ and the solar δm^2 and therefore can be neglected. We eventually obtain (see also Refs. [24, 29–33])

$$\begin{aligned} P(\nu_\mu \rightarrow \nu_e) &= |e^{-i(\Delta_{32}+\delta)} \sin 2\theta_{13} \sin \theta_{23} \sin \Delta_{31} + \sin 2\theta_{12} \cos \theta_{23} \cos \theta_{13} \sin \Delta_{21}|^2 \\ &= \sin^2 \theta_{23} \sin^2 2\theta_{13} \sin^2 \Delta_{31} + \cos^2 \theta_{13} \cos^2 \theta_{23} \sin^2 2\theta_{12} \sin^2 \Delta_{21} \\ &\quad + J_r \sin \Delta_{21} \sin \Delta_{31} (\cos \Delta_{32} \cos \delta - \sin \Delta_{32} \sin \delta). \end{aligned} \quad (2.18)$$

The first and second terms are the probability of $\nu_\mu \rightarrow \nu_e$ associated with the atmospheric and solar Δm^2 's, respectively, whereas the third term is the interference between these two probabilities. The term proportional to $\sin \delta$ is responsible for CP violation since it changes sign when going from neutrinos to anti-neutrinos.³

To illustrate the growing importance of the CP violating term as $\sin^2 2\theta_{13}$ gets smaller, we have plotted the neutrino anti-neutrino asymmetry, $|P_\nu - P_{\bar{\nu}}|/(P_\nu + P_{\bar{\nu}})$,

³The inclusion of the $\mathcal{O}(\sin \theta_{13})$ terms in $U_{\mu 2}^* U_{e 2}$ gives the full expression for $P(\nu_\mu \rightarrow \nu_e)$ by multiplying the first term by $(1 - 2 \sin^2 \theta_{12} \sin \Delta_{12} \cos \Delta_{32} / \sin \Delta_{31})$ and the second term by $|1 - e^{-i\delta} \sin \theta_{13} \tan \theta_{12} \tan \theta_{23}|^2$ while the third term is unchanged. Both of these factors are very close to unity for any reasonable NuMI experimental setup.

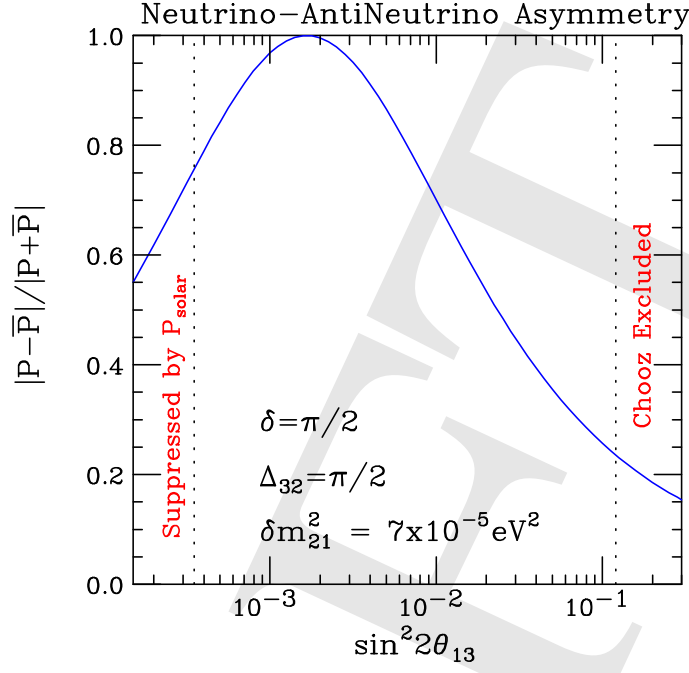


Figure 2.2: The vacuum asymmetry $|P(\nu_\mu \rightarrow \nu_e) - P(\bar{\nu}_\mu \rightarrow \bar{\nu}_e)|/|P(\nu_\mu \rightarrow \nu_e) + P(\bar{\nu}_\mu \rightarrow \bar{\nu}_e)|$ versus $\sin^2 2\theta_{13}$ at oscillation maximum, $\Delta_{32} = \frac{\pi}{2}$, assuming that the CP violation is maximal, $\delta = \frac{\pi}{2}$. At the peak of this asymmetry the amplitudes for $\nu_\mu \rightarrow \nu_e$ from the atmospheric and solar Δm^2 's are equal in magnitude. Above (below) the peak the atmospheric (solar) amplitude dominates.

versus $\sin^2 2\theta_{13}$ in Figure 2.2 at the first oscillation maximum assuming maximum CP violation, i.e., $\Delta_{31} = \pi/2$ and $\delta = \pi/2$. The asymmetry grows as $\sin^2 2\theta_{13}$ gets smaller until the amplitude for $\nu_\mu \rightarrow \nu_e$ from the atmospheric Δm^2 is equal in magnitude to the amplitude from the solar Δm^2 . At this value of $\sin^2 2\theta_{13}$ there is maximum destructive (constructive) interference for neutrinos (anti-neutrinos) and therefore a maximum asymmetry of unity. The value of $\sin^2 2\theta_{13}$ at this peak asymmetry is given by

$$\sin^2 2\theta_{13} \big|_{\text{peak}} \approx \frac{\sin^2 2\theta_{12}}{\tan^2 \theta_{23}} \left(\frac{\pi}{2} \frac{\Delta m_{21}^2}{\Delta m_{31}^2} \right)^2 \sim 0.002 \quad (2.19)$$

Even at the CHOOZ bound for $\sin^2 2\theta_{13}$, the asymmetry is greater than 20%. This asymmetry scales as $\sin \delta$ for values of δ away from $\frac{\pi}{2}$.

The effects of matter can easily be included in our expression for $P(\nu_\mu \rightarrow \nu_e)$ by replacing $\sin^n \Delta_{21}$ and $\sin^n \Delta_{31}$ for all n in all three terms using

$$\sin \Delta_{ij} \rightarrow \frac{\Delta_{ij}}{(\Delta_{ij} \mp aL)} \sin(\Delta_{ij} \mp aL) \quad (2.20)$$

$$\text{where } a = \frac{G_F N_e}{\sqrt{2}} \approx (3700 \text{ km})^{-1} \left(\frac{\rho}{2.8 \text{ g} \cdot \text{cm}^{-3}} \right). \quad (2.21)$$

The minus (plus) sign is for neutrinos (anti-neutrinos). The factors $\sin \Delta_{32}$ and $\cos \Delta_{32}$ remain unchanged by matter effects. This rule comes from the invariance of the product $\Delta m_{ij}^2 \sin 2\theta_{ij}$ evaluated in matter and in vacuum.

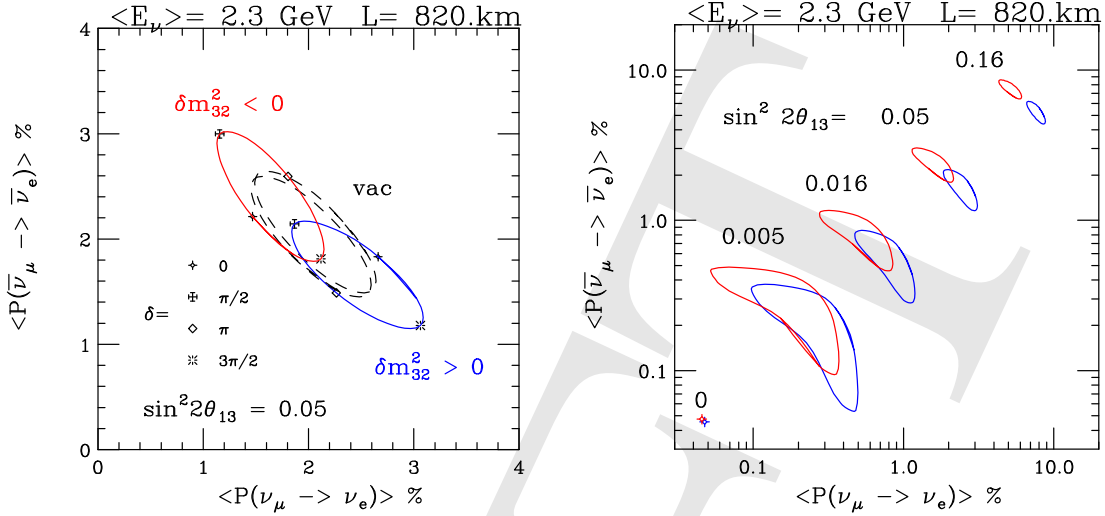


Figure 2.3: The bi-probability plots $P(\nu_\mu \rightarrow \nu_e)$ versus $P(\bar{\nu}_\mu \rightarrow \bar{\nu}_e)$ assuming a constant matter density of $\rho = 2.8 \text{ g} \cdot \text{cm}^{-3}$ at a distance of 820 km and an average energy of 2.3 GeV with a 20% gaussian spread. The mixing parameters are fixed to be $|\Delta m_{31}^2| = 2.5 \times 10^{-3} \text{ eV}^2$, $\sin^2 2\theta_{23} = 1.0$, $\Delta m_{21}^2 = +7 \times 10^{-5} \text{ eV}^2$, $\sin^2 2\theta_{12} = 0.8$ with the labeled values of $\sin^2 2\theta_{13}$ and δ_{CP} .

A useful and instructive way to present the combined effects of matter and sub-leading terms is in the bi-probability plots of $P(\nu_\mu \rightarrow \nu_e)$ versus $P(\bar{\nu}_\mu \rightarrow \bar{\nu}_e)$, invented by Minakata and Nunokawa [34]. We show in Figure 2.3 an example of such a plot for a NUMI case. At the larger values of $\sin^2 2\theta_{13}$, the ellipses associated with the two possible mass hierarchies separate in matter, whereas they are approximately degenerate in vacuum. For example, for a mass hierarchy determination free from the correlation with δ_{CP} , the ellipses have to be completely separated. It is the sensitivity to the sign of Δm_{32}^2 and the CP violating phase in these plots which allows for the determination of these parameters in a sufficiently accurate experiment. For a single experiment, there can be correlations and degeneracies in the determined parameters but these degeneracies can be broken by further measurements.

In summary, ν_e appearance experiments in the neutrino and anti-neutrino channel can, in principle, measure the following quantities:

$$\sin^2 \theta_{23} \sin^2 \theta_{13}, \quad \text{sign}(\Delta m_{32}^2), \quad \cos \theta_{23} \sin \delta_{CP} \quad \text{and} \quad \cos \theta_{23} \cos \delta_{CP}. \quad (2.22)$$

Although the ν_e appearance measurements depends on all of these quantities, the sensitivity varies greatly. In this list, we have ordered the quantities from highest to lowest level of sensitivity.

2.5 Complementarity of reactor experiments

In vacuum, the $\bar{\nu}_e$ disappearance probability at short distances (1 – 2 km) is given to a high accuracy by

$$P(\bar{\nu}_e \rightarrow \bar{\nu}_e) \simeq 1 - \sin^2 2\theta_{13} \sin^2 \Delta_{31} \quad (2.23)$$

Measured variable	LBL $\nu_\mu \rightarrow \nu_\mu$	LBL $\nu_\mu \rightarrow \nu_e$ $\bar{\nu}_\mu \rightarrow \bar{\nu}_e$	Reactor $\bar{\nu}_e \rightarrow \bar{\nu}_e$	Comments
$ \Delta m_{32}^2 $	Y	N	N	Magnitude but not sign
$\sin^2 2\theta_{23}$	Y	N	N	$\theta_{23} \leftrightarrow \frac{\pi}{2} - \theta_{23}$ ambiguous
$\sin^2 \theta_{13}$	N	N	Y	Direct measurement
$\sin^2 \theta_{23} \sin^2 \theta_{13}$	N	Y	N	Combination of θ_{23} and θ_{13}
$\text{sign}(\Delta m_{31}^2)$	N	Y	N	Via matter effects
$\cos \theta_{23} \sin \delta_{CP}$	N	Y	N	CP violation
$\cos \theta_{23} \cos \delta_{CP}$	N	Y	N	Very difficult

Table 2.1: Summary of different measurements at long baseline and reactor neutrino oscillation channels.

and matter effects are insignificant. Therefore a high precision reactor experiment could determine $\sin^2 2\theta_{13}$ provided it is larger than $\sim 1\%$. Since θ_{13} is already known to be small from other solar and atmospheric neutrino experiments, this measurement does not suffer from the $\theta \leftrightarrow \pi/2 - \theta$ ambiguity that the ν_μ disappearance experiment does. Hence, the reactor experiment makes a direct measurement of $\sin^2 \theta_{13}$ independent of θ_{23} , $\text{sign}(\Delta m_{23}^2)$, δ_{CP} , and matter effects. However, note that this implies that a reactor experiment can, for example, not measure δ_{CP} or the neutrino mass hierarchy.

The fact that this measurement of $\sin^2 \theta_{13}$ is independent of all other parameters makes this experiment truly complementary to the ν_e appearance experiments and will be especially useful to untangle the $\theta_{23} \leftrightarrow \frac{\pi}{2} - \theta_{23}$ ambiguity (if present) and the correlation between $\sin^2 2\theta_{13}$ and δ_{CP} when combined with the long baseline measurements. In Table 2.1 we summarize the quantities which the ν_μ LBL disappearance, ν_e LBL appearance and the Reactor experiments can measure.

2.6 The LSND anomaly and “new” physics

The LSND experiment [11] measured, mainly, the neutrino flux produced by pion decay in flight ($\pi^+ \rightarrow \mu^+ \nu_\mu$) and antimuon decay at rest ($\mu^+ \rightarrow e^+ \nu_e \bar{\nu}_\mu$). It observed a small electron-type antineutrino flux about 30 meters away from the production region [11]. The originally absent $\bar{\nu}_e$ -flux can be interpreted as evidence that $\bar{\nu}_\mu$ is transforming into $\bar{\nu}_e$ with $P_{\bar{\mu}\bar{e}}$ of the order a fraction of a percent, which one would not expect at this L/E within the standard three-flavor picture. If interpreted in terms of neutrino oscillations, the LSND anomaly points to a mass-squared difference $\Delta m_{\text{LSND}}^2 \sim 1 \text{ eV}^2$ (even within conservative errors, $\Delta m_{\text{LSND}}^2 \gg 10^{-3} \text{ eV}^2$). The LSND result will be confirmed or refuted by the on-going MiniBooNE experiment, perhaps as early as the end of Summer 2005 (see [35] and references therein).

It is easy to understand why the LSND anomaly does not “fit” in the three flavor mixing scheme described in detail earlier. With three neutrinos, one can define only two independent mass-squared differences, and these are completely determined by

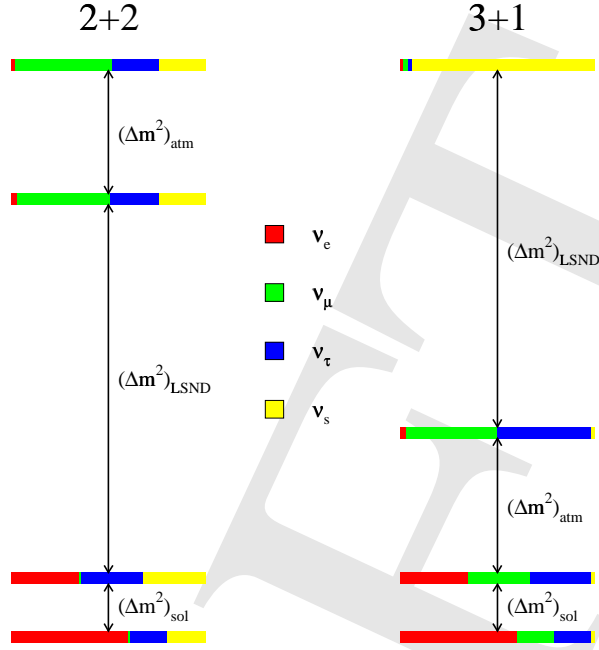


Figure 2.4: Two possible mass-patterns potentially capable of addressing all neutrino data, including those from LSND. The one on the left (right) is characteristic of a “2+2” (“3+1”) mass-scheme.

the solar, atmospheric, reactor, and accelerator data. As discussed earlier, both mass-squared differences are much smaller than Δm_{LSND}^2 . So far, the Karmen 2 experiment [36], which could have confirmed the LSND anomaly, did not observe a signal, ruling out a significant portion of the LSND allowed parameter space. Thus, given that the LSND results have not yet been confirmed by another experiment, it is a widely discussed possibility that “ordinary” three-flavor oscillations are responsible for “all-but-LSND-data”, whereas the LSND anomaly could come from more exotic new physics. Reinforcing this bias is the fact that, if indeed present, the LSND anomaly requires a very small transition probability.

One possible solution to the LSND anomaly is to add extra, Standard Model (SM) singlet (sterile) neutrinos, capable of mixing with the ordinary (active) neutrinos.⁴ While this allows one to define at least three mass-squared differences, it is not guaranteed that one is capable of fitting all neutrino data with four (or more) neutrino mixing. Indeed, detailed analyses [20, 38] suggest that four neutrino mixing schemes are either very poor or at best mediocre fits to all neutrino data.

The reason for this can be qualitatively understood: There are two general neutrino mass-patterns with four neutrinos, which are capable of describing one large and two small mass-squared differences. These are referred to as the “2+2” and “3+1” schemes as illustrated in Figure 2.4. As far as the 2+2 schemes are concerned, short baseline neutrino data constrain $|U_{\mu 1}|$, $|U_{\mu 2}|$, $|U_{e 3}|$, and $|U_{e 4}|$ to be

⁴According to data from the LEP experiments, there are no extra very light “neutrino” degrees of freedom that couple to the Z^0 -boson with SM-like couplings (*cf.*, [37] for the most updated analysis). Hence, any additional neutrinos are constrained to be SM singlets.

small. If all of these were set to zero, atmospheric oscillations would be driven by $|\nu_\mu\rangle \leftrightarrow \cos\zeta|\nu_\tau\rangle + \sin\zeta|\nu_s\rangle$ mixing, where ν_s is a sterile neutrino and ζ is a mixing angle that characterizes the sterile component of the muon-type neutrino. By unitarity, solar oscillations would then be driven by $|\nu_e\rangle \leftrightarrow -\sin\zeta|\nu_\tau\rangle + \cos\zeta|\nu_s\rangle$ mixing. Both solar and atmospheric data constrain ζ . Atmospheric neutrino data are sensitive to a sterile component via Earth matter effects and via the interaction of the tau-type neutrinos inside the detector. Solar data are sensitive to a sterile component via matter effects in the Sun and in the Earth, and also because tau-type neutrinos interact via neutral current interactions inside of SNO and Super-Kamiokande. Both solar and atmospheric data observe no evidence for a sterile neutrino component. Hence, atmospheric data set an upper bound for $\sin^2\zeta$, while the solar data constrain $\cos^2\zeta$. By combining both data sets, $\cos^2\zeta + \sin^2\zeta$ is already constrained to be less than one [20, 38], which is “ruling out” the 2+2 scheme. Some attempts have been made to understand what happens when the conditions $|U_{\mu 1}| = |U_{\mu 2}| = |U_{e 3}| = |U_{e 4}| = 0$ are lifted consistent with experimental bounds (see, for example, Ref. [39]) but one expects that these sub-leading effects will not lead to a significantly better fit to all data.

The 3+1 schemes fit the atmospheric and solar data just fine, given that sterile neutrino effects are just a small perturbation to the ordinary three neutrino fit to all-but-LSND data. However, they are constrained by the short-baseline searches for ν_e and ν_μ disappearance driven by the LSND frequency. The LSND $\nu_\mu \leftrightarrow \nu_e$ oscillations are given by

$$P_{e\mu} \simeq 4|U_{e4}|^2|U_{\mu 4}|^2 \sin^2\left(\frac{\Delta m_{\text{LSND}}^2 L}{4E}\right), \quad (2.24)$$

while the survival probability of a species $\alpha = e, \mu$ is given by

$$P_{\alpha\alpha} \simeq 1 - 4|U_{\alpha 4}|^2(1 - |U_{\alpha 4}|^2) \sin^2\left(\frac{\Delta m_{\text{LSND}}^2 L}{4E}\right). \quad (2.25)$$

The absence of electron-type and muon-type neutrino disappearance constrains $|U_{e4}|^2$ and $|U_{\mu 4}|^2$ to be small, while the LSND data require $|U_{e4}|^2 \times |U_{\mu 4}|^2$ to be larger than a fraction of a percent [40, 41]. The tension in the current data is not enough to rule out the 3+1 scheme, but it does lead to a rather poor fit [20, 38].

Five neutrino mixing schemes have also been explored (see, for example, [42]). They are in principle “3+1+1” schemes (“2+2+1” schemes do not much better than 2+2 schemes) and are designed in a way that the tension between the short-baseline and the LSND data is alleviated. With five neutrinos, it is possible to fit all the neutrino data properly, but a major point of criticism is that the choices for mixing parameters and mass-squared differences are rather “finely tuned”.

More exotic solutions to the LSND anomaly have been proposed, and none of them seem to fit all data particularly well. In the following, we discuss some of them. The possibility that there are rare lepton-flavor violating $\mu^+ \rightarrow e^+ \nu_e \bar{\nu}_e$ decays [43] could explain the LSND data as long as the branching ratio for the flavor-violating decay was of order a fraction of a percent. Such decays, however, should also have been observed by the Karmen experiment, which disfavored this hypothesis at around

the 90% confidence level [44]. Recently available precision data of the Michel electron energy spectrum [45] seem to safely rule out flavor changing muon decays as a solution to the LSND anomaly.

Postulating that neutrinos and antineutrinos have different masses and mixing angles (*cf.*, [46]; see also Refs. [47, 48]) received a significant amount of attention in the past three years. The original idea was inspired by the fact that solar data required the disappearance of electron-type *neutrinos*, while those from LSND required the appearance of electron-type *antineutrinos*. If neutrinos and antineutrinos oscillated at different frequencies (different Δm^2), all data could be rendered compatible. Aside from all sorts of theoretical issues, the original CPT-violating setup was ruled out when KamLAND published the first evidence for antineutrino oscillations at solar frequencies. A second manifestation of CPT-violating solutions to the LSND data consisted of postulating that atmospheric oscillations in the antineutrino sector were driven by Δm_{LSND}^2 . This possibility is strongly disfavored (at the three sigma level) by the atmospheric data [49].

Other ideas include four neutrino schemes *combined with* with CPT-violation [50] or “mass varying neutrinos” [51], violations of the unitary evolution of quantum mechanical systems [52], and violation of Lorentz invariance [53]. It is fair to say that the last two are yet to be tested rigorously.

Given the fact that none of the proposed solutions to the LSND anomaly seems to be completely satisfactory, it is fair to say that if MiniBooNE confirms the observations made by LSND, there is a good chance we have uncovered a novel physical phenomenon, *i.e.*, we still have to think about more plausible approaches to accommodate the LSND result. If the LSND anomaly is confirmed, all the necessary experimental and theoretical efforts will most likely concentrate, first, on uncovering the mechanism responsible for the LSND flavor change. This will likely require (a) detailed analysis of all available data and (b) a series of other experimental neutrino efforts, capable of mapping out the LSND/MiniBooNE potential parameter spaces. These efforts will most likely include new $\nu_\mu \rightarrow \nu_e$ searches at different short baselines.

If, for the sake of completeness, we assumed that 3+1 neutrino mixing schemes are indeed correct, post-MiniBooNE physics would include a complex program to try to reconstruct the 4×4 neutrino mixing matrix, including the several sources of CP-invariance violation (see, for example, Refs. [54, 55]).

On the other hand, taking the LSND anomaly seriously, there is no reason to assume that there is no other “new physics” affecting neutrino oscillations. Thus, it is another possibility that though MiniBooNE rejects LSND, nevertheless some “new physics” will be found at a NUMI-like experiment. In this case, new approaches to attack this problem will be needed.

In summary, the important measurements that could be made using a long baseline experiment are

- Observation of $\nu_\mu \rightarrow \nu_e$ at an L/E of ~ 500 km/GeV which would determine the ν_e role in atmospheric neutrino flavor transitions. In the neutrino oscillation scenario this is a measure of $\sin^2 \theta_{13}$.

- Matter effects can be used to distinguish the two mass hierarchies and therefore determine the sign of Δm_{31}^2 .
- Because the Large Mixing Angle region is the solution to the solar neutrino puzzle there is sensitivity to the CP violating phase in the channel $\nu_\mu \rightarrow \nu_e$.
- Precision measurements in $\nu_\mu \rightarrow \nu_\mu$ channel can measure how close θ_{23} is to $\pi/4$, that is maximal mixing.

Thus, there is a very rich neutrino physics program to be explored in a ν_e appearance experiment. Details of experimental and beam possibilities will be explored in the subsequent chapters.

On the other hand, if MiniBOONE confirms LSND, more detailed studies in the short baseline region have to be performed to understand the underlying “new physics”. In this case, depending on the actual result, a new strategy for short and long baseline experiments has to be developed. In either case, a large number of protons is needed to reach a sufficiently high statistics of the experiment(s).

Chapter 3

Theoretical Motivations for Neutrino Oscillation Measurements

Two of the main theoretical challenges in neutrino physics are the explanation of the tiny neutrino masses and the large generation mixing in the lepton sector. A lot of models have been proposed for these purposes. In many cases, their predictions for the mixing angle θ_{13} are well within the reach of next-generation long baseline experiments, so that these experiments are able to test and potentially rule out many models. The size of quantum corrections to θ_{13} can also be comparable to the expected sensitivities, which means that the experiments have the potential to restrict the parameters relevant for these corrections as well. From measurements of the neutrino mass hierarchy and deviations from maximal mixing, further important input for model building can be expected. In addition, the detection of leptonic CP violation could be another motivation to suspect that neutrinos played a role in generating the baryon asymmetry of the universe. In the long run, neutrino physics has the potential to yield the most precise information on flavor parameters. A tiny θ_{13} , or a θ_{23} extremely close to $\pi/4$ would disfavor a numerical coincidence and provide a strong hint for some new symmetry.

3.1 Neutrino Masses and Physics beyond the SM

One may ask whether theoretical reasons for a non-zero mixing angle θ_{13} and deviations from maximal atmospheric mixing of a magnitude accessible by new experiments exist. A related question is what impact an improved precision of oscillation experiments will have on the theoretical understanding of neutrino masses. These questions are connected to the origin of neutrino masses. Apparent regularities in the fermionic field content make it very tempting to introduce right-handed neutrino fields. Since

these are gauge singlets, they can have masses much larger than the electroweak scale. The diagonalization of the resulting mass matrices yields generically very small neutrino masses, which are of Majorana type in the most economical scheme. This is the well-known see-saw mechanism [13–17]. It can be nicely accommodated in embeddings of the Standard Model (SM) into Grand Unified Theories (GUTs) with a larger gauge symmetry, such as $SO(10)$. Thus, the generation of neutrino masses is related to physics close to the GUT scale in this framework, so that the measurement of neutrino properties may open up a window for learning about this new physics. In passing, we would like to note that there are several interesting alternative mechanisms for explaining small neutrino masses, which are based on similar principles as the simplest see-saw scheme, but can lead to a different phenomenology. For instance, one can predict Dirac neutrinos rather than Majorana neutrinos [56–60]. Let us stress, however, that the importance of a better knowledge of the mixing parameters is independent of the nature of neutrino masses.

3.2 Model Predictions

In this section, we discuss the predictions of neutrino mass models from the point of view of the different parameters and compare them to the expected sensitivities of future long-baseline experiments.

3.2.1 Motivation for Non-Zero θ_{13}

A reason for expecting a particular value of θ_{13} does clearly not exist as long as one extends the SM only minimally to accommodate neutrino masses. The value of θ_{13} is then simply unknown and could take an arbitrarily small value, *i.e.*, including zero. The situation changes in neutrino mass models, which make additional assumptions about the lepton flavor structure. Even then one should acknowledge that, in principle, any value of θ_{13} can be accommodated. Indeed, before the discovery of large leptonic mixing, many theorists who considered lepton mixing expected it to be similar to quark mixing, characterized by small angles. Experiment led theory in showing the striking results that $\sin^2 2\theta_{23} \simeq 1$ and $\tan^2 \theta_{12} \simeq 0.42$, while θ_{13} is small. Indeed, the most remarkable property of leptonic mixing is that two angles are large. Therefore, today there is no particular reason to expect the third angle, θ_{13} , to be extremely small or even zero. This can be seen in neutrino mass models which are able to predict a large θ_{12} and θ_{23} , utilizing various approaches such as Grand Unification, flavor symmetries, sequential right-handed neutrino dominance, textures, or combinations of these. Many of them are based on a version of the see-saw mechanism. They often have a tendency to predict also a sizable value of θ_{13} which is not too far from current experimental bounds. A similar behavior is found in so-called “anarchic mass matrices”. Starting essentially with random neutrino mass matrix elements one finds that large mixings are actually quite natural [61–64].

An overview of various predictions is given in Table 3.1. For more extensive reviews, see, for example, Refs. [65–69]. The conclusion from these considerations of

Model(s)	Refs.	$\sin \theta_{13}$	$\sin^2 2\theta_{13}$
Minimal SO(10)	[70]	0.18	0.13
Orbifold SO(10)	[71]	0.1	0.04
SO(10) + Flavor symmetry	[72]	$5.5 \cdot 10^{-4}$	$1.2 \cdot 10^{-6}$
	[73]	0.014	$7.8 \cdot 10^{-4}$
	[74–76]	0.05 .. 0.1	0.01 .. 0.04
	[77–79]	0.15 .. 0.22	0.09 .. 0.18
	[80]	0.01 .. 0.06	$4 \cdot 10^{-4}$.. 0.01
SO(10) + Texture	[81]	0.1	0.04
	[82]	0.15	0.09
SU(2) _L × SU(2) _R × SU(4) _c	[83–85]	0	0
	[86–88]	$\lesssim 0.03$	$\lesssim 0.004$
	[89–91]	0.005 .. 0.07	10^{-4} .. 0.02
	[88, 92–95]	0.1 .. 0.2	0.04 .. 0.15
Textures	[96]	0.01 .. 0.05	$4 \cdot 10^{-4}$.. 0.01
	[97–100]	0.08 .. 0.2	0.03 .. 0.15
3×2 see-saw	[101]	0.1	0.04
	[102] (n.h.)	0.07	0.02
	(i.h.)	> 0.006	$> 1.6 \cdot 10^{-4}$
Anarchy	[63]	> 0.1	> 0.04
Renormalization group enhancement	[103]	0.08 .. 0.1	0.03 .. 0.04
M-Theory model	[59]	0.005	10^{-4}

Table 3.1: Selection of predictions for θ_{13} . The numbers should be considered as order of magnitude statements. The abbreviations “n.h.” and “i.h.” refer to the normal and inverted hierarchies, respectively.

neutrino mass models is that a value of θ_{13} close to the CHOOZ bound would be quite natural, while smaller values become harder and harder to understand as the limit on θ_{13} is improved.

3.2.2 Deviations from Maximal θ_{23}

Let us now analyze theoretical expectations for the deviation from maximal atmospheric mixing. Again, there is a large variety of models aiming to explain the neutrino properties observed in atmospheric oscillation experiments, *cf.*, Table 3.2. There are models where the predicted θ_{23} lies in a range that does not include maximal mixing at all [70, 75, 87, 88, 91, 113]. In many other cases, a large atmospheric angle can be explained, while almost maximal mixing would require some tuning, see, for example, Refs. [78, 80, 81, 95, 103, 116–118]. Other works, for instance Refs. [71, 73, 74, 104], predict a value of θ_{23} rather close to $\pi/4$ at leading order, but various sources cause deviations that are typically still within the reach of future experiments.

In many cases, these deviations are related to small parameters, such as mass ratios. For example, even if we assume that maximal θ_{23} is predicted from properties of the neutrino mass matrix, corrections can stem from the charged lepton sector, with

Model(s)	Refs.	$ 0.5 - \sin^2 \theta_{23} $
Minimal SO(10)	[70]	> 0.16
SO(10) + Flavor symmetry	[73, 74, 104]	$\lesssim 0.05$
SO(10) + Texture	[80]	$\lesssim 0.11$
Flavor symmetries	[83, 84, 92, 93, 105–107]	0
	[86]	0.02
	[108]	0.04
	[91]	0.04 .. 0.1
	[87, 88]	$\gtrsim 0.07$
Sequential RH neutrino dominance	[109–111]	0.1
+ Flavor symmetries	[75, 94, 112]	0.1
+ Type II see-saw upgrade	[89]	0.01 .. 0.1
Texture zeros	[96]	0.07
	[113]	> 0.1
Perturbations of textures	[114]	$\lesssim 0.16$
	[64, 115]	0.005 .. 0.1
M-Theory model	[59]	0.02

Table 3.2: Selection of theoretical expectations for $|0.5 - \sin^2 \theta_{23}|$ at tree level. The numbers should be considered as order of magnitude statements.

a typical order of magnitude of $|0.5 - \sin^2 \theta_{23}| = \mathcal{O}(m_\mu/m_\tau) \sim 0.06$. Analogously, assuming that maximal θ_{23} is predicted from the charged lepton mass matrix, a hierarchical neutrino mass matrix might induce $|0.5 - \sin^2 \theta_{23}| = \mathcal{O}(m_2/m_3) \sim 0.17$ [90]. Deviations of this order of magnitude are also typical in models based on sequential right-handed neutrino dominance, where maximal θ_{23} in leading order can originate from the dominant right-handed neutrino and the subdominant contribution leads to corrections (see, for example, Refs. [75, 94, 109, 110, 112]).

3.2.3 Mass Schemes

Another important experimental input for model building is the neutrino mass scheme. GUT models with a standard type I see-saw mechanism tend to predict a normal hierarchy (see, for example, the reviews Refs. [67, 68]), while an inverted hierarchy is often obtained in the context of symmetries such as $L_e - L_\mu - L_\tau$ [119, 120]. For accommodating a relatively large absolute mass scale, *i.e.*, quasi-degenerate masses, the type II see-saw mechanism [121–123] turns out to be particularly suitable (see *e.g.* Ref. [89]). In any case, a specific model is usually only compatible with a normal or an inverted mass ordering, so that the measurement of the sign of Δm_{31}^2 would be very restrictive. In order to probe the nature of neutrino masses (Majorana or Dirac) and to constrain their absolute values, non-oscillation experiments such as searches for neutrinoless double beta decay or cosmological observations are required. For these experiments, the measurement of the sign of Δm_{31}^2 will be important, too. For example, a negative Δm_{31}^2 implies a lower limit on the effective mass for neutrinoless double beta decay (in the case of Majorana neutrinos) which can be reached with the

next generation of experiments.

3.2.4 Dirac and Majorana CP Phases

Given the present state of fermion mass models, only very few of them make predictions for the Dirac and Majorana CP phases. One example are classes of models using a type-II upgrade for explaining a quasi-degenerate mass spectrum, which predict that all CP phases become smaller as the absolute neutrino mass scale increases [89]. A motivation for expecting to find non-vanishing CP phases stems from leptogenesis [124], which provides an attractive mechanism for explaining the observed baryon asymmetry of the universe and which requires CP violation in the Yukawa couplings. However, in the most general case, the CP violation for leptogenesis is not related to the low-energy CP phases in the effective neutrino mass matrix [125, 126]. This changes for specific models where flavor symmetries and texture zeros restrict the structure of the coupling matrices. Then, in general, relations between the CP violation for leptogenesis and the low-energy CP phases emerge. In such models, the requirement of successful leptogenesis typically predicts in particular a non-zero Dirac phase δ , accessible to neutrino oscillation experiments (see, for example, Refs. [101, 127]).

3.3 Implications of Quantum Corrections

Neutrino masses and mixing parameters are subject to quantum corrections (renormalization group running) between low scales, where measurements are performed, and high scales, where models employing flavor symmetries, GUT relations, or textures typically operate. Consequently, even in the “worst case” scenario, where θ_{13} is predicted to be exactly zero, quantum corrections cause θ_{13} to run to a finite value at low energy in general. Strictly speaking, $\theta_{13} = 0$ cannot be excluded completely by this argument, as the high-energy value could be just as large as the change due to the running and of opposite sign. However, a severe cancellation of this kind would be unnatural, since the physics generating the value at high energy is not related to that responsible for the quantum corrections.

The size of these quantum effects can easily be estimated using the differential equations derived in Ref. [128] (see also Refs. [129, 130] for related works). It immediately follows that the effects are negligible in the SM due to the smallness of the charged lepton Yukawa couplings. In the MSSM (Minimal Supersymmetric Standard Model), they are enhanced by $\tan \beta$, the ratio of the two Higgs vacuum expectation values, which means that the situation can change. In addition to the oscillation parameters, the running depends on the mass of the lightest neutrino, the value of the Majorana CP phases in the lepton mixing matrix, and $\tan \beta$. The estimated change of $\sin^2 2\theta_{13}$ in the MSSM is shown in Figure 3.1. One finds a shift larger than 0.01 for a considerable parameter range, so that one can hope to measure a finite value of θ_{13} already in the next generation of experiments. Conversely, limits on model parameters would be obtained if an experiment were to set an upper bound on $\sin^2 2\theta_{13}$ in the range of 0.01. In any case, it should be clear that a precision of the same order

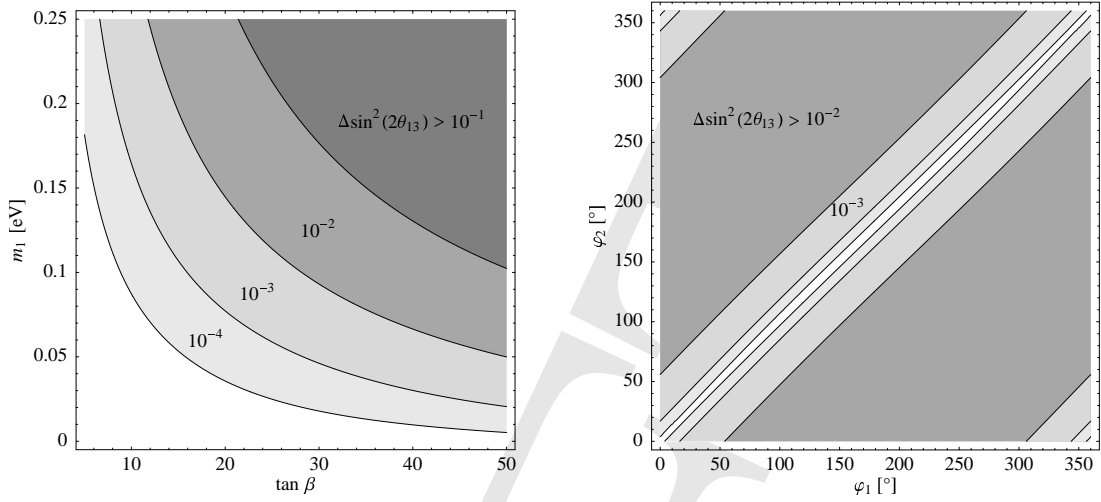


Figure 3.1: Corrections to θ_{13} from the running between 10^2 and 10^{12} GeV in the MSSM, calculated using the initial conditions $\theta_{13} = 0$ and LMA best-fit values for the remaining parameters, as well as a normal mass hierarchy. In the left figure, the corrections are shown as a function of $\tan \beta$ and m_1 , the mass of the lightest neutrino (with Majorana phases $\varphi_1 = 0$ and $\varphi_2 = \pi$). The right plot illustrates the dependence on the Majorana CP phases φ_1 and φ_2 (as defined in Ref. [128]) for $\tan \beta = 50$ and $m_1 = 0.08$ eV. The contour lines are defined as in the left diagram. (Plots taken from Ref. [128].)

of magnitude as the quantum corrections is very interesting in a number of ways.

Analogously, for a model predicting exactly maximal atmospheric mixing, one expects to measure deviations of the order of magnitude of the running effects. Again, one finds corrections to θ_{23} comparable to the precision of future experiments for a considerable part of the parameter space [128, 131].

Note that our estimates are conservative, since we have not taken into account the contributions of neutrino Yukawa couplings above the see-saw scale [132–138] and possible corrections from physics above the GUT scale [139].

The absolute neutrino mass scale is an important factor in determining the size of radiative corrections. As one can see from Figure 3.1, they are largest for quasi-degenerate neutrinos. In this case, it is even possible that the mass ordering is changed in the MSSM with a large $\tan \beta$, i.e., an inverted hierarchy at low energies can be compatible with a normal hierarchy at high energies [128]. This could relax the restrictions on GUT models, if an inverted hierarchy were to be observed experimentally.

Finally, significant radiative corrections to the values of the CP phases are likely, if the neutrino mass hierarchy is not strongly hierarchical. An interesting possibility in this context is the radiative generation of a non-zero Dirac phase [128, 130]. Thus, even if this phase vanishes at some high scale, the low-energy value can be large, which means that leptonic CP violation could also be created by quantum corrections.

3.4 Impact of Future Measurements on Theory

The predictions of neutrino mass models summarized in Tables 3.1 and 3.2, as well as the effects of quantum corrections estimated in Section 3.3 provide good reasons to be optimistic that deviations from zero θ_{13} and maximal atmospheric mixing are large enough to be measurable. If a non-vanishing θ_{13} is found, the power of the measurement to discriminate between different models will depend not only on the precision of the experiment, but also on that of the theoretical predictions. Therefore, it is desirable to improve the latter as well. If maximal atmospheric neutrino mixing is excluded experimentally by a broad margin, this will favor models which can accommodate or even predict significant deviations. However, it will probably be harder to distinguish between the models compatible with the data than in the case of θ_{13} , since the predictions for θ_{23} tend to be less specific.

On the other hand, a negative search for θ_{13} in experiments with a high precision would be very restrictive and rule out many models. Experimental confirmation of a nearly maximal θ_{23} would also eliminate several proposals. However, the large class of models which can accommodate but not predict $\theta_{23} = \pi/4$ would rather be disfavored than strictly ruled out, since one typically expects deviations, as argued in Section 3.2.2. Both a very small θ_{13} and a value of θ_{23} very close to $\pi/4$ corresponds to a rather particular configuration of lepton mixing parameters, which is clearly not compatible with the assumption of a neutrino mass matrix without any structure and would require some theoretical reason. One option is employing flavor symmetries that enforce zero θ_{13} or virtually maximal atmospheric mixing, see, for instance, Refs. [83–85, 92, 93, 105–107].

As discussed in Section 3.3, high-precision measurements are also very interesting in the context of quantum corrections to neutrino masses and mixings. They have the potential to restrict the relevant parameters by disfavoring parameter space regions where the corrections are larger than the measured value of or upper limit on θ_{13} or $\theta_{23} - \pi/4$.

Finally, a determination of the neutrino mass ordering would be another crucial piece of information with a good potential to disfavor certain models.

To conclude, there exist very good theoretical reasons to improve the sensitivity limits of oscillation experiments. The obtained information on the lepton flavour structure is crucial input for lepton mass models. The expected experimental improvements also serve as a motivation for theorists to improve the precision of their predictions to match that of the measurements, in order to make a discrimination between various models easier. From a broader perspective, the experiments discussed in this study probe whether the values of θ_{13} and θ_{23} are mere numerical coincidences or the result of some underlying symmetry. If the smallness of neutrino masses is indeed due to the see-saw mechanism, they may also provide a way to indirectly explore physics at energy scales far beyond the reach of accelerators.

DRAFT

Chapter 4

Scenarios for Neutrino Oscillations at Proton Driver Startup

In the time before a Proton Driver might begin sending neutrinos the next generation of LBL experiments, MINOS, CNGS, T2K, and the proposed NOvA will likely have published results as well as the small scale reactor experiment Double-Chooz, and probably a medium scale reactor experiment as well. MiniBooNE will have resolved the question of whether the LSND result was caused by neutrino oscillations and, judging by the history of neutrino physics, there will be surprise results not yet anticipated. This creates a variety of scenarios for the landscape of neutrino oscillations at Proton Driver startup which are delineated in this chapter. Subsequent chapters will show that in every one of these scenarios a Proton Driver is needed to take the next step.

4.1 Oscillation Measurements Before Proton Driver Startup

It is necessary to consider what will be happening in the field of neutrino oscillations between the present time and when a Proton Driver might start sending beam. In this chapter the potential upcoming experimental results and the possible scenarios for neutrino oscillation physics at Proton Driver startup are described. Future chapters will show how a Proton Driver is needed to take the next step regardless which scenario transpires.

We can expect new oscillation results from 8 experiments that fall into 4 categories: The conventional beam experiments MINOS, ICARUS, and OPERA, the first generation superbeam experiments T2K and NOvA, the reactor experiments Double-Chooz and the generic ReactorII setup, and the short baseline MiniBooNE experiment. The main characteristics of these are summarized in Table 4.1 and described in more detail in

the following sections.

The calculations in this chapter are taken from Refs. [140] and [141]. These references should be consulted for full details.

4.1.1 Conventional beam experiments

Conventional beam experiments use an accelerator for neutrino production: A proton beam hits a target and produces a pion beam (with a contribution of kaons). The resulting pions mainly decay into muon neutrinos with some electron neutrino contamination. The far detector is usually located in the center of the beam. The primary goal of these beams is the improvement of the precision of the atmospheric oscillation parameters. In addition, an improvement of the CHOOZ limit for $\sin^2 2\theta_{13}$ is expected. For more details, see Ref. [21] for the MINOS experiment and Refs. [142, 143] for the CNGS experiments.

The neutrino beam for the MINOS experiment is produced at Fermilab. Protons with an energy of about 120 GeV hit a graphite target with an intended exposure of $3.7 \cdot 10^{20}$ protons on target (pot) per year. A two-horn focusing system directs the pions towards the Soudan mine 735 km away, where the magnetized iron far detector is located. The flavor content of the beam is, because of the decay characteristics of the pions, almost only ν_μ with a contamination of approximately 1% ν_e . The mean neutrino energy is at $\langle E_\nu \rangle \sim 3$ GeV, which is small compared to the τ -production threshold. The main purpose is to observe $\nu_\mu \rightarrow \nu_\mu$ disappearance with high statistics, and thus to determine the “atmospheric” oscillation parameters. In addition, the $\nu_\mu \rightarrow \nu_e$ appearance channel will provide some information on $\sin^2 2\theta_{13}$.

The CNGS beam is produced at CERN and directed towards the Gran Sasso Laboratory, where the ICARUS and OPERA detectors are located at a baseline of 732 km. The primary protons are accelerated in the SPS to 400 GeV, and the luminosity is planned to be $4.5 \cdot 10^{19}$ pot y^{-1} . Again the beam mainly contains ν_μ with a small contamination of ν_e at the level of 1%. The main difference to the MINOS beam is the higher neutrino energy. The mean energy is 17 GeV, well above the τ -production threshold. Therefore, the CNGS experiments will be able to study the ν_τ -appearance in the $\nu_\mu \rightarrow \nu_\tau$ channel. Two far detectors with very different technologies designed for ν_τ detection will be used for the CNGS experiment. The OPERA detector is an emulsion cloud chamber, whereas ICARUS is based on a liquid Argon TPC. In addition to the ν_τ detection, it is possible to identify electrons and muons in the OPERA and ICARUS detectors. This allows study of the $\nu_\mu \rightarrow \nu_e$ appearance channel providing information on $\sin^2 2\theta_{13}$, and the ν_μ disappearance channel, which contributes significantly to the determination of the atmospheric oscillation parameters.

4.1.2 The first-generation superbeams T2K and NOvA

Superbeams are based upon the technology of conventional beam experiments with some technical improvements. All superbeams use a near detector for a better control of the systematics and are aiming for higher target powers than the conventional beam experiments. In addition, the detectors are better optimized for the considered

Label	L	$\langle E_\nu \rangle$	P_{Source}	Detector technology	m_{Det}	t_{run}
Conventional beam experiments:						
MINOS	735 km	3 GeV	$3.7 \cdot 10^{20}$ pot/y	Magn. iron calorim.	5.4 kt	5 yr
ICARUS	732 km	17 GeV	$4.5 \cdot 10^{19}$ pot/y	Liquid Argon TPC	2.35 kt	5 yr
OPERA	732 km	17 GeV	$4.5 \cdot 10^{19}$ pot/y	Emul. cloud chamb.	1.65 kt	5 yr
Superbeams:						
T2K	295 km	0.76 GeV	$1.0 \cdot 10^{21}$ pot/y	Water Cherenkov	22.5 kt	5 yr
NOvA	812 km	2.22 GeV	$4.0 \cdot 10^{20}$ pot/y	Low-Z-calorimeter	50 kt	5 yr
Reactor experiments:						
D-Chooz	1.05 km	~ 4 MeV	2×4.25 GW	Liquid Scintillator	11.3 t	3 yr
Reactor-II	1.70 km	~ 4 MeV	8 GW	Liquid Scintillator	200 t	5 yr
Short Baseline experiments:						
MiniBooNE	0.54 km	~ 0.7 GeV	$\sim 3 \cdot 10^{20}$ pot/y	Oil Cherenkov	450 t	3 yr

Table 4.1: The different classes of experiments and the considered setups. The table shows the label of the experiment, the baseline L , the mean neutrino energy $\langle E_\nu \rangle$, the source power P_{Source} (for beams: in protons on target per year, for reactors: in gigawatts of thermal reactor power), the detector technology, the fiducial detector mass m_{Det} , and the running time t_{run} . Note that most results are, to a first approximation, a function of the product of running time, detector mass, and source power. Table modified from Ref. [140].

purpose. Since the primary goal of superbeams is the $\sin^2 2\theta_{13}$ sensitivity, the $\nu_\mu \rightarrow \nu_e$ appearance channel is expected to provide the most interesting results. In order to reduce the irreducible fraction of ν_e from meson decays and the unwanted high-energy tail in the neutrino energy spectrum, one uses the *off-axis*-technology [144] to produce a narrow-band beam, i.e., a neutrino beam with a sharply peaking energy spectrum. For this technology, the far detector is situated slightly off the beam axis.

The J-PARC to Super-Kamiokande superbeam experiment is called T2K, and is supposed to have a target power of 0.77 MW with 10^{21} pot per year [28]. It uses the Super-Kamiokande detector, a water Cherenkov detector with a fiducial mass of 22.5 kt at a baseline of $L = 295$ km and an off-axis angle of 2° . The Super-Kamiokande detector has excellent electron-muon separation and neutral current rejection capabilities. Since the mean neutrino energy is 0.76 GeV, quasi-elastic scattering is the dominant detection process.

The NuMI off-axis experiment [145], is called NOvA, and is planned to be a low-Z-calorimeter with a fiducial mass of 50 kt [146]. Because of the higher average neutrino energy of about 2.2 GeV, deep inelastic scattering is the dominant detection process. Thus, the hadronic fraction of the energy deposition is larger at these energies, which makes the low-Z-calorimeter the more efficient detector technology. For the baseline and off-axis angle, many configurations are under discussion. As it has been demonstrated in Refs. [25–27], a NOvA baseline significantly longer than 712 km increases the overall physics potential because of the larger contribution of matter effects. In this work, a baseline of 812 km and an off-axis angle of 0.72° are used. These corresponds to a location close to the proposed Ash River site, the longest possible baseline within the United States. The beam is supposed to have a target power of about 0.43 MW

with $4.0 \cdot 10^{20}$ pot per year.

4.1.3 The reactor experiments Double-Chooz and Reactor-II

The key idea of the new proposed reactor experiments is the use of a near detector at a distance of few hundred meters away from the reactor core. If near and far detectors are built as identically as possible, systematic uncertainties related to the neutrino flux will cancel. In addition, detectors considerably larger than the CHOOZ detector are anticipated, which have been demonstrated to be feasible by KamLAND [10]. Except for these improvements, such a reactor experiment would be very similar to previous experiments, such as CHOOZ [147] or Palo Verde [148]. The basic principle is the detection of antineutrinos by the inverse β -decay process, which are produced by β -decay in a nuclear fission reactor.

For the Double-Chooz experiment, we assume a total number of 60 000 un-oscillated events in the far detector [149], which corresponds (for 100% detection efficiency) to the integrated luminosity of $288 \text{ t} \cdot \text{GW} \cdot \text{yr}$, compared to the original CHOOZ experiment with $12.25 \text{ t} \cdot \text{GW} \cdot \text{yr}$ leading to about 2 500 un-oscillated events [6]. The integrated luminosity is given as the product of thermal reactor power, running time, and detector mass. Note that, at least for a background-free measurement, one can scale the individual factors such that their product remains constant. The possibility to re-use the cavity of the original CHOOZ experiment is a striking feature of the Double-Chooz proposal, although it confines the far detector to a baseline of 1.05 km, which is slightly too short for the current best-fit value $\Delta m_{31}^2 \simeq 2 \cdot 10^{-3} \text{ eV}^2$.

If a positive signal for $\sin^2 2\theta_{13}$ is found soon, *i.e.*, $\sin^2 2\theta_{13}$ turns out to be large, it will be the primary objective to push the knowledge on $\sin^2 2\theta_{13}$ and δ_{CP} with the next generations of experiments. From the initial measurements of superbeams, $\sin^2 2\theta_{13}$ and δ_{CP} will be highly correlated. In order to disentangle these parameters, some complementary information is needed. For this purpose, one can either use extensive antineutrino running at a beam experiment, or use an additional large reactor experiment to measure $\sin^2 2\theta_{13}$ precisely [23, 150]. The large, schematic, reactor experiment Reactor-II from Ref. [23] at the optimal baseline of $L = 1.7 \text{ km}$ demonstrates the combined potential of all such experiments. It has 636 200 un-oscillated events, which corresponds to an integrated luminosity of $8 000 \text{ t} \cdot \text{GW} \cdot \text{yr}$. Such a reactor experiment could, for example, be built at the Diablo Canyon or Braidwood power plants [151, 152].

4.1.4 The Short Baseline Experiment MiniBooNE

In order to resolve the LSND anomaly described in Chapter 2 the MiniBooNE experiment [12] was proposed in 1997, approved, and started taking data in 2002. It uses the 8 GeV protons from the Fermilab Booster, a Beryllium target, and a single focussing horn to produce a conventional muon neutrino beam of average energy $\sim 0.7 \text{ GeV}$. The MiniBooNE detector is located $\sim 540 \text{ m}$ from the beam target. It is a steel tank, 610 cm in radius, holding mineral oil and viewed by ~ 1500 8 inch Hamamatsu PMTs. By looking for ν_e appearance they will confirm or refute neutrino oscillations as the

source of the LSND anomaly. The experiment is expecting to publish results towards the end of 2005.

4.2 The $\sin^2 2\theta_{13}$ bound from different experiments at Proton Driver Startup

Let us now assume that the conventional beam experiments MINOS, ICARUS, and OPERA have been running five years each, and that the Double-Chooz experiment has accumulated three years of data. In addition, we assume that the superbeam experiments T2K and NOvA have reached the integrated luminosities as given in Table 4.1. (For earlier, more extensive discussions of the potential of superbeam experiments, we refer to Ref. [26].)

In Figure 4.1, we show the $\sin^2 2\theta_{13}$ sensitivity for the considered experiments. The final sensitivity limit is obtained after successively switching on systematics, correlations, and degeneracies as the rightmost edge of the bars.¹ Figure 4.1 demonstrates that the beam experiments are dominated by correlations and degeneracies, whereas the reactor experiments are dominated by systematics. It can be clearly seen that the $(\sin^2 2\theta_{13})_{\text{eff}}$ sensitivity limit (between systematics and correlation bar), or the precision of a combination of parameters leading to a positive signal, is much better for the superbeams than for the reactor experiments. Therefore, though the reactor experiments have a good potential to extract $\sin^2 2\theta_{13}$ directly, the superbeams results will in addition contain a lot of indirect information about δ_{CP} and the mass hierarchy, which might be resolved by the combination with complementary information.

A very important parameter for future $\sin^2 2\theta_{13}$ measurements is the true value of Δm_{31}^2 , which currently is constrained to the interval $0.0011 \text{ eV}^2 \lesssim |\Delta m_{31}^2| \lesssim 0.0032 \text{ eV}^2$ at 3σ [155]. From Figure 4.2, one can easily see that the true value of Δm_{31}^2 strongly affects the $\sin^2 2\theta_{13}$ sensitivity limit. This figure demonstrates that for all experiments the $\sin^2 2\theta_{13}$ sensitivity becomes worse for small values of $|\Delta m_{31}^2|$ within the currently allowed range. It should be noted, however, that the current $\sin^2 2\theta_{13}$ bound (dark-gray shaded region) is also worse for small values of $|\Delta m_{31}^2|$ than for large values.

4.3 The measurements of Δm_{31}^2 and θ_{23}

In this section, we investigate the ability of the conventional beam experiments and superbeams to measure the leading atmospheric parameters Δm_{31}^2 and θ_{23} . We do not include the reactor experiments in this discussion, since they are rather insensitive to Δm_{31}^2 , and cannot access θ_{23} at all. The measurement of these parameters is dominated by the $\nu_\mu \rightarrow \nu_\mu$ disappearance channel in the beam experiments.

¹Note that earlier similar figures, such as in Refs. [23, 26], are computed with different parameter values, which leads to changes of the final sensitivity limits. The largest of these changes come from the adjusted atmospheric best-fit values and NOvA parameters.

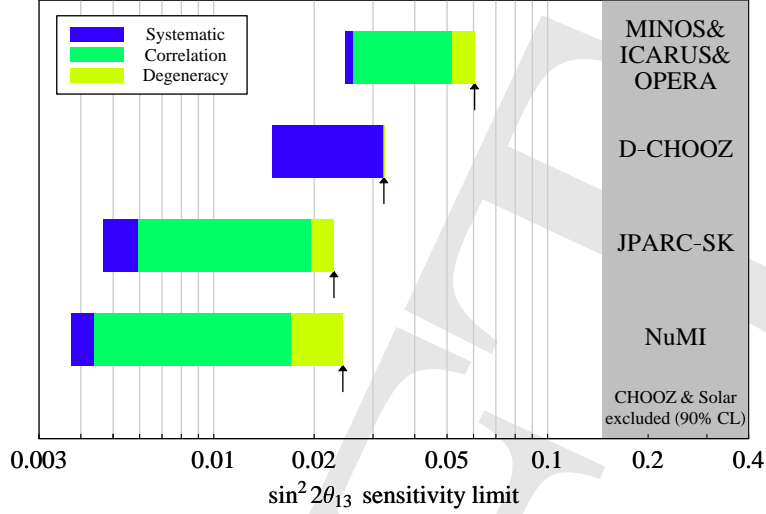


Figure 4.1: The $\sin^2 2\theta_{13}$ sensitivity limit at the 90% CL for MINOS, ICARUS, and OPERA combined, Double-Chooz, T2K, and NOvA. The left edges of the bars are obtained for the statistics limits only, whereas the right edges are obtained after successively switching on systematics, correlations, and degeneracies, i.e., they correspond to the final $\sin^2 2\theta_{13}$ sensitivity limits. The gray-shaded region corresponds to the current $\sin^2 2\theta_{13}$ bound at 90% CL. For the true values of the oscillation parameters, we use $|\Delta m_{31}^2| = 2.0 \cdot 10^{-3} \text{ eV}^2$, $\sin^2 2\theta_{23} = 1$, $\Delta m_{21}^2 = 7.0 \cdot 10^{-5} \text{ eV}^2$, $\sin^2 2\theta_{12} = 0.8$ [8, 153–155], and a normal mass hierarchy. Figure taken from Ref. [140].

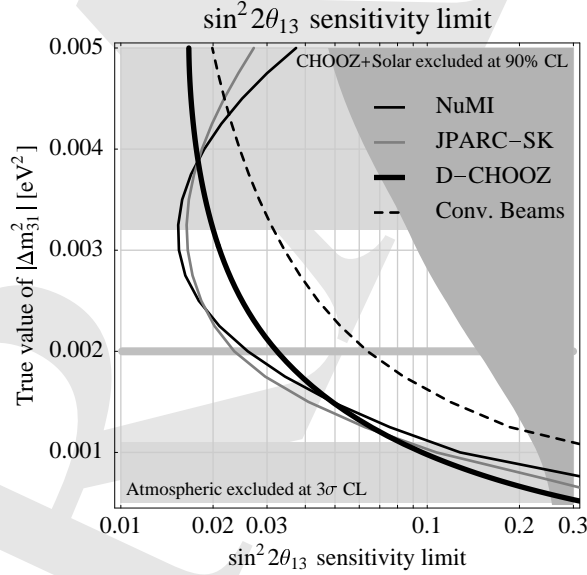


Figure 4.2: The $\sin^2 2\theta_{13}$ sensitivity limits at 90% CL from the experiments NOvA, T2K, Double-Chooz, and the combined conventional beams (MINOS, ICARUS, OPERA) as function of the true value of $|\Delta m_{31}^2|$. The dark-gray shaded region refers to the current $\sin^2 2\theta_{13}$ bound from CHOOZ and the solar experiments (90% CL) [154]. Same parameter values as in Figure 4.1. Figure taken from Ref. [140].

In Figure 4.3, we compare the predicted allowed regions for Δm_{31}^2 and $\sin^2 \theta_{23}$ from the combined conventional beams (MINOS, ICARUS, OPERA), T2K, NOvA, and all beam experiments combined to the current allowed region from Super-Kamiokande

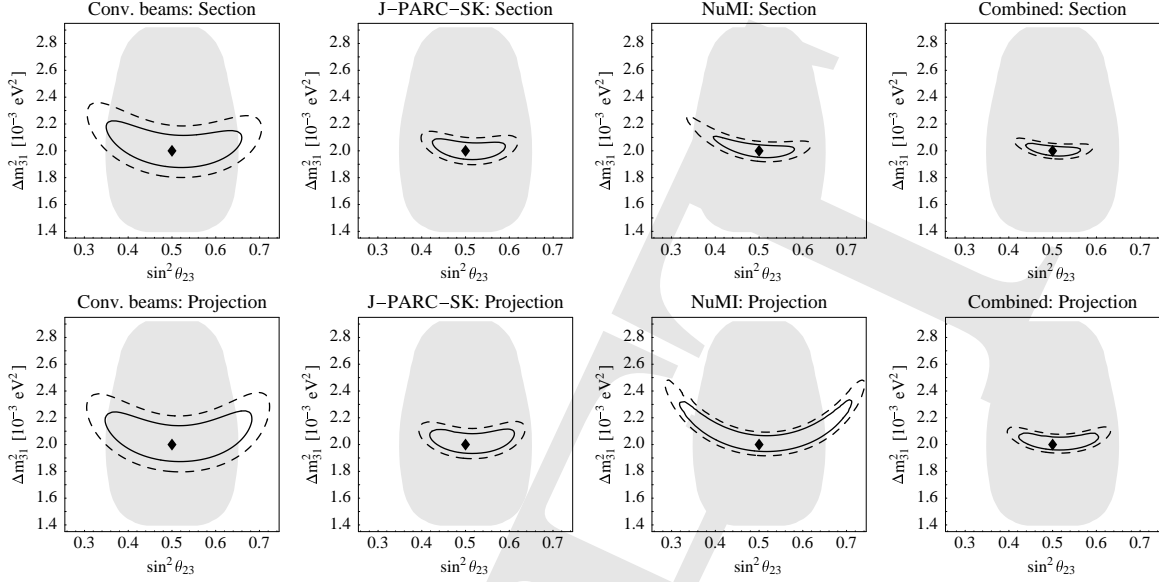


Figure 4.3: The 90% CL (solid curves) and 3σ (dashed curves) allowed regions (2 d.o.f.) in the $\sin^2 \theta_{23}$ - Δm_{31}^2 -plane for the combined conventional beams (MINOS, ICARUS, OPERA), T2K, NOvA, and all beam experiments combined. The upper row shows a section of the fit manifold (with the un-displayed oscillation parameters fixed at their true values), and the lower row shows the projection onto the $\sin^2 \theta_{23}$ - Δm_{31}^2 -plane as the final result. The shaded regions correspond to the 90% CL allowed region from current atmospheric neutrino data [155]. For the true values of the oscillation parameters, we choose the same parameter values as in Figure 4.1, $\sin^2 2\theta_{13} = 0.1$ close to the CHOOZ bound [6] and $\delta_{CP} = 0$. Figure taken from Ref. [140].

atmospheric neutrino data. We show the fit-manifold section in the $\sin^2 \theta_{23}$ - Δm_{31}^2 -plane (upper row), as well as the projection onto this plane (lower row). For a section, all oscillation parameters which are not shown are fixed at their true values, whereas for a projection the χ^2 -function is minimized over these parameters. Therefore, the projection corresponds to the final result, since it includes the fact that the other fit parameters are not exactly known. In general, the χ^2 -value becomes smaller by the minimization over the not shown fit parameters, which means that the allowed regions become larger. In Figure 4.3 the $\text{sgn}(\Delta m_{31}^2)$ -degeneracy is not included, since it usually does not produce large effects in the disappearance channels. In addition, we use the true values $\sin^2 2\theta_{13} = 0.1$ and $\delta_{CP} = 0^\circ$. Although the fit-manifold sections shown in the upper row of Figure 4.3 depend to some extent on this choice, the effect for the final results of the disappearance channels is very small, *i.e.*, the lower row of Figure 4.3 is hardly changed for $\sin^2 2\theta_{13} = 0$.

The first thing to learn from Figure 4.3 is that the precision on Δm_{31}^2 will drastically improve with the next generation of experiments, whereas our knowledge on θ_{23} will be increased rather modestly. The combination of all the beam experiments will improve the current precision from the Super-Kamiokande atmospheric neutrino data [155] on $\sin^2 \theta_{23}$ roughly by a factor of two, while the precision on Δm_{31}^2 will be improved by an order of magnitude. Neither the three conventional beams combined nor NOvA will obtain a precision on θ_{23} better than current Super-Kamiokande data, only T2K might improve the precision slightly. We note however, that the θ_{23} accu-

Experiment/Combination	$ \Delta m_{31}^2 $	θ_{23}	$\sin^2 \theta_{23}$
MINOS + OPERA + ICARUS	$2_{-0.18}^{+0.34} \cdot 10^{-3} \text{ eV}^2$	$(\pi/4)_{-0.19}^{+0.22}$	$0.5_{-0.18}^{+0.21}$
T2K	$2_{-0.09}^{+0.15} \cdot 10^{-3} \text{ eV}^2$	$(\pi/4)_{-0.10}^{+0.13}$	$0.5_{-0.10}^{+0.13}$
NOvA	$2_{-0.07}^{+0.43} \cdot 10^{-3} \text{ eV}^2$	$(\pi/4)_{-0.21}^{+0.24}$	$0.5_{-0.20}^{+0.23}$
All beam experiments combined	$2_{-0.06}^{+0.12} \cdot 10^{-3} \text{ eV}^2$	$(\pi/4)_{-0.10}^{+0.13}$	$0.5_{-0.09}^{+0.12}$

Table 4.2: The expected allowed ranges (3σ , 1 d.o.f.) for the atmospheric oscillation parameters. For the true values of the oscillation parameters, we choose the same values as in Figure 4.3. The impact of an inverted mass hierarchy, and different values for $\sin^2 2\theta_{13}$ or δ_{CP} on these final results is rather small. Table taken from Ref. [140].

racy of the long-baseline experiments strongly depends on the true value of Δm_{31}^2 , and it will be improved if Δm_{31}^2 turns out to be larger than the current best-fit point.

In Table 4.2 is shown the prediction for the 3σ -allowed ranges of the atmospheric oscillation parameters from the conventional beam experiments and first generation superbeam experiments for one degree of freedom.

4.4 The MiniBooNE Measurement

This section will describe the MiniBooNE sensitivity to LSND oscillations and the possible outcomes of the measurement.

4.5 The Scenarios

This section will explicitly list the 6 scenarios described in more details in the previous sections and set up the rest of the document.

Chapter 5

Scenario 1: $\sin^2 2\theta_{13}$ Greater Than ~ 0.04

For a very large value of $\sin^2 2\theta_{13}$, the MINOS experiment might in fact be the first place to see a hint of ν_e appearance, as would be the CNGS program. In parallel, one may expect that a reactor experiment, such as D-CHOOZ, directly measures $\sin^2 2\theta_{13}$. In this case, the next logical step would be to use the proton driver at the existing beamline (and possibly a larger detector and longer running times) to push the then existing NO ν A setup to its limits. There are three major applications: First, may want to have a high confidence establishment of $\sin^2 2\theta_{13} > 0$ and a precision measurement of $\sin^2 2\theta_{13}$. Second, the proton driver would clearly increase the mass hierarchy sensitivity to a substantial fraction of all possible values of δ_{CP} . And third, CP violation measurements would require antineutrino running to resolve the correlation between $\sin^2 2\theta_{13}$ and δ_{CP} . Because of the lower antineutrino cross section and the lower π^- production rate, about three times as many protons are required in this mode to achieve a statistical weight comparative to the neutrino running mode and to become better sensitive to CP effects.

5.1 The NO ν A experiment

As it has been discussed before in Chapter 2, the $\nu_\mu \rightarrow \nu_e$ neutrino oscillation channel carries the very interesting information on the unknown neutrino oscillation parameters. The NO ν A experiment is designed to search for this $\nu_\mu \rightarrow \nu_e$ signal, where more details on the experiment can be found in Appendix A.1. The discovery limit for the $\nu_\mu \rightarrow \nu_e$ signal can be found in Figure 5.1 as function of the three unknown parameters $\sin^2 2\theta_{13}$, δ_{CP} , and the neutrino mass hierarchy (true values). The vertical axis

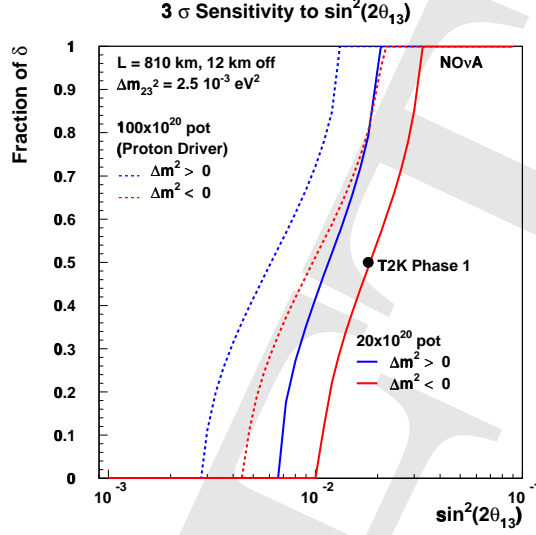


Figure 5.1: Three standard deviation discovery limits for the observation of $\nu_\mu \rightarrow \nu_e$ oscillations for the NO ν A detector (assuming $\Delta m_{32}^2 = 0.0025 \text{ eV}^2$). See the text for more details.

represents the fraction of possible δ_{CP} values for which a 3σ discovery could be made. In other words, zero represents the limit for the most favorable value of δ_{CP} for a given $\sin^2 2\theta_{13}$ (typically around $\delta_{\text{CP}} \sim 3\pi/2$), one represents the least favorable value of δ (typically around $\delta_{\text{CP}} \sim \pi/2$). For the purpose of risk minimization, one wants to have a good sensitivity for a fraction of δ_{CP} as large as possible. For the protons on target, the value of 20×10^{20} pot represents an estimate of what Fermilab might be able to deliver in a five-year run with incremental Booster and Main Injector improvements, while 100×10^{20} pot represents the expectation with the Booster replaced by the Proton Driver. A 5% systematic error on the background determination has been included in these and the other calculations presented here, but the statistical errors on the backgrounds always dominate. The three standard-deviation sensitivity of the T2K (phase 1) proposal [28] is also shown in this figure. This plot shows clearly that even without a proton driver, if $\sin^2 2\theta_{13}$ is greater than 0.04 then NO ν A will have a 3σ sensitivity, regardless of the neutrino mass hierarchy, and regardless of what the CP-violating phase δ_{CP} may be. Therefore, it is obvious that the proton driver will in this case help to establish ν_e appearance at a very high confidence level and to provide a precision measurement of $\sin^2 2\theta_{13}$.

As soon as $\sin^2 2\theta_{13}$ is established, the determination of the neutrino mass hierarchy using the $\nu_\mu \rightarrow \nu_e$ signal will be the next step for NO ν A, since NO ν A will be worldwide the only experiment with a long enough baseline to observe large matter effects. Figure 5.2 shows the 95% confidence level resolution of the mass hierarchy as a function of $\sin^2 2\theta_{13}$. The assumed scenario is that within three years of neutrino running a 3σ signal is observed for ν_e appearance, after which the running is switched to antineutrinos for studying the mass hierarchy and CP effects. Thus, Figure 5.2 assumes three years of each neutrino and antineutrino running, both with and without

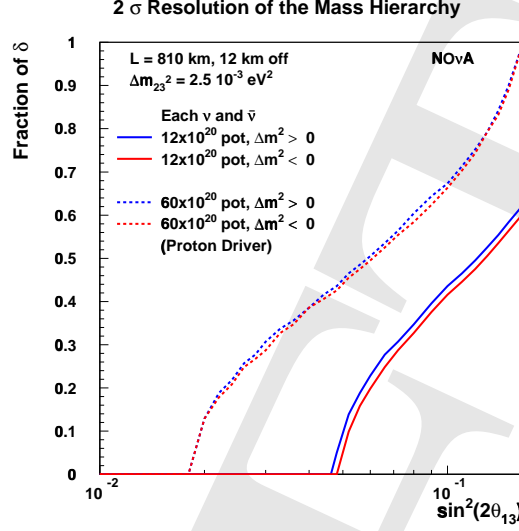


Figure 5.2: The 95% confidence level resolution of the mass hierarchy versus $\sin^2 2\theta_{13}$ for three years of running each neutrinos and antineutrinos, with and without the Proton Driver.

the Proton Driver. The shapes of the curves come from the fact that there is a limited range of δ_{CP} values for which two measurements can resolve the mass hierarchy, and this range decreases with decreasing values of $\sin^2 2\theta_{13}$.

As far as the statistics is concerned, for both the resolution of the mass ordering and for the measurement of CP violation, it is worth noting that the Proton Driver changes a 1σ effect into a 3σ effect. As an estimate, a factor of nine in statistics is required to do this for one degree of freedom. However, for a measurement with two degrees of freedom, such as that for the allowed region for $\sin^2 2\theta_{13}$ and δ_{CP} , only a factor of about five is required since $\Delta\chi^2 = 2.23$ corresponds to a 1σ effect, while $\Delta\chi^2 = 11.83$ corresponds to a 3σ effect. This is exactly the factor of five provided by the proton driver.

Except from statistics, the correlation between $\sin^2 2\theta_{13}$ and δ_{CP} affects the mass hierarchy and CP measurements, which can be resolved by either extensive antineutrino running or a large reactor experiment (see, *e.g.*, Ref. [23]). In fact, the optimum splitting of the running time between neutrinos and antineutrinos would be about $2/7$ neutrino running and $5/7$ antineutrino (for $NO\nu A$) to obtain equal statistical weights of the neutrino and antineutrino channels (see, *e.g.*, Ref. [26]). However, in this case one would have a too short neutrino running time ($2/7 * 6 \text{ yr} \sim 1.7 \text{ yr}$) to establish $\sin^2 2\theta_{13}$ first. This implies that an extension of the antineutrino running over the above used six years would help to improve the measurements, where the proton driver is needed to compensate for the lower antineutrino cross sections and π^- production rate. For example, for three years of neutrino running without proton driver, more than ten years of antineutrino running would provide similar statistics. Therefore, it is obvious that one cannot only use longer running times (or larger detectors) to compensate for the lower antineutrino event rates, but one needs a proton

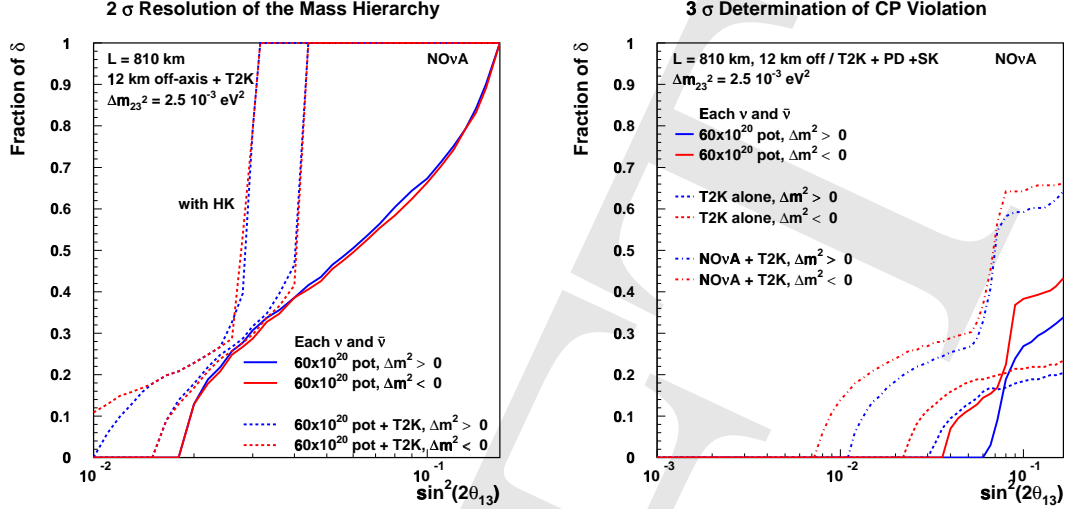


Figure 5.3: The sensitivity to the mass hierarchy (2σ , left panel) and to CP violation (3σ , right panel) for NO ν A and NO ν A combined with T2K. In the left panel, the curves labeled “HK” assume that the T2K detector is Hyper-Kamiokande; the other set of dashed curves assume that it is Super-Kamiokande. In all cases, it is assumed that both NO ν A and T2K run three years each on neutrinos and antineutrinos, where in the right panel also an upgraded proton source for T2K is assumed.

driver.

5.2 Synergy with T2K Measurements

If the neutrino oscillation parameters, such as the mass ordering, cannot be resolved by NO ν A alone, then combining NO ν A measurements with the measurement of another experiment will be necessary. As it has been demonstrated in Refs. [25–27], the combination with another superbeam (such as T2K) would clearly lead to risk minimization with respect to δ_{CP} and lead to a genuine synergy between the two experiments. The combination with T2K is shown in Figure 5.3 for the mass hierarchy (left panel) and CP violation (right panel) measurements.

For the mass hierarchy determination (left panel), the combination with T2K might not be necessary for a small fraction of about one fourth of all values of δ_{CP} . However, we do not know δ_{CP} before these measurements, which means that a fraction of δ_{CP} as large as possible would clearly minimize the risk to observe nothing. From Figure 5.3, one can read off that already with the Super-Kamiokande detector, the mass hierarchy can be resolved for all values of δ_{CP} in the complete range $\sin^2 2\theta_{13} \gtrsim 0.04$ discussed in this chapter, *i.e.*, the risk with respect to the unknown value of δ_{CP} will be eliminated. The reason for this can be understood as follows: We are comparing two distributions that have approximately the same structure due to the CP phase, but that differ by a factor of 2.3 in the matter effect. Thus, sufficient statistics to pass the 95% confidence level threshold happens for all values of δ_{CP} at

approximately the same point to separate the positive- and negative-sign solutions. A more detailed discussion of the underlying phenomenology as function of δ_{CP} can be found in Refs. [27, 156].

The relationship between the resolution of the mass hierarchy and the observation of CP violation varies from experiment to experiment. Very short baseline experiments, such as the beta beam experiments being planned in Europe [157] have very small matter effects and can measure the CP violation phase δ without regard to the determination of the mass hierarchy. Long baseline experiments such as NO ν A generally require a resolution of the mass hierarchy to measure the CP phase because maximal CP violation for one mass ordering can have the same or similar neutrino and antineutrino oscillation probabilities as no CP violation for the other mass ordering.

Below we will explore the capability of NO ν A to measure the CP violating phase δ and the power of combinations of NO ν A measurements with those of other experiments. One should keep in mind that CP-violating effects are proportional to the first power of θ_{13} , while CP-conserving effects are, for the most part, proportional to the square of θ_{13} , *cf.*, Eq. (2.18). This has led some to argue that the ability to measure δ is independent, to some extent, of the value of $\sin^2 2\theta_{13}$ (*cf.*, Figure 2.2). We will see that there are regions of $\sin^2 2\theta_{13}$ in which the probability of measurement is flat. We will also see that there can be peaks and dips in the probability as a function of $\sin^2 2\theta_{13}$ due to the complex relationship between CP-violating effects and matter effects.

For CP violation, we use as a measure the fraction of possible δ_{CP} values for which there is a three standard deviation demonstration of CP violation, that is, that δ is neither zero nor π for both mass orderings. Of course, this fraction can never be 100%, since there will always be some range of δ_{CP} values very close to zero or π . A rough way to convert this measure into a one standard deviation measure of δ_{CP} is that a small, but non-zero fraction corresponds to 30 degrees, a 25% fraction to 22.5 degrees, a 50% fraction to 15 degrees, and so on.

Neither NO ν A nor T2K can demonstrate CP violation, even at the two standard deviation level, with six years of running without an enhanced proton source.¹ However, both experiments gain some ability with their proposed proton drivers. This is shown in Figure 5.3 (right panel), in which both experiments are assumed to have run three years each on neutrinos and antineutrinos and the T2K detector is assumed to be Super-Kamiokande. T2K has a broader reach than NO ν A in $\sin^2 2\theta_{13}$, but saturates at a lower fraction of δ_{CP} due to its inability to resolve the mass hierarchy.

Combining measurements from both experiments gives a large gain in both the breadth and precision of the measurement. The sharp rise around $\sin^2 2\theta_{13} = 0.05$ is due to the resolution of the mass ordering, as discussed above and seen in the left panel of Figure 5.3. Thus, only the combination NO ν A plus proton driver with T2K has a considerable potential for a large fraction of δ_{CP} values in the discussed range $\sin^2 2\theta_{13} \gtrsim 0.04$.

¹Note that this does not necessarily mean that one cannot learn anything about δ_{CP} at all. For example, though one may not be able to establish CP violation, one might still be able to exclude a certain fraction of the parameter space for δ_{CP} (see, for instance, Ref. [140]).

In conclusion, for $\sin^2 2\theta_{13} \gtrsim 0.04$ the proton driver for NO ν A could provide a precise measurement of $\sin^2 2\theta_{13}$, have a very good mass hierarchy measurement potential, and help the establishment of leptonic CP violation for a wide range of δ_{CP} values.

Chapter 6

Scenario 2: $\sin^2 2\theta_{13}$ Between ~ 0.01 and ~ 0.04

For this range of $\sin^2 2\theta_{13}$, the MINOS and CNGS experiments will likely only set lower limits on $\nu_\mu \rightarrow \nu_e$ oscillations, but the NO ν A and T2K experiments would observe a small signal. In addition, there could be some hint for $\sin^2 2\theta_{13}$ from a reactor experiment. In this case, there is a strong physics case for a super-beam upgrade in some form, which requires both a proton driver and considerably more detector mass and running time. One of the top priorities would then be to obtain a highly significant $\sin^2 2\theta_{13}$ signal, which requires a substantial luminosity increase in whatever form. If one wants in addition resolve the mass hierarchy and to be sensitive to leptonic CP violation, two general strategies are possible: First, one could use a longer baseline to use the matter effects to enhance or suppress the $\sin^2 2\theta_{13}$ signal and to determine the neutrino mass hierarchy. And second, one could go to the second or third oscillation maximum to obtain more relative weight in the CP violating terms. For example, either an additional detector in the NUMI beam line or a broad band beam could observe more than one oscillation maximum, which would clearly help to disentangle the oscillation parameters. Which of these approaches is the most promising choice depends on the actual parameter values, the complementarity and competitiveness to other efforts (such as T2HK or a national underground laboratory), and needs further study. However, the proton driver will be needed for all of these scenarios.

If θ_{13} is in this range, then the NO ν A detector together with the proton driver will be able to establish $\nu_\mu \rightarrow \nu_e$ oscillations for all values of δ_{CP} in the considered range $\sin^2 2\theta_{13} \gtrsim 0.01$. This can be immediately read off Figure 5.1. In this case, the proton driver could then help a high precision measurement of $\sin^2 2\theta_{13}$. However, as we

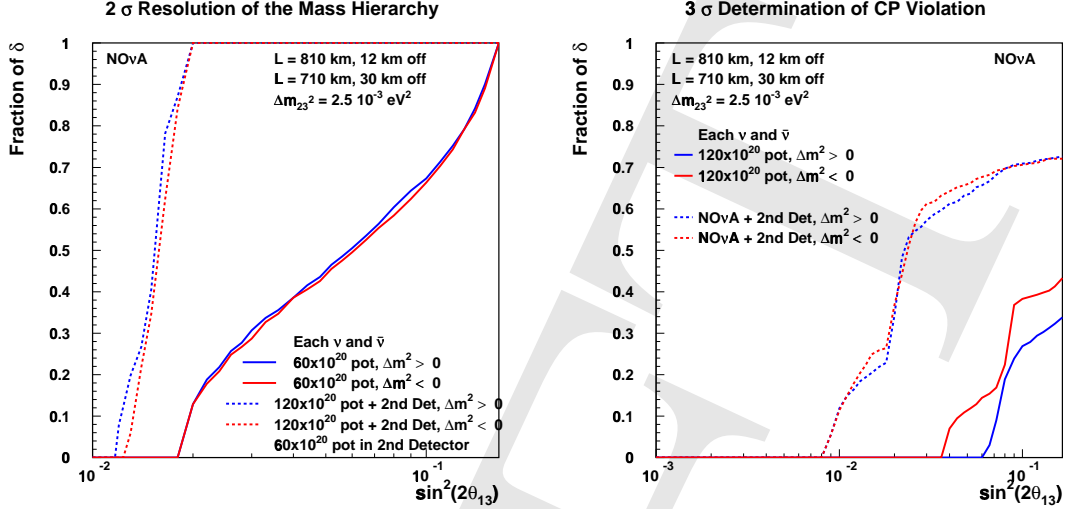


Figure 6.1: A comparison of the mass hierarchy sensitivity (2σ , left panel) and the CP violation sensitivity (3σ , right panel) between NO ν A alone (solid curves) and the combination of NO ν A and an additional NuMI detector sited to measure the second oscillation maximum (dashed curves). See the text and labels in figures for details of the scenarios.

have discussed in the last chapter, the NO ν A detector alone even together with T2K will not be sufficient to measure the neutrino mass hierarchy or leptonic CP violation down to $\sin^2 2\theta_{13} \sim 0.01$. Therefore, we will in this chapter first of all show different approaches to study these parameters with larger or additional detectors. In addition, as useful as it may be in the shorter terms, the NuMI beamline need not define the entire future of long-baseline neutrino oscillation measurements at Fermilab. A new, even longer baseline, beamline could be built. Such a beamline could permit full use of very high proton intensities, coupling of the long-baseline measurements with a very large multi-purpose detector at an underground laboratory and full measurement of the oscillated neutrino spectrum over both the first and second oscillation maxima. We will show several examples for such a new beamline and their physics potential.

6.1 Use Other or New Detectors with NO ν A

One attractive approach would be to do a measurement with an additional detector on the NuMI beamline to measure events at the second oscillation maximum. At the second maximum the matter effect is smaller by a factor of three and the CP violating effects are larger by a factor of three. There will be sufficient information available at that time that it will be known whether this technique will work and how much detector mass will be required. For the purpose of a calculation, we consider the following scenario. After two years of running with the Proton Driver, it is realized that a second off-axis detector will be needed and it is constructed in four years and then runs for an additional six years. Thus, there will be twelve years of NO ν A data

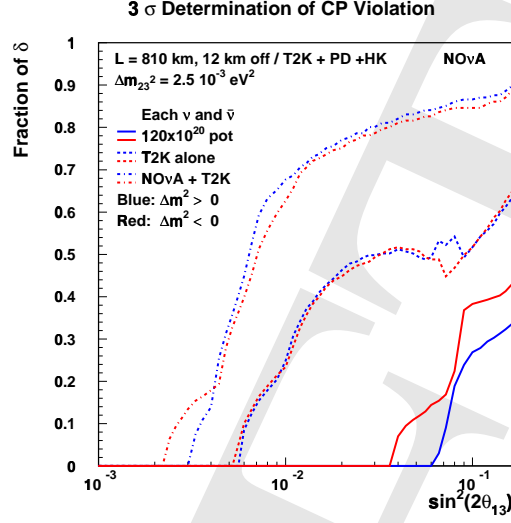


Figure 6.2: The fraction of δ values for which CP violation can be demonstrated at three standard deviations. A three year run on each of neutrinos and antineutrinos is assumed for NO ν A with the Proton Driver and for T2K with an enhanced proton source and Hyper-Kamiokande as the detector.

with the Proton Driver and six years of data with the second detector, both split equally between neutrinos and antineutrinos. It is assumed that the second detector would have the same mass as NO ν A for this illustration. The results are shown in Figure 6.1. The mass hierarchy (left panel) is resolved for all values of δ for values of $\sin^2 2\theta_{13}$ greater than about 0.01 to 0.02. In addition, CP violation (right panel) can be established for a large fraction of δ_{CP} values. Therefore, using a second detector in the NUMI beamline together with the proton driver could provide the anticipated sensitivities in the range $\sin^2 2\theta_{13} \gtrsim 0.02$.

Alternatively, a proton source and detector upgrade of T2K would help tremendously for CP violation. Figure 6.2 shows the same information as in the right panel in Figure 5.3, but for Hyper-Kamiokande as T2K detector. The twenty-fold increase in mass gives it high statistical precision. The role of NO ν A is to resolve the mass hierarchy so that the precision can be used. In fact, one can see that in that case the CP violation sensitivity covers a large fraction of δ_{CP} for the range $\sin^2 2\theta_{13} \gtrsim 0.01$.

6.2 Narrow Band Beams from Fermilab to Homestake

As part of the APS study, the physics sensitivity of a new beamline aimed from Fermilab to Homestake has been investigated. The new beamline would utilize both 120 GeV and 8 GeV protons from a proton driver. It is described in more detail in the appendix, but it can be summarized as several narrow band beams run in succession, so that the backgrounds can be kept low, yet many energies can be accessed

throughout the course of the experiment. The neutrino beam coming from the 8 GeV protons would be a broad band beam, and the MiniBooNE beamline design was assumed.

The best CP violation and mass hierarchy sensitivity is achieved if the mass hierarchy is the “normal” one and running with just neutrinos. However, if there is an inverted mass hierarchy then it is important to run with both neutrinos and anti-neutrinos to achieve the best sensitivity. Note that running with anti-neutrinos reduces the sensitivity with the normal hierarchy due to overall reduced statistics. However, we calculate the following curves based on an equal mix of neutrinos and anti-neutrinos. Figure 6.2 (top) shows the region of parameter space (to the right of the curves) in which at least a 3σ ν_e appearance signal will be observed for a nominal five year run with half neutrino and half anti-neutrino running. The blue curve is for the normal hierarchy and the red for the inverted hierarchy. A 125 kT detector with event ID efficiency of 50% with negligible NC backgrounds has been assumed. The middle panel shows the region of parameter space for which at least a 2σ resolution will be possible on the mass hierarchy. Finally, the lowest panel in Figure 6.2 shows the parameter space for which a 3σ measurement of non-zero CP violating phase can be measured. These three plots are all calculated in the same way as the similar plots for the NO ν A Experiment.

6.3 Broadband Beam to Homestake or WIPP

While the previous section focused on sending several narrow band beams to a large underground detector and seeing several oscillation peaks, still another strategy would involve sending one broad band beam over a long distance and using an improved detector technology to reduce backgrounds, while still taking advantage of the improvements due to matter effect amplification. Detailed studies have been done by a Brookhaven-based study group, but clearly these studies are not site-specific. In fact, this strategy has been simulated for a 2540km baseline, which is approximately the distance from Fermilab to WIPP, which is one possibility for an underground lab, as well as a baseline of 1290, which is the distance from Fermilab to Homestake. Clearly the shorter distance affords a higher event rate for the same detector mass, while the longer distance gives oscillation maxima and minima at higher energies where the detector response is better and the backgrounds are not as high.

Because these studies were originally done to address the capabilities of the AGS at Brookhaven, a 1-2MW proton source assuming 28GeV protons was assumed. For the superconducting linac proton driver being considered for Fermilab, 2MW could be provided at 28 GeV or at 120 GeV, since the Main Injector could be filled with protons more quickly in the lower energy case. Since the neutrinos of interest are only in the few GeV range, there is not an obvious advantage in going to higher proton energies.

The major difference between the 1290 and 2540 km baselines is that the shorter baseline has a higher correlation between the parameters, δ_{CP} and $\sin^2 2\theta_{13}$, has better resolution on $\sin^2 2\theta_{13}$, and has worse sensitivity to systematic errors on the back-

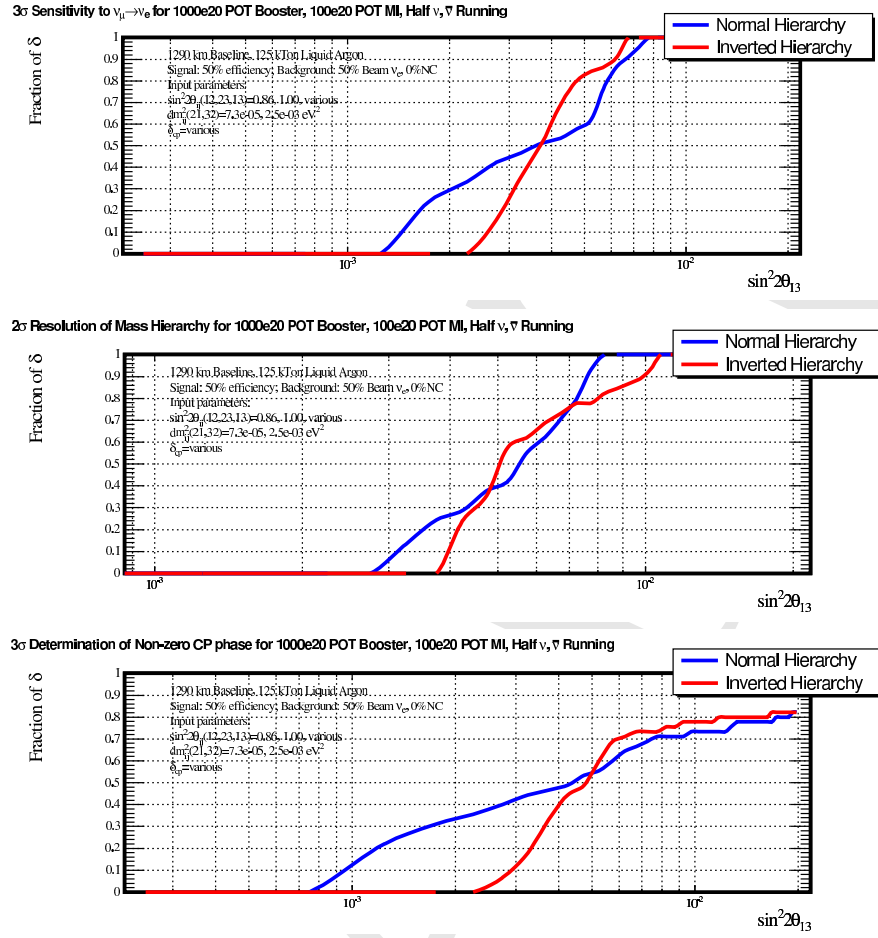


Figure 6.3: The region of parameter space (to the right of the curves) in which at least (top) a 3σ ν_e appearance signal will be observed (middle) the mass hierarchy can be resolved with greater than 2σ sensitivity, or (bottom) the CP violating phase δ can be resolved to be non-zero with greater than 3σ sensitivity, all for a nominal five year run with half neutrino and half anti-neutrino running. The blue curve is for the normal hierarchy and the red for the inverted hierarchy. A 125 kT detector with event ID efficiency of 50% with negligible NC backgrounds has been assumed.

ground and the spectrum shape. If the systematic errors exceed 10%, the shorter baseline will most likely have worse performance for measuring the CP parameter.

If there is no excess of electron events observed then this experiment, at either baseline, can set a limit on the value of $\sin^2 2\theta_{13}$ as a function of δ_{CP} . Such 95 and 99% C.L. sensitivity limits are shown in Figure 6.4. These set of plots illustrate various considerations that must be evaluated for the very long baseline project. After running initially in the neutrino mode with 1 MW of beam power, if an excess signal is found then a measurement of δ_{CP} versus $\sin^2 2\theta_{13}$ can be made as shown in Figure ??, at the same time the mass hierarchy is determined from the strength of the signal in the higher energy region. If there is no signal in the neutrino mode then either θ_{13} is too small for the regular mass hierarchy (RO) or the mass hierarchy is reversed (UO) and parameters are in the “unlucky” region ($-140^\circ < \delta_{CP} < 30^\circ$). For the shorter baseline

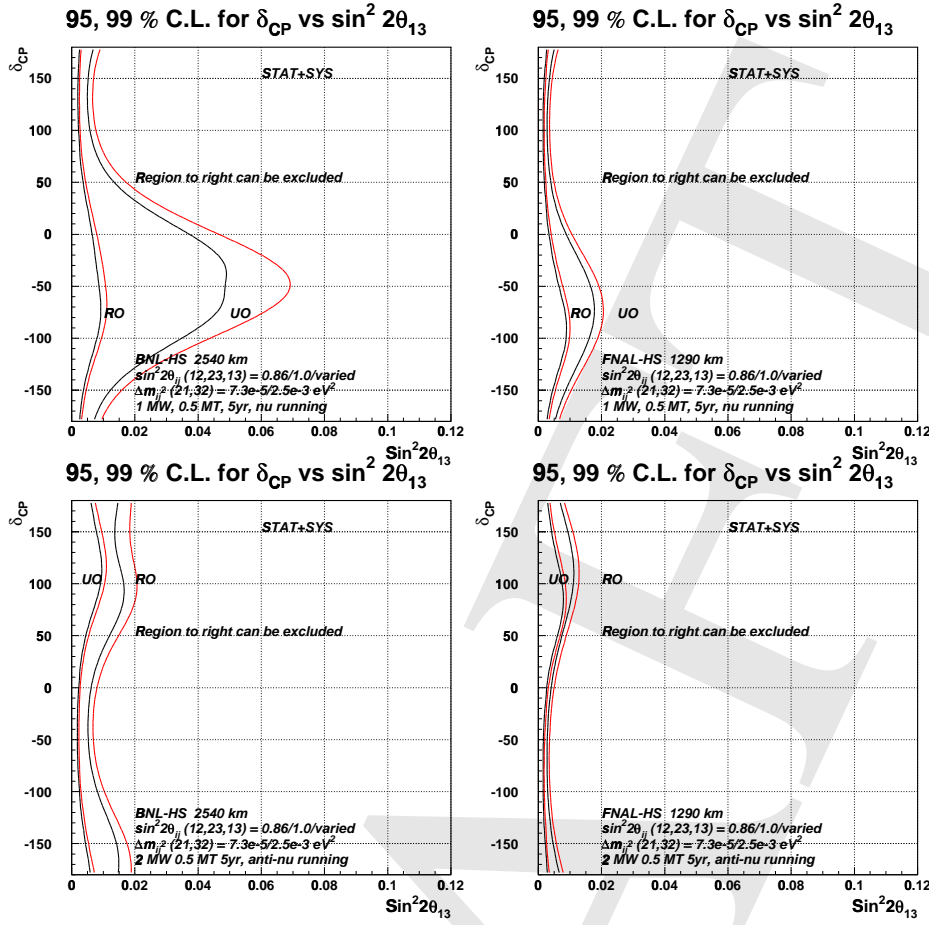


Figure 6.4: Expected limit on $\sin^2 2\theta_{13}$ as a function of δ_{CP} for BNL-HS neutrino running only (top left), FNAL-HS neutrino running only (top right), BNL-HS anti-neutrino running only (bottom left), FNAL-HS anti-neutrino running only (bottom right).

of 1290 km, the θ_{13} sensitivity for the reversed hierarchy is not reduced as much as for 2540 km because both the CP-sensitivity and the matter effect are weaker. Although this yields a better limit for $\sin^2 2\theta_{13}$ in the absence of signal, it affects the precision on δ_{CP} and the determination of the mass hierarchy.

If there is no signal in the neutrino mode, one would still run in the anti-neutrino mode to cover the “unlucky” parameter space for the appearance signal. A combination of neutrino and anti-neutrino running will yield a stringent limit approaching $\sin^2 2\theta_{13} \sim 0.003$ independent of the value of δ_{CP} . The simulation results shown here include wrong sign contamination in both the background and signal for anti-neutrinos. Interestingly, since more than 20% of the event rate in the anti-neutrino case actually arises from the neutrino contamination, the $\sin^2 2\theta_{13}$ limit in the anti-neutrino case exhibits less dependence on δ_{CP} and the mass hierarchy.

If there is a signal in the neutrino mode, then the measurement of δ_{CP} can actually be made from neutrino data alone in the 3-generation model, but it will still be important to run in the anti-neutrino mode. First of all combining this mode with neutrino mode would give better precision, but would also over-constraint the 3-generation model, and allow a search for possible new physics either in the mixing or

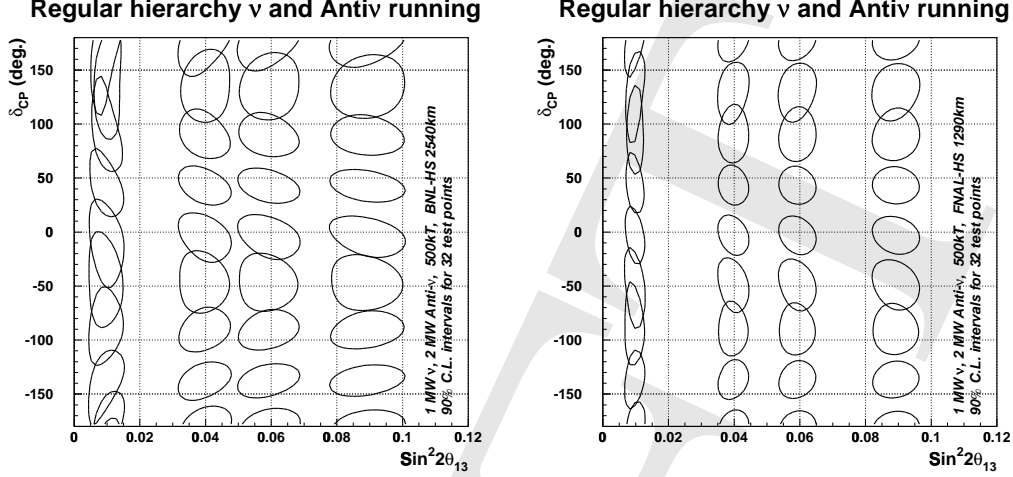


Figure 6.5: 90% confidence level error contours in $\sin^2 2\theta_{13}$ versus δ_{CP} for statistical and systematic errors for 32 test points. This simulation is for combining both neutrino and anti-neutrino data. Left is for BNL-HS and right is for FNAL-HS. We assume 10% systematic errors for this plot. Figure taken from Ref. [158].

in the interactions of neutrinos.

The sensitivity to systematic errors and the dependence on the mass hierarchy can be relieved by using data from both neutrino and anti-neutrino running. Figure 6.5 shows the 90% confidence level interval for 32 test points in the δ_{CP} and $\sin^2 2\theta_{13}$ plane after both neutrino and anti-neutrino data. A number of observations can be made: Figure 6.5 is for the regular mass hierarchy. The plot for the reversed mass hierarchy is similar. After both neutrino and anti-neutrino data the hierarchy will be resolved to more than 10 sigma (somewhat less significance for the shorter baseline) for $\sin^2 2\theta_{13}$ as small as 0.01. The resolution on δ_{CP} is seen to be approximately independent of $\sin^2 2\theta_{13}$ for $\sin^2 2\theta_{13} > 0.01$. When $\sin^2 2\theta_{13}$ is so small that the background becomes dominant, the δ_{CP} resolution becomes poor. The resolution on δ_{CP} is seen to be approximately the same for 2540 and 1290 km, except for small $\sin^2 2\theta_{13}$ where large statistics at 1290 km are seen to overcome the background. The resolution on $\sin^2 2\theta_{13}$ is, however, better for the shorter baseline because the sensitivity comes from the first node of oscillations which has much higher statistics at the shorter baseline.

6.4 Very Long Baselines

The potential of higher energy neutrino beams with very long baseline ($L > 7000$ km) has, for example, been explored in Refs. [159,160]. The $\nu_\mu \rightarrow \nu_e$ signal at these baselines can be highly amplified by matter effects, improving the signal-to-background ratio [161–163].

A very long baseline experiment can play a complementary role to shorter baseline experiments. The short-baseline experiment measures a CP-violating combination of

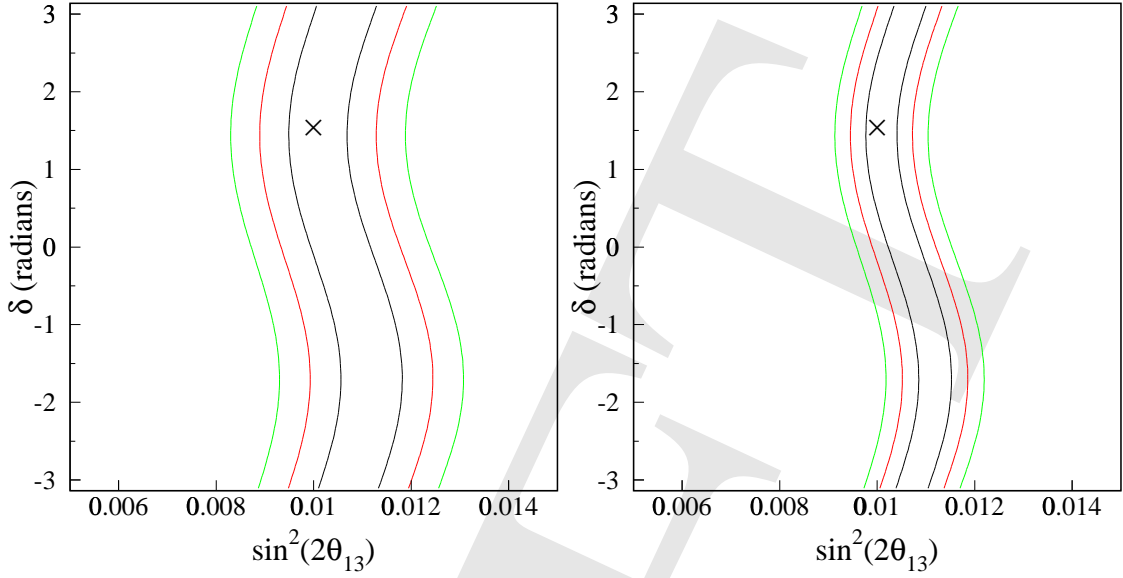


Figure 6.6: The allowed region in the $\sin^2 2\theta_{13}$ - δ_{CP} plane for FNAL-Kamioka (or China) as described in the main text. The left panel is for two years of running time with the Fermilab beam, the right panel for eight years. For the oscillation parameters, $\sin^2 2\theta_{13} = 0.01$, $\delta_{\text{CP}} = \pi/2$, $\Delta m_{31}^2 = 3.5 \cdot 10^{-3} \text{ eV}^2$, $\Delta m_{21}^2 = 5.0 \cdot 10^{-5} \text{ eV}^2$, $\sin^2 2\theta_{23} = 1.0$, and $\sin^2 2\theta_{12} = 0.8$ were chosen.

atmospheric and solar oscillations. The long-baseline experiment determines the sign of Δm_{31}^2 , constrains the matter effects, whereas it is highly independent of δ_{CP} effects. For example, CP effects vanish identically at the “magic baseline” $L \sim 7500 \text{ km}$, which allows a degeneracy-free measurement of $\sin^2 2\theta_{13}$ and the mass hierarchy [164, 165].

For a superbeam, the main principles of such a very long baseline experiment could be:

1. Combine information from very short and very long baselines in order to determine the mass hierarchy and CP-violating oscillation parameters.
2. Match the spectrum of the long-baseline neutrino beam to the energy at which matter effects produce the maximum amplification of the signal.
3. Design the long-baseline neutrino beam to have an energy spectrum with a rapid cut-off above the signal region. Since most backgrounds feed-down from the neutrino energy to a lower visible energy, this reduces the background in the signal region.

The potential for an optimized long-baseline experiment to complement a short-baseline experiment has been analyzed in Ref. [166], where a Hyper-Kamiokande detector (with 40 times more fiducial mass than Super-Kamiokande) is used as a target for two neutrino beams: One from JHF, with a baseline of 295 km, and one from Fermilab, with a baseline of 9300 km. However, the concept of this proposal does not depend on the details of this choice, and could be adapted for other locations, such as a large neutrino detector near Beijing [167]. Recent discussions have pointed

out the possibility that a detector at the Beijing site could be a liquid Argon detector with a mass of one or two hundred kilotons. Combined with a broadband beam, we expect results similar to those in Ref. [166]. In Figure 6.6 we show the potential of such a baseline in the $\sin^2 2\theta_{13}$ - δ_{CP} -plane. Obviously, the precision of $\sin^2 2\theta_{13}$ is not strongly affected by the correlation with δ_{CP} , which means that the combination with a short baseline could provide a very good determination of both parameters. For more details, see Ref. [166].

DRAFT

Chapter 7

Scenario 3: $\sin^2 2\theta_{13}$ Less Than ~ 0.01

If $\sin^2 2\theta_{13}$ is less than about 0.01, most likely none of the currently existing or proposed experiments will find a $\sin^2 2\theta_{13}$ signal. In this case, there is a strong motivation to go directly to a high precision instrument, such as a neutrino factory or a higher gamma β -beam. With such an experiment, measurements of $\sin^2 2\theta_{13}$, the mass hierarchy, and δ_{CP} should, in principle, be possible at least down to $\sin^2 2\theta_{13} \sim 10^{-4}$. Any of these experiments could be done with a low-GeV proton driver, but in addition require some other pieces of sophisticated technology.

7.1 Neutrino Factory

New accelerator technologies offer the possibility of building, not too many years in the future, an accelerator complex to produce and capture more than 10^{20} muons per year. It has been proposed to build a Neutrino Factory [168, 169] by accelerating the muons from this intense source to energies of several GeV, injecting the muons into a storage ring having long straight sections, and exploiting the intense neutrino beams that are produced by muons decaying in the straight sections. The decays: $\mu^- \rightarrow e^- \nu_\mu \bar{\nu}_e$ and $\mu^+ \rightarrow e^+ \bar{\nu}_\mu \nu_e$ offer exciting possibilities to pursue the study of neutrino oscillations and neutrino interactions with exquisite precision.

If $\sin^2 2\theta_{13} < O(0.01)$ much of the basic neutrino oscillation physics program will be beyond the reach of conventional neutrino beams. The exquisite precision offered by a Neutrino Factory will be required to make progress. However, to create a sufficiently intense muon source, a Neutrino Factory requires an intense multi-GeV proton source capable of producing a primary proton beam with a beam power of 1 MW or more on target. This is just the proton source required in the medium term for Neutrino Superbeams. A 2 MW Proton driver at Fermilab could provide a natural

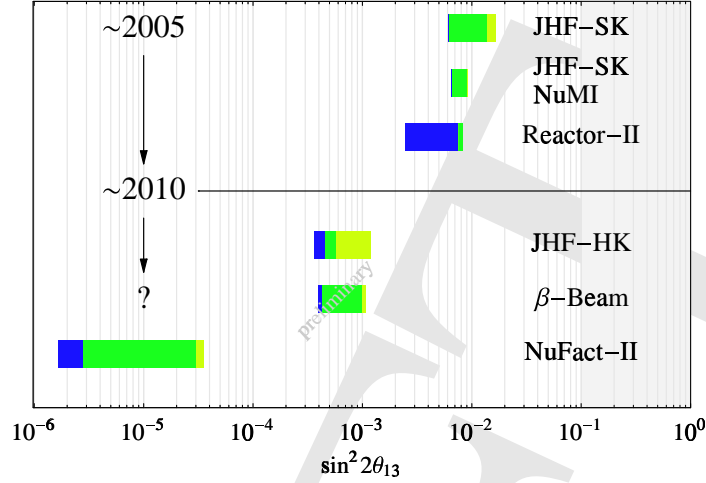


Figure 7.1: Sensitivity to a non-zero $\sin^2 2\theta_{13}$. The shaded regions within the bars show the degradation of the sensitivities due to irreducible experimental systematics, the effects of correlations, and the effects of false solutions in the three-flavor mixing parameter space. The rightmost limit of the bars therefore gives the expected sensitivities for each experiment. Figure from the authors of Refs. [140, 170].

evolution from the presently approved neutrino program, to a Neutrino Superbeam program based on a new Proton Driver, and finally to a Neutrino Factory program.

In the following subsections we begin by describing the Neutrino Factory and the possible evolution from Superbeams to Neutrino Factory, and then discuss the physics reach attainable with a Neutrino Factory.

A new Fermilab Proton Driver would provide the first system required for a Neutrino Factory. The Target, Capture, and Decay Channel could be constructed to provide an intense low energy muon source for low energy muon experiments (see the Muon Working Group Report). This could be done either as part of the initial Proton Driver facility, or as a second phase. At this point Fermilab would have a strong World class neutrino physics program, a strong World class muon physics program, and the ideal test-bed for further development and optimization of Neutrino Factory technology. The remaining subsystems (bunching, phase rotation, cooling, acceleration, and storage ring) might then be constructed in one further step, to produce a Neutrino Factory sometime within the next two decades. Alternatively, if a Linear Collider is constructed near Fermilab, the remaining Neutrino Factory systems could be built in stages to create an increasingly sophisticated muon source, with the Neutrino Factory being built in the longer-term future, after the Linear Collider. In either scenario, each stage would be motivated by its own stand-alone physics program.

7.1.1 Neutrino Factory Physics Reach

Neutrino factories are attractive because, when compared with conventional neutrino beams, they yield higher signal rates with lower background fractions and lower systematic uncertainties. These characteristics enable neutrino factory experiments to

be sensitive to values of θ_{13} that are beyond the reach of any other approach. Detailed studies [170] (see Fig. 1) have shown that a non-zero value of $\sin^2 2\theta_{13}$ could be measured for values as small as $O(10^{-4})$. In addition, both the neutrino mass hierarchy and CP violation in the lepton sector could be measured over this entire range. Even if $\theta_{13} = 0$ the probability for $\nu_e \rightarrow \nu_\mu$ oscillations in a long-baseline experiment is finite, and a Neutrino Factory would still make the first observation of $\nu_e \rightarrow \nu_\mu$ transitions in an appearance experiment, and put a sufficiently stringent limit on the magnitude of θ_{13} to suggest perhaps the presence of a new conservation law.

In addition to exquisite sensitivity, it should be noted that Neutrino Factories provide a new sort of neutrino beam containing both electron-type neutrinos and muon-type neutrinos. The experimental data samples can be divided into sub-samples tagged by the presence of (i) a “right-sign” muon, (ii) a “wrong-sign” muon, (iii) an electron or positron (assuming the charge cannot be measured), (iv) a positive tau-lepton, (v) a negative tau-lepton, or (vi) the absence of any lepton. The measurements can be made with positive muons stored in the Neutrino Factory, and with negative muons stored. Thus, there are 12 measured differential spectra that can be simultaneously fit to obtain the oscillation parameters. This provides neutrino factory experiments with a wealth of measurements that, in addition to offering exquisite precision, also offer the flexibility to exploit surprises that may turn up along the way.

7.2 BetaBeam

7.2.1 Background

The concept of Beta Beam facility was first proposed by P. Zucchelli in 2002 [171], and has since been studied by a group at CERN. More recently, a wider collaboration was formed with funding from the European Union.

The idea is to accelerate beta-unstable nuclides to high energy and storing them in a decay ring, to produce a very pure beam of electron neutrinos (or anti-neutrinos). As the kinematics of the beta decay is well understood, the energy distribution of the neutrinos can be predicted to a very high accuracy. Furthermore, as the energy of the beta decay is low compared with that for muon decay, the resulting neutrino beam has a small divergence. Two ion are considered, ${}^6\text{He}$ for producing antineutrinos and ${}^{18}\text{Ne}$ for neutrinos, both have lifetimes on the order of 1s.

A proton driver is required to produce the radioactive ions. The CERN study assumes using a fraction of the proposed Super Proton Linac (SPL) capacity, providing about 400kW of 2.2GeV protons. The target system is patterned after that of the proposed EURISOL facility [172], and ionization would be done with a very high frequency Electron Cyclotron Resonance (ECR) source under development in Grenoble. The radioactive beam would then be accelerated in a 20-100 MeV linac, followed by a rapid cycling synchrotron (RCS). At this point, the existing CERN PS and SPS machines would take over and accelerate the beam to the desired gamma of 150, following which the beam would be stored in a decay ring with 2500m straight sections,

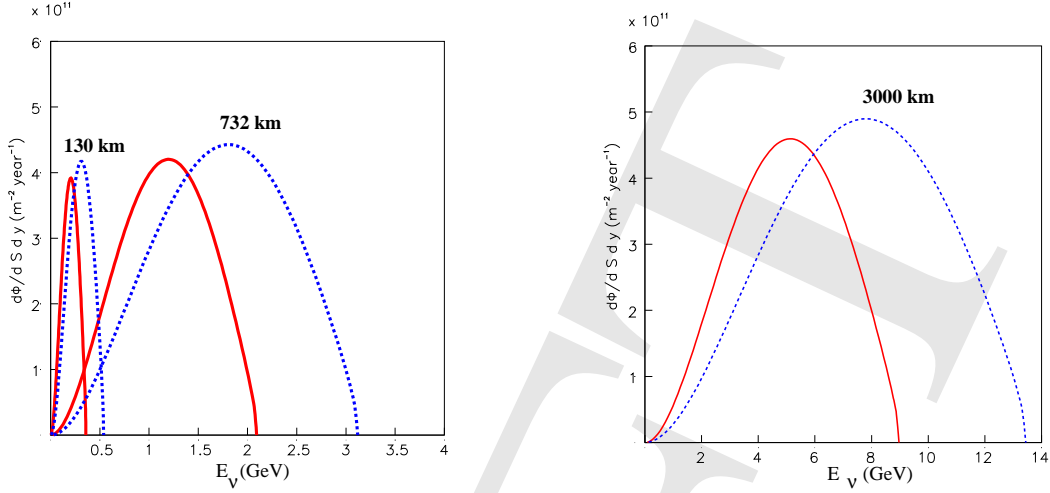


Figure 7.2: (Color) Comparison of Beta Beam neutrino fluxes for the three setups described in the text, shown as a function of the neutrino energy for $\bar{\nu}_e$ (solid) and ν_e (dashed). Figures from Ref. [173].

one of which would be pointed at an experiment in the Frejus tunnel.

7.2.2 Physics with a beta beam

The Beta Beam concept is quite new, and the performance of Beta Beam experiments is less well established than the e.g. the case of a Neutrino Factory. Recent calculations of the $\sin^2 2\theta_{13}$ sensitivity for low energy Beta Beam scenarios (by the authors of [170]) have included the effects of systematic uncertainties, correlations, and false solutions in parameter space. Although the expected signal rates are relatively modest compared to a Neutrino Factory, low energy Beta Beams offer an improvement in the $\sin^2 2\theta_{13}$ sensitivity beyond that achievable with a high-performance Superbeam. This realization has led to the consideration of higher energy Beta Beams [173].

γ	L (km)	$\bar{\nu}_e$ CC	ν_e CC	$\langle E_\nu \rangle$ (GeV)
60/100	130	1.9	25.7	0.2/0.3
350/580	730	48.6	194.2	1.17/1.87
1500/2500	3000	244.5	800.2	5.01/7.55

Table 7.1: Number of charged current events without oscillations per kton-year for the three reference setups described in the text. Also is shown the average neutrino energy. Table from Ref. [173].

In particular, it has been proposed that the energies be increased by at least a factor of a few beyond the SPS baseline so that the neutrino and antineutrino energies are well above the Fermi motion region, which would enable useful spectral information to be extracted from the Beta Beam measurements. In addition, this would increase the signal rates (Table 7.1), since the cross section grows with energy, and if the energy were sufficiently high to result in significant matter effects, then

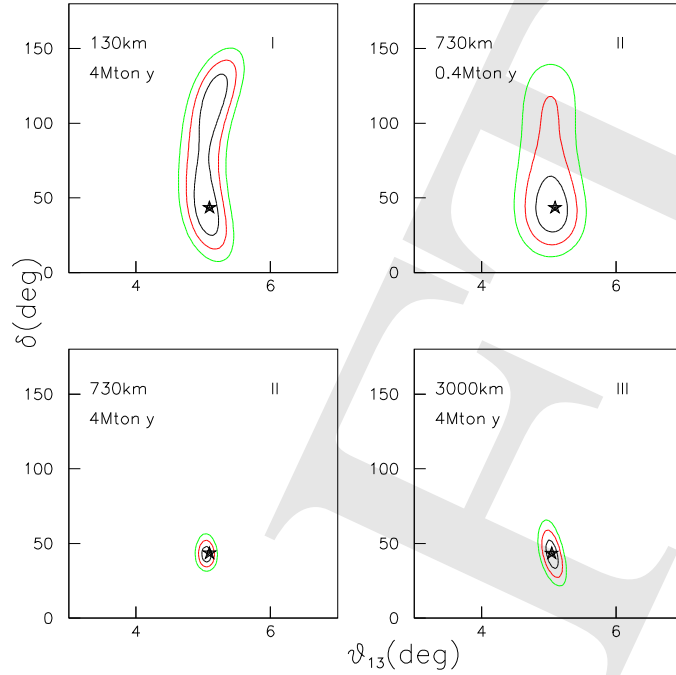


Figure 7.3: (Color) Low-, Medium-, and High-Energy Beta Beam sensitivities. The estimated 1σ , 2σ and 3σ contours are shown for the setups described in the text. See Ref. [173].

it would be possible (if θ_{13} is sufficiently large) to use Beta Beams to determine the neutrino mass hierarchy. The particular scenarios that have been considered [173] are:

Low Energy Beta Beam: This is the standard CERN scenario using the SPS for acceleration, and a 1 megaton water Cerenkov detector in the Fréjus tunnel ($\gamma = 60$, $L = 130$ km).

Medium Energy Beta Beam: This would require the Fermilab Tevatron (or equivalent) for acceleration, and a 1 megaton water Cerenkov detector in the Soudan mine ($\gamma = 350$, $L = 730$ km).

High Energy Beta Beam: This would require the LHC for acceleration, with $\gamma = 1500$, $L = 3000$ km.

In all three cases, the running time is assumed to be 10 years. The improvement in statistical precision enabled by the higher energy Beta Beam scenarios is illustrated in Table 7.1 and Fig. 7.3. The figure shows, for the three scenarios, the 1σ , 2σ , and 3σ contours in the (θ_{13}, δ) -plane. Note that the expected sensitivity for the medium energy case with a “small” water Cerenkov detector is comparable to the low energy case with the megaton water Cerenkov detector. However, the medium energy

sensitivity is dramatically improved with the much bigger detector. The further improvement obtained by going to LHC energies seems to be marginal. Given the likelihood that the LHC would not be available as a Beta Beam accelerator for a very long time, perhaps the most interesting scenario is the medium energy one, at Fermilab.

Chapter 8

The Special Cases

The previous three chapters have described the three possible scenarios for the value of $\sin^2 2\theta_{13}$ at the time of Proton Driver startup and how a Proton Driver is needed to take the next step in each case. In this chapter the three special cases are described: 1) LSND Oscillations Confirmed by MiniBooNE, 2) $\sin^2 2\theta_{23}$ Still Consistent with 1, and 3) Something Unexpected. It is explained how a Proton Driver is the necessary next stage in each of these cases also.

8.1 Special Case 1: $\sin^2 2\theta_{23}$ Still Consistent with 1

8.1.1 $\text{NO}\nu\text{A}$ Measurement

One of the important current questions in neutrino physics is the value of θ_{23} . Current data from the SuperKamiokande experiment [174] are consistent with maximal atmospheric-scale mixing, that is with $\theta_{23} = 45^\circ$. However, the current best 90% C. L. upper limit is only $\sin^2 2\theta_{23} \geq 0.90$, which corresponds to $35.8^\circ \leq \theta_{23} \leq 54.2^\circ$ or $0.342 \leq \sin^2(\theta_{23}) \leq 0.658$. Obtaining a much more restrictive range for θ_{23} is important for three reasons:

1. Maximal atmospheric-scale mixing could indicate a previously unknown symmetry in neutrino mixing.
2. $\nu_\mu \rightarrow \nu_e$ oscillations at the atmospheric mass scale are largely proportional to $\sin^2(\theta_{23}) \sin^2(2\theta_{13})$, so a reasonably precise knowledge of $\sin^2 \theta_{23}$ is required for an extraction of $\sin^2 2\theta_{13}$ from $\nu_\mu \rightarrow \nu_e$ oscillations or for a comparison of reactor and accelerator results.
3. If atmospheric-scale mixing is not maximal, there is a two fold ambiguity in θ_{23} , which is probably best resolved by a comparison of reactor and accelerator results.

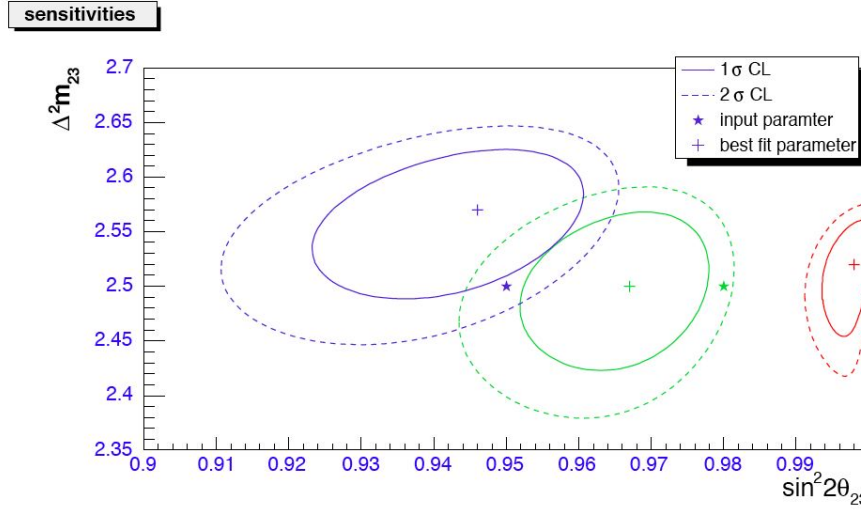


Figure 8.1:

The totally active version of the NO ν A detector, which is currently under study, is very well suited to perform a precise measurement of $\sin^2 2\theta_{13}$. The technique is to use only quasi-elastic ν_μ charged current events, which are defined as those with only a muon track and a possible recoil proton. The total energies of these events are measured with suitable corrections for saturation and inactive material and a maximum likelihood fit is done simultaneously for both Δm_{32}^2 and $\sin^2 2\theta_{23}$. The results depend on the excellent energy resolution of the totally active NO ν A design. We anticipate that quasi-elastic event energies can be measured with a 2% resolution [175].

The results are shown in Figs. 8.1 and 8.2 for five years of neutrino running. Fig. 8.1 is for running without the Proton Driver, corresponding to 18.5×10^{20} protons on target, while Fig. 8.2 is for running with the Proton Driver, corresponding to 100×10^{20} protons on target. The improvement due to the higher flux of the Proton Driver is obvious. If the atmospheric-scale oscillations are maximal, then, with the Proton Driver, NO ν A might conservatively be able to set a 90% C.L. of $\sin^2(2\theta_{23}) \leq 0.996$. Note also that Δm_{32}^2 can be determined to about 0.8%.

8.1.2 Broadband Beam Measurement

We propose to use clean single muon events [176] and calculate the neutrino energy from the energy and angle of these muons assuming they are all from quasi-elastic interactions. The expected spectrum is shown in Figure 8.3; the simulation includes effects of Fermi motion, detector resolution, and backgrounds from non-quasielastic events.

A great advantage of the very long baseline and multiple oscillation pattern in the spectrum is that the effect of systematic errors from flux normalization, background subtraction, and spectrum distortion due to nuclear effects or detector calibration can

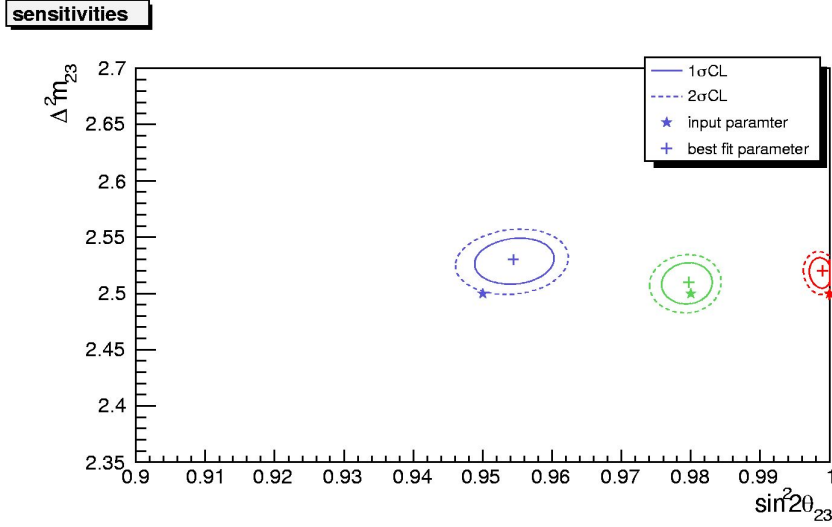


Figure 8.2:

be small. Nevertheless, since the statistics and the size of the expected distortion of the spectrum are both large in the disappearance measurement, the final error on the precise determination of the parameters will most likely have significant contribution from systematic errors. In Figure 8.4 we show the 1 sigma resolutions that could be achieved on Δm_{32}^2 and $\sin^2 2\theta_{23}$. The black lines (labeled (1)) show the resolutions for purely statistical errors. For the red lines (labeled (2)) we have included a 5% bin-to-bin systematic uncertainty in the spectrum shape and a 5% systematic uncertainty in the overall normalization. These uncertainties could include modeling of cross sections or knowledge of the background spectra. For the Δm_{32}^2 resolutions we also show the expected resolution for an additional systematic error of 1% on the global energy scale (blue line labeled (3)). This uncertainty for the Super Kamioka water Cherenkov detector is estimated to be 2.5% in the multi-GeV region [177].

Although the resolution on Δm_{32}^2 will be dominated by systematic errors for the proposed experimental arrangement, a measurement approaching 1 – 2% precision can clearly be made. On the other hand, the resolution on $\sin^2 2\theta_{23}$ is dominated by the statistical power at the first node. This results in a factor of ~ 2 better resolution with 1290 km than with 2540 km using the same sized detector.

Running in the anti-neutrino mode with 2 MW of beam power will yield approximately the same spectra and resolutions on Δm_{32}^2 and $\sin^2 2\theta_{23}$. By comparing the measurements with the results from neutrino running a test of CPT is possible. In such a comparison many systematic errors, such as the global energy scale, common to the neutrino and anti-neutrino data sets should cancel yielding a comparison with

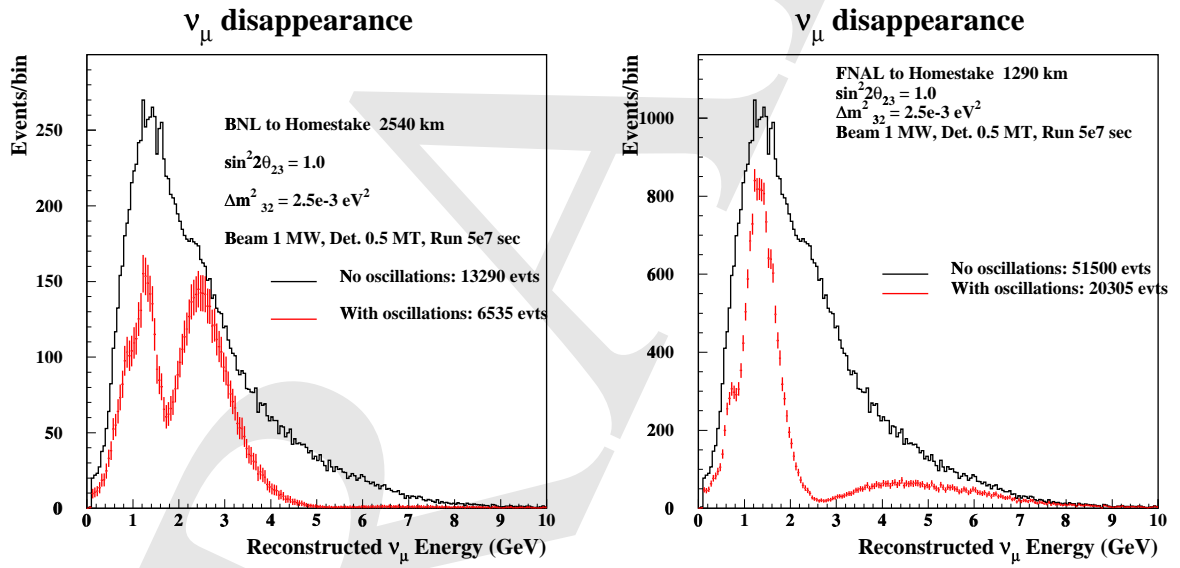


Figure 8.3: Simulated spectrum of detected muon neutrinos for 1 MW beam and 500 kT detector exposed for 5×10^7 sec. Left side is for baseline of 2540 km, right side for baseline of 1290 km. The oscillation parameters assumed are shown in the figure. Only clean single muon events are assumed to be used for this measurement (see text).

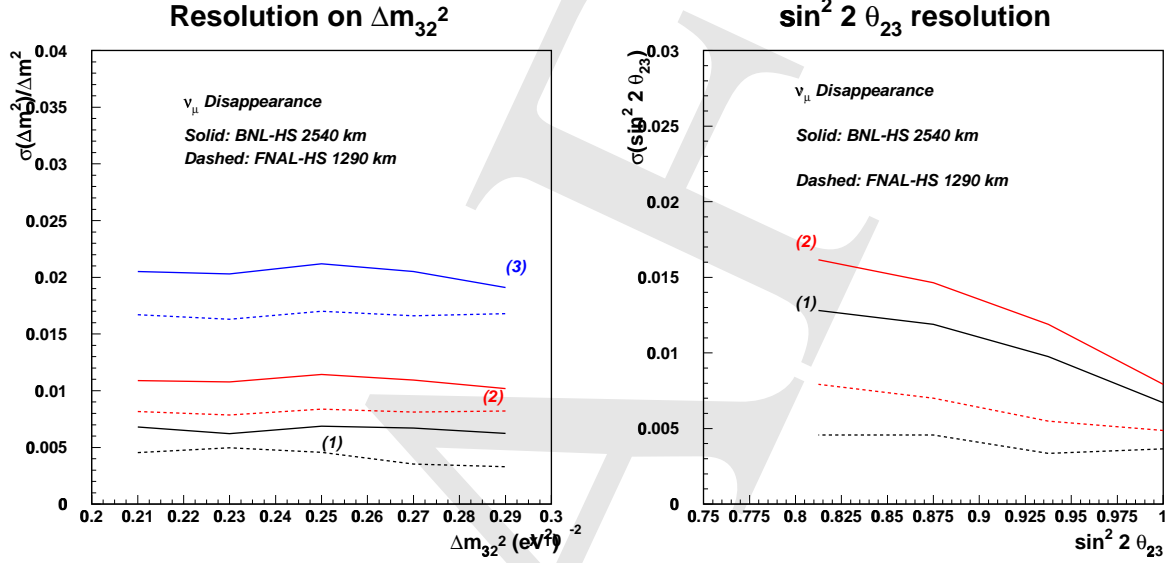


Figure 8.4: 1σ resolutions on Δm^2_{32} (left) and $\sin^2 2\theta_{23}$ (right) expected after analysis of the oscillation spectra from Figure 8.3. The solid curves are for BNL-HS 2540 km baseline, and the dashed are for FNAL-HS 1290 km baseline. The curves labeled 1 and 2 correspond to statistics only and statistics and systematics, respectively (similarly for dashed curves of the same color). The curve labeled (3) on the left has an additional contribution of 1% systematic error on the global energy scale.

errors less than 1%.

Finally, we remark that it is important to make precision measurements of both Δm^2_{32} and $\sin^2 2\theta_{23}$ not only because they are fundamental parameters, but also because they are needed for interpreting the appearance ($\nu_\mu \rightarrow \nu_e$) result. Knowledge of both Δm^2_{21} and Δm^2_{32} are essential in fitting the shape of the appearance signal to extract other parameters. In addition, it will be very important to definitively understand if $\sin^2 2\theta_{23}$ is close to 1.0 or is < 1.0 . If $\sin^2 2\theta_{23} < 1.0$ then there will be an ambiguity in $\theta_{23} \rightarrow \pi/2 - \theta_{23}$. As we will describe below this ambiguity will affect the interpretation of the appearance spectrum.

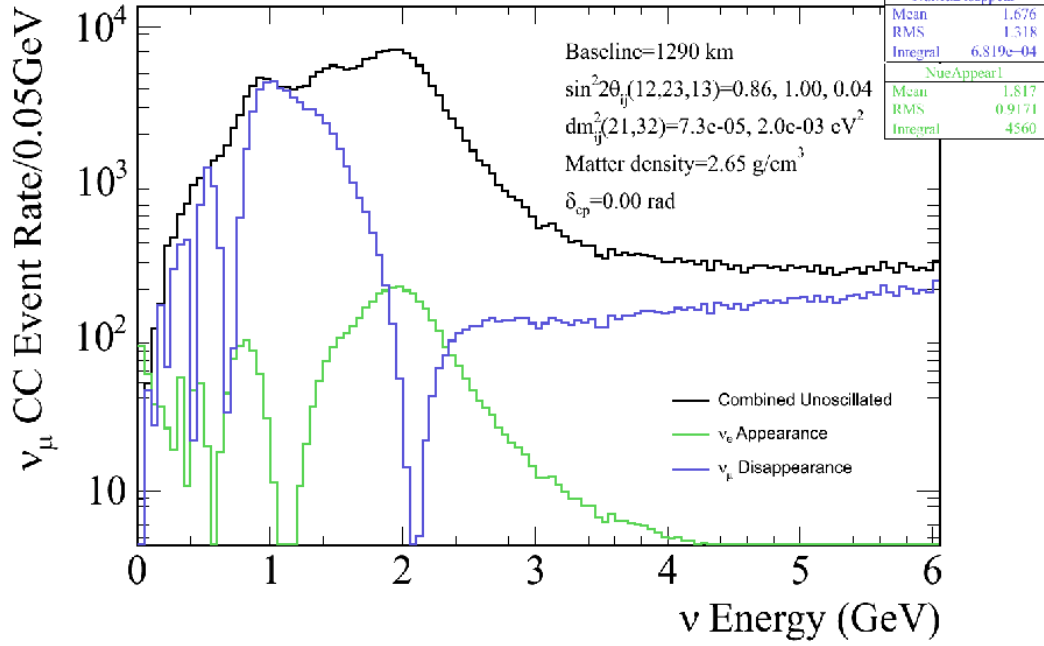


Figure 8.5: Expected rate of neutrino events at Homestake given $\Delta m^2 = 0.002$, $\sin^2 2\theta_{23} = 1.0$, $\sin^2 2\theta_{13} = 0.04$, $\delta_{CP} = 0.0$ and with the normal mass hierarchy. The first oscillation maximum occurs at $E_\nu = 2.0$ GeV and the second oscillation maximum occurs at $E_\nu = 0.7$ GeV.

8.1.3 FeHo Measurement

Figure 8.5 shows the expected neutrino event rates at Homestake given $\Delta m^2 = 0.002$ eV², $\sin^2 2\theta_{23} = 1.0$, $\sin^2 2\theta_{13} = 0.04$, $\delta_{CP} = 0.0$ and with the normal mass hierarchy. The first oscillation maximum occurs at $E_\nu = 2.0$ GeV and the second oscillation maximum occurs at $E_\nu = 0.7$ GeV. It is worth noting that the 8 GeV protons directly from the 8 GeV proton driver are an contributor to measurements near the second oscillation maximum. Use of these protons makes both higher total power available as well as more neutrinos at the less than 1 GeV energies required.

Figure 8.6 shows the sensitivity of a 500 kT water Cerenkov detector to the ν_μ disappearance parameters. Although the Super-K response functions have been used, possible systematic uncertainties in extrapolation of the beam to the far detector have not been included in these sensitivities.

Confidence Levels

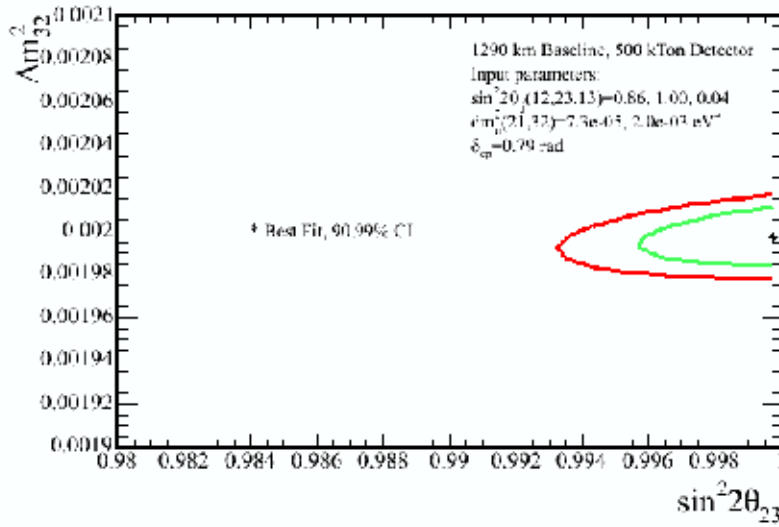


Figure 8.6: Expected 90% and 99% CL contours on measurement of Δm^2 and $\sin^2 2\theta_{23}$ for actual input values $\Delta m^2 = 0.002 \text{ eV}^2$ and $\sin^2 2\theta_{23} = 1.00$ using a 500 kT water Cerenkov detector at Homestake. All expected event confusions and energy smearing have been included in the calculation but it is assumed that the systematic uncertainty in the detector response is negligible. In fact, significant work will be required to make this true but here we simply assume that such work will be done.

8.2 Special Case 2: LSND Oscillations Confirmed by MiniBooNE

8.2.1 Decay at Rest Source

Should the MiniBooNE experiment at FermiLab confirm the LSND signal, then new experiments will be required to understand the underlying mechanism of these oscillations. New models include sterile neutrinos [42], CP [178] or CPT [179] violation, and other possibilities. Described below are several types of measurements with a stopped pion/muon source which could tease out the contributions to these large Δm^2 oscillations.

The precision experiments required to observe the new physics described above requires an intense source of neutrinos which is well characterized. Neutrinos from stopped pion decay is such a source, having well defined flux, energy spectrum, and low backgrounds. Fortunately, such classes of accelerators are either being built, or are being proposed. The first such prospect is the 1.4 MW, 1.3 GeV, short duty-factor Spallation Neutron Source (SNS) at ORNL [180], which is currently being built and will be fully commissioned by 2008. The second is a proposal for a 2 MW, 8 GeV, Proton Driver (PD) at FNAL [181].

The dominate decay scheme that produces neutrinos from a stopped pion source

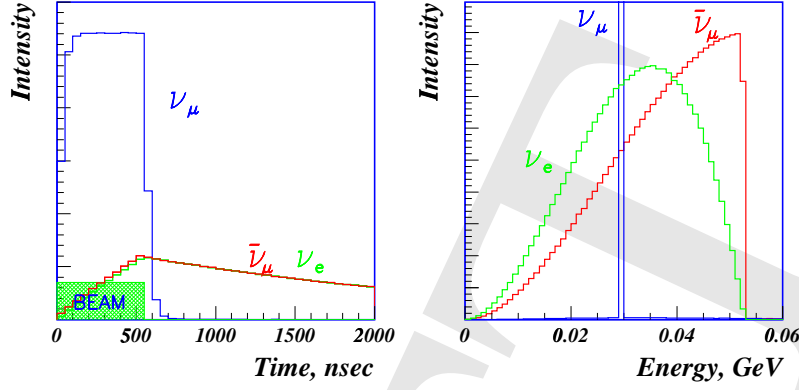


Figure 8.7: The neutrino time and energy spectra of the different neutrino species produced isotropically from a stopped pion/muon source.

is

$$\pi^+ \rightarrow \mu^+ \nu_\mu, \quad \tau = 26 \text{ nsec} \quad (8.1)$$

followed by

$$\mu^+ \rightarrow e^+ \bar{\nu}_\mu \nu_e, \quad \tau = 2.2 \text{ } \mu\text{sec}. \quad (8.2)$$

The neutrinos from stopped π^- 's are highly suppressed because the negative pions are almost completely absorbed in the surrounding material. Thus, neutrinos from the π^- decay chain are significantly depleted and can be estimated from the measured $\nu_\mu u$, $\bar{\nu}_\mu u$, and ν_e flux. Figure 8.7 shows the neutrino spectra and timing plots from a stopped pion source. As shown in the right hand plot, the ν_μ energy is monoenergetic ($E_{\nu_\mu} = 29.8 \text{ MeV}$), while the $\bar{\nu}_\mu u$ and ν_e have known Michel decay distributions, with an end point energy of 52.8 MeV. Furthermore, the left hand plot shows the SNS beam timing and the time distributions for the three neutrino species. One of the advantages of the SNS relative to the similar LAMPF machine is the short beam time of 695 nsec (the FNAL-PD will have a similar short beam time). With a simple timing selection after the beam, one can achieve a fairly pure $\nu_\mu u$ sample, with only a 14% contamination of each neutrino type $\bar{\nu}_\mu u$ and ν_e .

Table 8.1 shows the expected proton rates for both SNS and FNAL beamlines, normalized to a full year of running, i.e. 3.15×10^7 seconds. The FNAL Proton Driver proposal is broken down into a 8 GeV, 2 MW and a 5 GeV, 1.25 MW beamline. The FNAL 8 GeV option will provide about 2.5 times more protons per year than the SNS. However, the FNAL PD is only a proposal, while the SNS is under construction and will be operational by 2008, which makes it more timely. Furthermore, the SNS is planning an upgrade for 2014, which will deliver 3MW to two sources, which makes for the interesting situation of multiple baselines with a single detector.

The SNS or FNAL-PD stopped pion/muon source will provide very high (and precisely known) fluxes of neutrinos from π^+ and μ^+ decay at rest with a very low duty factor for cosmic-ray suppression. Furthermore, the oscillation signals are easily identifiable with well-known cross sections, and the backgrounds are quite low, so that an LSND signal at 0.3 eV^2 , for example, would have a signal to background greater than 10 to 1. By copying the MiniBooNE detector design [12] with only a few

	FNAL (8 GeV)	FNAL (5 GeV)	SNS
P/yr	1.6×10^{22}	1.6×10^{22}	6.7×10^{22}
DAR $\nu(\nu/P)$	1.5	0.9	0.13
DAR $\nu(\nu/yr)$	7.3×10^{22}	4.4×10^{22}	2.9×10^{22}

Table 8.1: Proton intensity at FNAL and SNS. The numbers are taken from Ref. [181], assuming 3.16×10^7 s/yr operation.

minor changes (higher phototube coverage, better phototubes, and the addition of b-PBD scintillator), then one would be able to make a very precise measurement of the oscillation parameters, search for multiple Δm^2 contributions, search for CP and CPT violation by the comparison of neutrino and anti-neutrino oscillation parameters, and search for sterile neutrinos via the neutral-current reaction $\nu_x {}^{12}\text{C} \rightarrow \nu_x {}^{12}\text{C}^*$ (15.11). The precise distance of the detector from the source depends on the value of Δm^2 determined by MiniBooNE: $\Delta m^2 \sim 1 \text{ eV}^2$ would suggest a distance of $\sim 60 \text{ m}$, while $\Delta m^2 \sim 0.3 \text{ eV}^2$ would suggest a distance of $\sim 200 \text{ m}$. At the SNS the detector could not be placed closer than 60 m, while for the FNAL-PD, there is no such constraint, with distances as close as 10 m possible, which allow for higher Δm^2 sensitivity up to 10 eV^2 .

The signal and backgrounds for a new short baseline neutrino oscillation experiment can be reliably estimated based on the experience from the LSND experiment [182]. Compared to LSND, an SNS/FNAL-PD experiment should observe an oscillation event rate that is an order of magnitude higher, due to the 5 times larger mass and the 2 times larger neutrino flux. For the FNAL-PD, this flux would be 5 times larger. Based on the LSND oscillation parameters, an SNS (FNAL-PD) experiment should observe about 350 (875) $\bar{\nu}_\mu p \rightarrow e^+ n$ events per year due to $\bar{\nu}_\mu \rightarrow \bar{\nu}_e$ oscillations. The only significant neutrino background is μ^- decay at rest in the beam dump followed by $\bar{\nu}_e p \rightarrow e^+ n$ scattering in the detector and is estimated to be only about 10 events per year. The cosmic-ray background is small due to the low SNS/FNAL-PD duty factor (more than 2 orders of magnitude lower than LAMPF). It is estimated to be < 20 events per year. Therefore, the total background should be < 30 events per year, giving a signal to background of about 10(25) to 1! As the neutrino energy can be well measured from the e^+ energy and angle and the neutrino distance can be well determined from the event position inside the detector, the L_ν/E_ν resolution is very good and the neutrino oscillation parameters can be accurately determined from the shape of the E_ν or L_ν/E_ν distribution. Fig. 8.8 shows how the energy distribution is very sensitive to the precise values of Δm^2 and $\sin^2 2\theta$ for a detector 60m from the SNS source (multiply the event rate by 2.5 for the FNAL 8GeV proton driver).

In addition to measuring $\bar{\nu}_\mu \rightarrow \bar{\nu}_e$ oscillations, an SNS/FNAL-PD neutrino experiment will also be able to measure $\nu_\mu \rightarrow \nu_e$ oscillations, via the reaction $\nu_e {}^{12}\text{C} \rightarrow e^- {}^{12}\text{N}_{gs}$, with up to a hundred events a year clearly detectable [183]. Comparing to the $\bar{\nu}_\mu \rightarrow \bar{\nu}_e$ rate will directly test CP and CPT violation models.

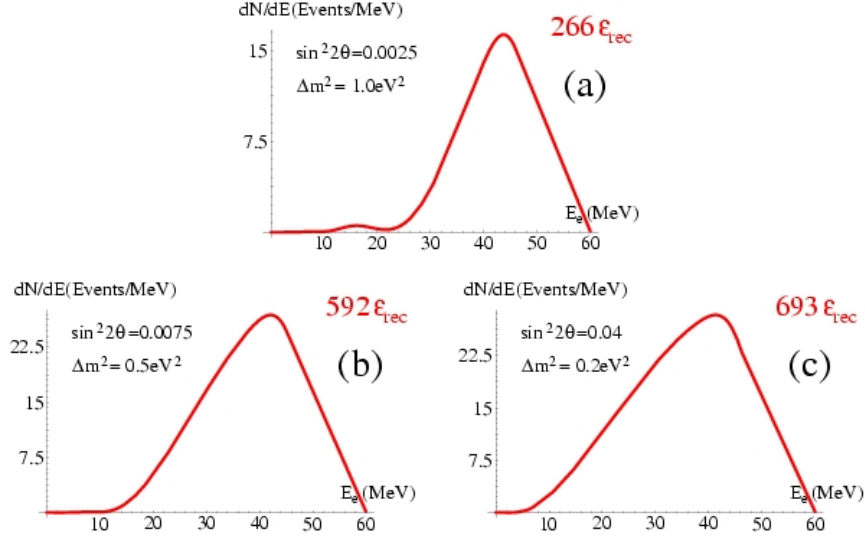


Figure 8.8: The reconstructed $\bar{\nu}_\mu \rightarrow \bar{\nu}_e$ oscillation energy distribution is very sensitive to the values of Δm^2 and $\sin^2 2\theta$. This figure comes from Ref. [183], which assumes the SNS source, a miniBooNE type detector distance of 60 m, and an energy resolution of 7%.

Finally, a search for sterile neutrinos can be done via the neutral-current (NC) reaction $\nu_x \, ^{12}\text{C} \rightarrow \nu_x \, ^{12}\text{C}^* (15.11)$, which emits a 15.11 MeV γ . A lower event rate than expected for the neutral-current reaction would be direct evidence for oscillations into sterile neutrinos. This reaction makes use of the mono-energetic ν_μ beam, so that for large Δm^2 and sufficiently large mixing, an oscillatory event rate would be observed in the detector as a function of distance. Figure 8.9 shows the solution space for a miniBooNE style detector at 100 m, and a small 100 ton oil detector at 10 m from the FNAL-PD 8 GeV stopped pion source [184]. Large Δm^2 solutions have oscillation lengths of a few meters, thus NC oscillations patterns can be clearly identified in the far detector (10 m fiducial volume). Low Δm^2 mass solutions appear as NC rate suppression of the far detector relative to the near detector. This detector/source setup is extremely sensitive to active-sterile neutrino oscillations, and can easily pick out the 3+2 sterile neutrino model solutions of $\Delta m^2 = 0.9 \text{ eV}^2$, $\sin^2 2\theta = 0.15$, and $\Delta m^2 = 22 \text{ eV}^2$, $\sin^2 2\theta = 0.19$ [42].

All of the above reactions have well known cross sections with uncertainties less than a few percent, and together with the perfectly-known neutrino energy shapes, are capable of making precision measurements of the oscillation parameters, searching for sterile neutrinos, and CP/CPT violation. An intense stopped pion/muon source is a golden opportunity for a next generation short baseline neutrino oscillation experiment. This would be ideal as a followup to a positive miniBooNE signal, and the clearest way to determine the source of new physics beyond the Standard Model.

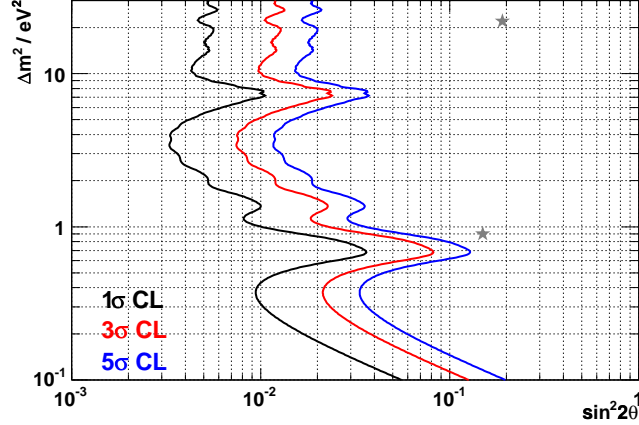


Figure 8.9: Sterile neutrino oscillation sensitivity with NC reaction $\nu_x \, ^{12}\text{C} \rightarrow \nu_x \, ^{12}\text{C}^*$ (15.11) for FNAL-PD 8GeV, with a MiniBooNE sized detector at 100m, and a small near detector at 10m. No systematic errors on flux, and three years of running. The two stars corresponds to the 3+2 sterile solutions as described in the text.

8.2.2 NuMI ν_μ to ν_τ

If MiniBooNE confirms LSND, it will confirm that neutrinos oscillate with a relatively large mass difference $\Delta m^2 > 0.1 \text{ eV}^2$ and that at least four neutrino mass eigenstates play a role. The followup would be to characterize the large-mass-scale oscillations as completely as possible, to determine the parameters for oscillations to active flavors and thereby constrain the sterile neutrino mixing component. Such a program would include a search for $\nu_\mu \rightarrow \nu_\tau$ at short baseline.

A $\nu_\mu \rightarrow \nu_\tau$ experiment requires a moderately high energy neutrino beam to permit charged current ν_τ interactions and a detector with high spacial resolution to observe the decay of the short-lived τ leptons. The τ production threshold is 3.5 GeV and a beam at least a few GeV above this energy would be optimal. Here we consider using the NuMI medium energy beam, where the event spectrum peaks at about 7 GeV. At these energies the τ typically travels less than a millimeter before decay.

To date, ν_τ interactions have been observed by only one experiment, DONUT at Fermilab [185], which used an emulsion target. Emulsion provides sub-micron position resolution, and the τ signature is a kink: a track emerging from the neutrino interaction vertex with a change in direction after a short path. At DONUT, the neutrino beam was produced by directing 800 GeV protons onto a 1-m-long tungsten beam dump. Neutrinos emerged from charmed meson decays in the dump, a significant fraction of which were ν_τ . Four τ candidate events were reconstructed in the emulsion target, which had an average mass during the exposure of 0.261 tons. This observation verified the existence of ν_τ and demonstrated the use of emulsion for its detection.

The most recent experiments to search for $\nu_\mu \rightarrow \nu_\tau$ were CHORUS [186] and NOMAD [187], which ran concurrently in the same beam at CERN and employed

different ν_τ detection techniques. CHORUS used an emulsion target of total mass 0.77 tons, while at NOMAD the target consisted of drift chambers with a fiducial mass of 2.7 tons. At NOMAD the τ decay vertex was not reconstructed — instead, τ candidates were identified based on kinematic criteria after reconstruction of all visible final state particles. CHORUS expected less than an event of background and found no ν_τ candidates. NOMAD found no excess of candidates above background expectations. Limits from these two experiments and earlier experiments are given in Fig. 8.10.

Fig. 8.10 also shows an indirect limit on $\nu_\mu \rightarrow \nu_\tau$ derived from reactor and atmospheric neutrino data in the context of the (3+1) neutrino model. A global analysis of neutrino oscillation data performed by Maltoni et al. [20] sets limits on four-neutrino mixing models. These authors find 90% C.L. limits on parameters $d_\mu < 0.04$ and $d_s > 0.75$, where $1 - d_\mu$ ($1 - d_s$) is the fraction of ν_μ (ν_s) participating in atmospheric oscillations. These results are used to set the short-baseline bound $\sin^2 \theta_{\mu\tau} < 0.04$ for the (3+1) neutrino model.

The state of the art in ν_τ detection will be advanced at two new experiments, OPERA [188] and ICARUS [189], which are to search for ν_τ appearance in the CNGS beam from the CERN SPS to the Gran Sasso Laboratory, a 730 km baseline. Both detectors are kiloton scale, representing a three order of magnitude increase in mass over previous ν_τ detectors. OPERA will use an emulsion-lead target with a mass of 1.8 kton. ICARUS will use a Liquid Argon time projection chamber with a total mass of 5 ktons planned. These experiments aim to observe $\nu_\mu \rightarrow \nu_\tau$ and confirm the atmospheric oscillation parameters. The CNGS neutrino beam turns on in 2006.

At NuMI, detectors of modest size compared to OPERA and ICARUS could search for ν_τ appearance in the LSND Δm^2 range with mixings significantly smaller than present limits. Fig. 8.11 shows the sensitivity expected with a 100 ton emulsion detector at the NuMI medium energy beam with 80×10^{20} protons on target. These sensitivities are derived by considering statistical uncertainties and assuming a τ detection efficiency (including branching ratios) of 9.1% and backgrounds of 3×10^{-5} per ν_μ event, both independent of energy. These parameters are similar to those expected by OPERA. Sensitivities using four different baselines are shown, and the 1 km baseline corresponds to placing the detector in the existing NuMI near detector hall. The NuMI secondary beam decay region is long compared to the nominal baseline, and these sensitivities take the average pion decay length into account. The background, which is due to ν_μ misidentification, scales with the flux and therefore falls like L^{-2} . The signal is to first order independent of L . Therefore a longer baseline provides an advantage. However, the NuMI beam points down at 3.3 degrees, so the the longer the baseline the deeper the location of the detector hall. The sensitivity is background-limited, so for small Δm^2 it scales with the detector mass only as $M^{1/4}$. It follows then that a 100-ton detector at $L = 1$ km offers similar low- Δm^2 sensitivity as a 1-ton detector at $L = 3.16$ km. Regardless of the exact baseline choice, the challenge in probing small $\sin^2 \theta_{\mu\tau}$ values with emulsion will be to scan efficiently a large number of ν_μ events. For example, with 10^{21} protons on target the NuMI medium energy beam will produce 660000 ν_μ events per ton at 2 km, yielding about 20 background events compared to 8200 identified ν_τ events assuming 100% transmutation.

Note, finally, that OPERA and ICARUS expect to observe $\nu_\mu \rightarrow \nu_\tau$ at the atmospheric Δm^2 . If such oscillations also occur with small amplitude at the LSND mass scale, then the ν_τ event samples at OPERA and ICARUS will contain contributions from both sources, and it will be impossible to pick those contributions apart. A short baseline experiment will be required to resolve the high- Δm^2 contribution.

8.2.3 Effect on LBL Measurements

Confirmation of LSND will support the supposition that sterile neutrinos must exist, and that the entire theory of neutrinos must be given a fresh look. The LBL experiments will be faced with two paths to explore: They might assume that sterile neutrinos do not mix with active neutrinos, in which case there may be no effect on the the experiment, and the interpretation of the results. If this assumption is not be valid, the experiments and the interpretation of the results will need to be reevaluated. Since the former case needs no further explanation, we'll explore some of the implications of the latter case in the remainder of this section.

We'll need some examples to set the stage so let's first consider the NoVA proposal. The 250 kiloton detector will be in the NuMI beamline, may be scintillator-based, located 810km from the source and 12 km off-axis. The collaboration assumes 3.7×10^{20} p.o.t/yr for five years. NoVA is a ν_e appearance experiment, but a search for sterile neutrinos involves a search for a depletion of neutral current events, if the NC events are not affected by oscillations. With these assumptions the collaboration claims a possible limit on $\nu_\mu \rightarrow \nu_s$ of about 7% [190], [191] in the atmospheric Δm^2 range.

T2K hopes to run with 10^{21} pot/yr, with a far detector 295 km from the source. The 50 Kiloton Super-Kamiokande will be the far detector in this initial stage. The detector will be sensitive to cerenkov and scintillation light. The neutral current interactions provide a means to measure the total flux of neutrinos of all flavors provided the cross-sections are well measured. Combined with the ν_e appearance measurement, the neutral current data provide a means for measuring the ν_μ disappearance into ν_τ and ν_s . The sensitivity of the experiment will increase in time as bigger and better detectors are brought on-line [28].

The existence of sterile neutrinos in the LSND mass range may limit the ability of LBL experiments to resolve the mass hierarchy and exclude a null CPV signal in neutrino interactions. These sterile neutrinos will oscillate with a very short wavelength, and appear at the LBL far detectors as ν_e or ν_μ interactions. They behave as an added intrinsic background, added to the beam related intrinsic backgrounds. This will limit the sensitivity of the experiments in $\sin^2(2\theta_{13})$ vs. $\text{CP}\delta$ space. Furthermore, if the LSND signal is CP violating, the reach in θ_{13} may be severely limited. These simulations are shown in Fig. 8.12.

The existence of sterile neutrinos was measured by the Super Kamiokanda Collaboration to explore the possibility that atmospheric neutrinos oscillate either into ν_τ or ν_s . The experiment measures the zenith angle variation in ν_μ flux, which effectively provides a measure of matter effects. The collaboration was able to set a limit at 99% confidence level that oscillations take place into ν_τ , and that there is no evidence for

sterile neutrinos [3]. This result limits the degree to which the LBL might hope to see a signal in the neutral current interactions, but many surprises may still be in store in the neutrino sector.

As we can see from the examples discussed in this section, the neutrino physics landscape may be complex and difficult to navigate. Future experiments will need some basic tools, such as accurate neutrino cross-sections in the 0.5 to 3 GeV range, and very high beam flux to fully exploit their capabilities. The neutral current signal can provide a lot of important insight into the nature of neutrino interactions, but only if the cross-sections are well understood. This implies that an ongoing program at existing facilities is needed to make these measurements possible. Sufficient accelerator-produced protons must be available to support existing physics programs, and make room for neutrino cross-section measurements that will support future experiments.

As seen in Figure 1, nominal assumptions regarding neutrino flux suggest that ten years of running will be needed to make a measurement of CP violation. The LBL experiments, simply because flux varies as $1/L^2$, will suffer from low statistics unless a very intense neutrino source is available. Remember the neutrino physics mantra: “We need more beam.”

8.3 Special Case 3: Something Else Unexpected

This section will contain a generic description of unexpected results by the time of Proton Driver startup, perhaps referring to some unexpected results from the history of neutrino physics. The section will conclude with the general statement that any unexpected results will be from comparatively few events and so will need the statistics provided by a proton driver to investigate them further.

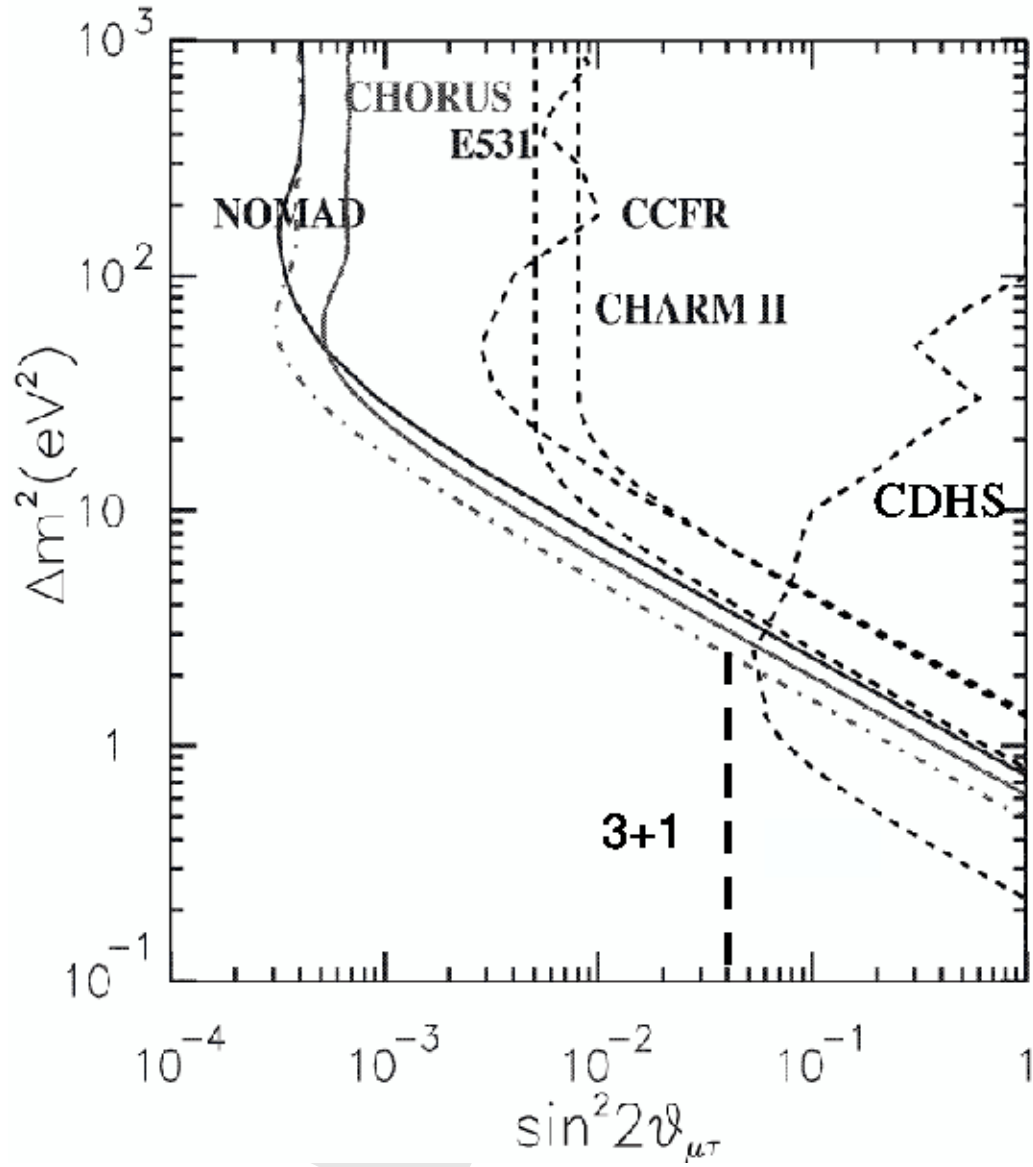


Figure 8.10: Limits at 90% C.L. on $\nu_\mu \rightarrow \nu_\tau$ oscillation from previous experiments (from Ref. [186]). The vertical dashed line is a limit from atmospheric and short baseline reactor data in the (3+1) neutrino model.

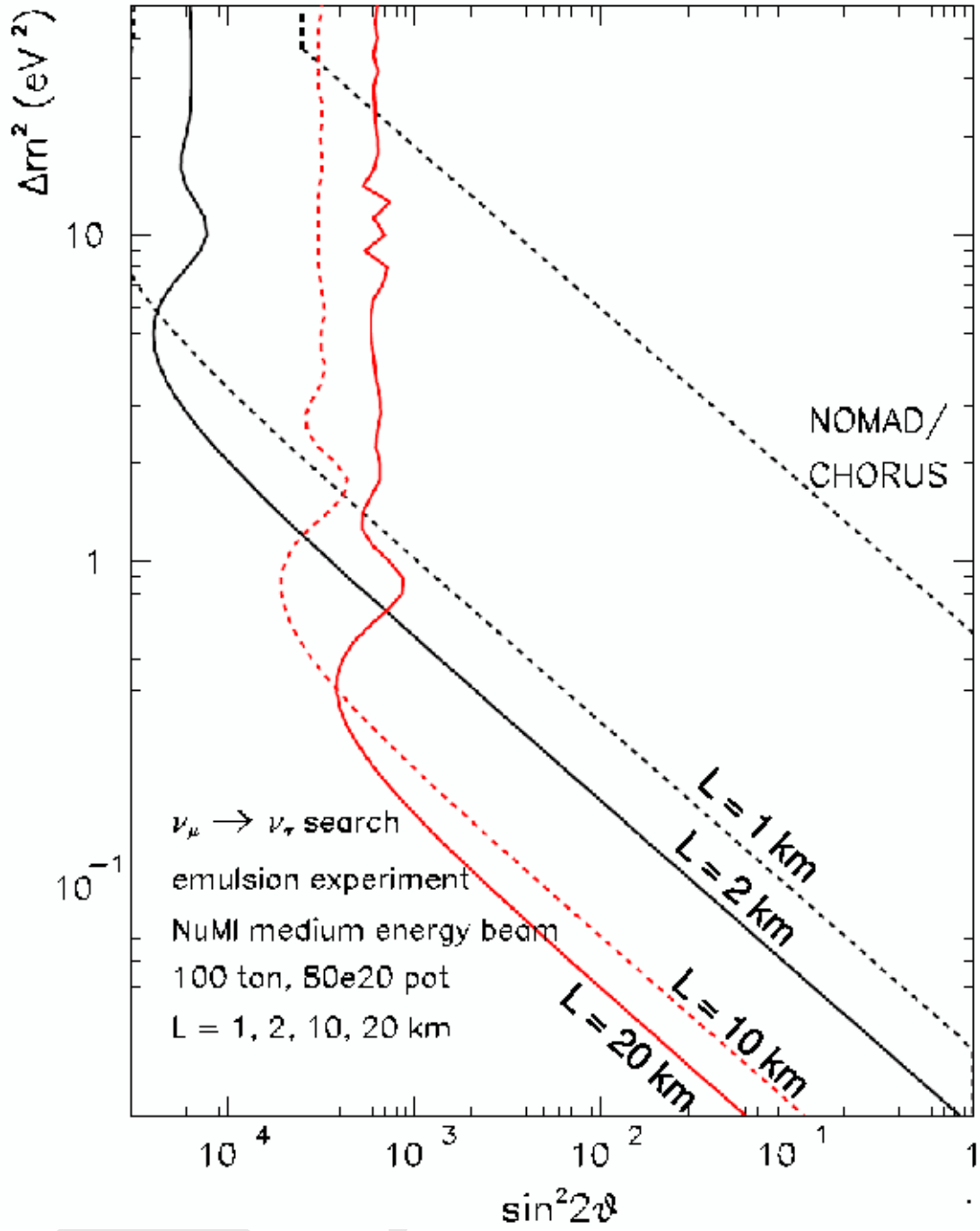


Figure 8.11: Expected 90% C.L. limits on $\nu_\mu \rightarrow \nu_\tau$ oscillation using the NuMI medium energy neutrino beam with 80×10^{20} protons on target and a 100 ton emulsion detector, assuming detection efficiencies and background levels similar to those of OPERA, as explained in the text. Four different baselines, $L = 1, 2, 10$, and 20 km, are shown. The present limits from NOMAD and CHORUS are also indicated.

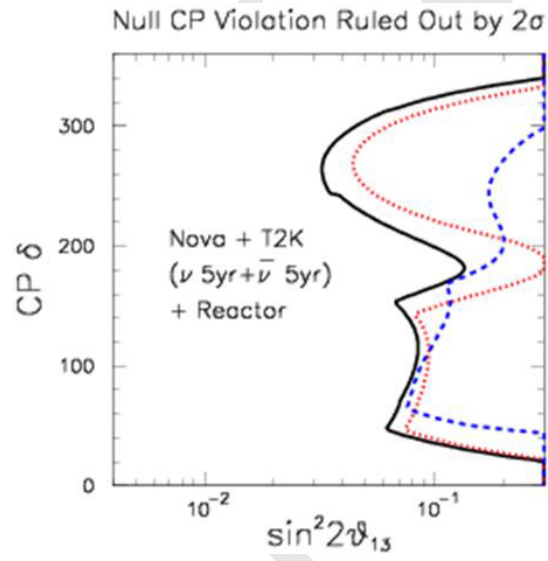


Figure 8.12: The excluded region to a two σ level in $\sin^2(2\theta_{13})$ vs. the CP phase δ for combined runs of NoVA and T2K of five years in ν mode and five years in $\bar{\nu}$ mode combined further with results from a reactor based experiment. Black line applies if LSND is refuted; Red dotted curve is with LSND confirmed by MiniBooNE and the signal is CP conserving; Blue dashed curve is for LSND confirmed by MiniBooNE and the signal is CP violating.

DRAFT

Chapter 9

Summary

DRAFT

DRAFT

Appendix A

Experiment descriptions

A.1 The NO ν A Experiment

NO ν A (NuMI Off-Axis ν_e Appearance Experiment) is a proposal to Fermilab (P-929 [191]) to use the Fermilab Main Injector neutrino beam (NuMI) [192] with a new surface detector situated 810 km from Fermilab in Minnesota just south of Voyager National Park. The primary physics goal of NO ν A is to look for oscillations of the ν_μ beam into ν_e and thus to measure the mixing angle θ_{13} . With anti-neutrino running NO ν A can also address the mass hierarchy question. These investigations would be enhanced by the increased neutrino beam intensity available with a Fermilab Proton Driver to the extent that measurements of CP violation in neutrino oscillations might be done by NO ν A. Additional measurements of Δm_{32}^2 and $\sin^2 2\theta_{23}$ and searches for sterile neutrinos are also part of a NO ν A physics program.

The NuMI beam facility has been designed for a proton intensity of 4×10^{13} protons per pulse every 1.9 sec – roughly 0.4 MW of beam power. The NO ν A proposal assumes this per pulse intensity would produce approximately 4×10^{20} protons per year and assumes 5 years of data taking. NO ν A would be located off-axis to the NuMI beamline to take advantage of the angle-energy relationship first pointed out for experiment E-889 at Brookhaven National Laboratory [144]. At 12 km off-axis (about 15 mrad), the experiment would see a nearly mono-energetic 2 GeV neutrino beam with a width (FWHM) of about 0.7 GeV, as shown in figure A.1. The farther off axis the detector is placed, the lower the peak neutrino energy.

The NO ν A detector is optimized to find ν_e charged current events identified by the presence of an electron in the final state. The experimental backgrounds to the $\nu_\mu \rightarrow \nu_e$ oscillation signals arise from two general sources. There are genuine events with electrons resulting from the intrinsic ν_e component in the beam and from τ decays produced in the charged current ν_τ interactions from $\nu_\mu \rightarrow \nu_\tau$ oscillations. The ν_τ background is very small in NO ν A since most of the ν_μ flux is below τ production threshold. The second background sources are potentially misidentified Neutral Current (NC) events or high y ν_μ CC events where one or more neutral pions in the final state masquerade as an electron or, less likely, that a hadron is misidentified as an electron. When compared to the on-axis beam, the off-axis configuration reduces the

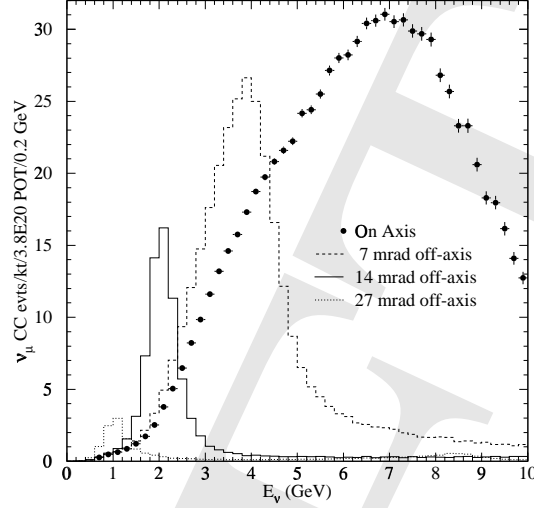


Figure A.1: Event rates at various off axis angles with respect to the NuMI beamline, for the medium energy configuration.

high energy tail of the neutrino beam, which reduces these NC and $\nu_\tau au$ backgrounds.

The NO ν A detector design is a low Z tracking calorimeter based on liquid scintillator contained in segmented plastic extrusions. Wavelength shifting fibers are used to transport the light to avalanche photodiodes (APDs) as the readout. A total mass of 25 kilotons is proposed [191]. The individual liquid scintillator cells are 3.9 cm x 16 m transverse to the neutrino beam and 4.5 cm thick along the beam direction. Sequential planes have the 16 m cell dimension in the horizontal, then the vertical direction, providing x and y coordinates for events. The extruded PVC plastic cells are loaded with 15% titanium dioxide for good reflectivity of the scintillator light. A looped 0.8 mm diameter wavelength shifting fiber is placed in each tube by folding a single fiber back on itself at the end of each cell. Both ends of the fiber are routed to the same APD pixel and every channel will have pulse height information. Approximately 42 photons per minimum ionizing particle are expected to reach the APD from the far end of the long cells and the APD would be run at a gain of 100 with a quantum efficiency of 85%. Peltier cooling is used to reduce the intrinsic APD noise so that a signal to noise level greater than 10 is achieved. The detector is 85% scintillator + 15% PVC and is therefore nearly "totally active". Two views of a typical event in the NO ν A detector are shown in Figure A-1. Individual tracks in the final state can be clearly separated from each other due to the transverse segmentation.

Electrons in NO ν A are distinguished from hadrons and muons by a generally broader pattern of hits along the track for electrons due to the electron shower. Thus ν_e charged current (CC) events are quite easily separated from ν_μ CC events. Electrons are distinguished from π^0 's by a finite separation between the vertex and the conversion points of the photons from the π^0 . This property is used to help remove NC backgrounds. The proposed detector has good energy resolution of about

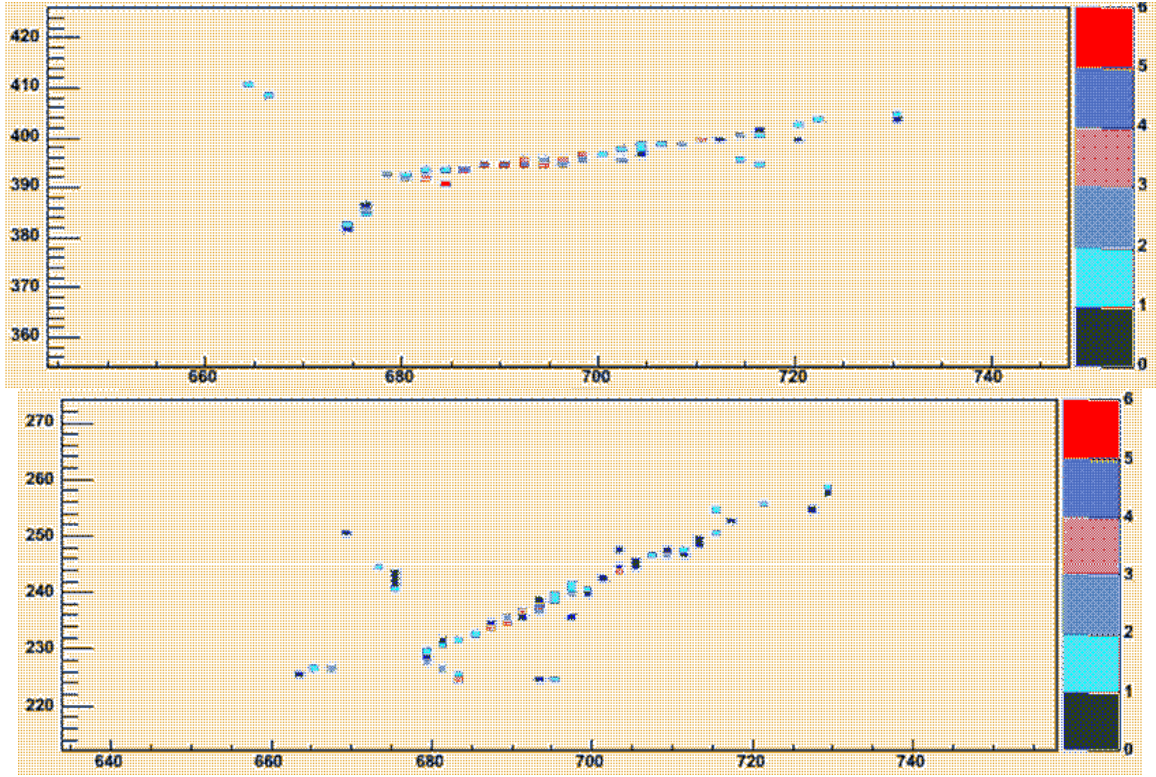


Figure A.2: A ν_e CC event in the NO ν A detector, $\nu_e + A \rightarrow p + e^- + \pi^0$ with $E_\nu = 1.65\text{GeV}$. The event is displayed using only the indicated color code to show the relative pulse height. The X-Z view on top and the Y-Z view on the bottom. The scale units are numbers of cells.

10%/sqrt(E) for ν_e CC events and this resolution can be used to remove NC and beam ν_e backgrounds inconsistent with the mono-energetic off-axis beam energy. Figure 2 illustrates the backgrounds (before any cuts) and possible signal that would be seen in NO ν A. The sensitivity of NO ν A in various θ_{13} scenarios is described in the main text.

As is typical in long baseline neutrino oscillation experiments, NO ν A would also have a Near Detector located off-axis at Fermilab to understand the un-oscillated beam backgrounds. This 120 ton device would be built with the same detector technology and would be located in the existing access tunnel upstream of the MINOS Near Detector Hall.

The NuMI beamline and MINOS detector will become operational in 2005 and NO ν A would capitalize on that investment with a second-generation detector which could begin operations as early as 2008 with a portion of the detector. The NO ν A collaboration views the proposed experiment as a second step in an incremental Fermilab program to measure all of the unknown parameters of neutrino oscillations. Each incremental step will provide guidance on the optimum direction for the succeeding step.

We view the NO ν A experiment as the next step in a step-by-step Fermilab neutrino program in which information from each step is used to plan future steps. We

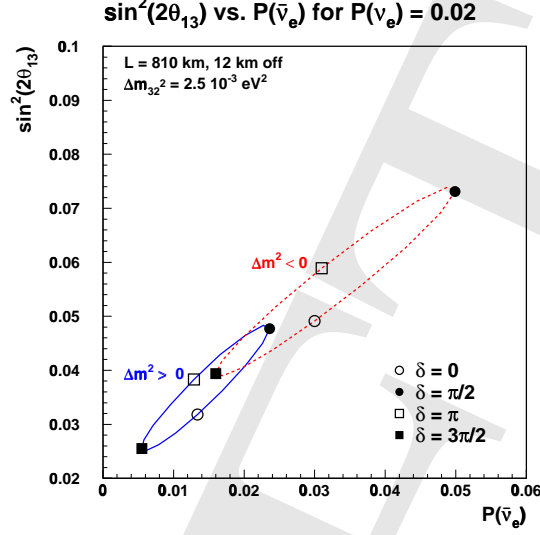


Figure A.3: Plot of the possible results of a measurement of a 2% neutrino oscillation probability. See text for an explanation

presume that NO ν A will begin operation prior to the completion of the Proton Driver, but the Proton Driver will greatly enhance its capabilities in all scenarios.

The primary goal of the proposed NO ν A experiment [?] is to measure $\nu_\mu \rightarrow \nu_e$ oscillations in order to determine the three oscillation parameters about which we presently have either no information or only an upper limit: $\sin^2 2\theta_{13}$, $\text{sign}(\Delta_{32}^2)$, and δ . In particular, provided that θ_{13} is in the range accessible to conventional neutrino beams, the unique contribution of the NO ν A and NuMI neutrino program will be the resolution of the mass hierarchy. This can only be done by experiments that measure the matter effect due to ν_e 's traveling long distances through the earth. Planned future experiments in both Japan [28] and Europe [157] are concentrating on base-lines that are too short for this purpose.

To understand how NO ν A addresses the measurement of these parameters, it is useful to inspect Fig. A.1. This figure shows all of the values of the parameters consistent with a perfectly measured 2% oscillation probability 12 km off-axis at an 810 km baseline. There are three parameters, $\sin^2 2\theta_{13}$, shown on the vertical axis, the two possible mass orderings, the normal hierarchy, shown by the solid blue curve and the inverted hierarchy, shown by the dashed red curve, and the CP phase δ , shown as values around the ellipses. The horizontal axis shows the result of a perfect measurement of the oscillation probability.

NO ν A is capable of making two measurements, the neutrino and the antineutrino oscillation probabilities near the first oscillation maximum. In some cases, these two measurements are capable, in principle, of measuring all three parameters, up to a two-fold ambiguity in the CP phase. For example a neutrino oscillation probability of 2% and an antineutrino oscillation probability of 4% or 1%, determine the mass hierarchy unambiguously. However, a neutrino oscillation probability of 2% and an

antineutrino oscillation probability of 2% cannot resolve the inherent ambiguity shown in Fig. A.1. A third measurement is needed in this case, either from an experiment done elsewhere at a different baseline, or from an additional measurement on the NuMI beamline, for example, on the second oscillation maximum.

As the neutrino oscillation probability decreases, the relative magnitude of the matter effect is unchanged, but the CP-sensitive effects increase since they are sensitive to only the first power of θ_{13} . Thus the overlap of the ellipses shown in Fig. A.1 become larger, making it less probable or more difficult to resolve the mass ordering with only two measurements.

A.2 Broadband Beam to Homestake or WIPP

If a large detector facility (as a part of NUSEL) [193–195] is located at Homestake (HS) the beam from BNL (FNAL) will have to traverse 2540km (1290km) through the earth. At BNL the beam would have to be built at an incline angle of about 11.3° . Current design for such a beam calls for the construction of a hill with a height of about 50 m [196]. Such a hill will have the proton target at the top of the hill and a 200 m long decay tunnel on the downslope. At FNAL the inclination will be about 5.7° . There is already experience at FNAL in building the NUMI beam [21]; this experience could be extended to build a new beam to HS. In either case, it is adequate to have a short decay tunnel (200 m) compared to the NUMI tunnel (750 m) to achieve the needed flux. The option of running with a narrow band beam using the off-axis technique [144] could be preserved if the decay tunnel is made sufficiently wide. For example, a 4 m diameter tunnel could allow one to move and rotate the target and horn assembly so that a 1° off-axis beam could be sent to the far detector.

With 1 MW of beam, a baseline of 2540 km, and a 500kT detector we calculate that we would obtain ~ 60000 muon charged current and ~ 20000 neutral current events for $5 \times 10^7 \text{ sec}$ of running in the neutrino mode in the absence of oscillations. For the same running conditions in the anti-neutrino mode (with the horn current reversed) we calculate a total of ~ 19000 anti-muon charged current and ~ 7000 neutral current events; approximately 20% of the event rate in the anti-neutrino beam will be due to wrong-sign neutrino interactions. For the shorter baseline of 1290 km from FNAL to HS, the event rates will be higher by a factor of $(2540/1290)^2$. For both neutrino and anti-neutrino running approximately $\sim 0.7\%$ of the charged current rate will be from electron charged current events which form a background to the $\nu_\mu \rightarrow \nu_e$ search. It will be desirable to obtain similar numbers of events in the anti-neutrino and the neutrino beam. Therefore, for the calculations in this paper we assume 1 MW operation for $5 \times 10^7 \text{ sec}$ in the neutrino mode and 2 MW operation for $5 \times 10^7 \text{ sec}$ in the anti-neutrino mode.

A large detector facility at NUSEL will most likely be used for a broad range of physics goals. Important considerations for such a detector are the fiducial mass, energy threshold, energy resolution, muon/electron discrimination, pattern recognition capability, time resolution, depth of the location, and the cost. Two classes of detectors are under consideration: water Cherenkov detector instrumented with

photo-multiplier tubes and a liquid Argon based time projection chamber.

A water Cherenkov detector built in the same manner as the super-Kamiokande experiment (with 20 inch photo-multipliers placed on the inside detector surface covering approximately 40% of the total area) [177] can achieve the 500 kT mass. This could be done by simply scaling the super-Kamiokande detector to larger size or by building several detector modules [193, 194]. Such a detector placed underground at NUSEL could have a low energy threshold (< 10 MeV), good energy resolution ($< 10\%$) for single particles, good muon/electron separation ($< 1\%$), and time resolution ($< \text{few ns}$). For the experiment we propose here it is important to obtain good energy resolution on the neutrino energy. This can be achieved in a water Cherenkov detector by separating quasi-elastic scattering events with well identified leptons in the final state from the rest of the charged current events. The fraction of quasi-elastic events in the total charged current rate with the spectrum used in this paper is about 23% for the neutrino beam and 39% for the anti-neutrino beam. Separation of quasi-elastic events from the charged current background is being used by the K2K experiment [4]. Further work is needed to make this event reconstruction work at higher energies. The reconstruction algorithm could be enhanced by the addition of ring imaging techniques to the detector [197].

A number of proponents have argued that a liquid Argon time projection chamber (LARTPC) could be built with total mass approaching 100 kT [195]. A fine grained detector such as this has much better resolution for separating tracks. It is possible therefore to use a large fraction of the charged current cross section (rather than only the quasi-elastic events) for determining the neutrino energy spectrum. The LARTPC will also have much better particle identification capability. Therefore, a LARTPC with a smaller total fiducial mass of ~ 100 kT than the 500 kT assumed for the water Cherenkov tank is expected to have similar performance for the physics.

For the purposes of this paper we will assume the same detector performance as described in [176]. For the physics sensitivity calculated in this paper we will assume 1 MW operation for $5 \times 10^7 \text{ sec}$ in the neutrino mode and 2 MW operation for $5 \times 10^7 \text{ sec}$ in the anti-neutrino mode. In both cases we will assume a detector fiducial mass of 500 kT. With the running times, the accelerator power level, and the detector mass fixed, we will consider two baselines: 1290 km (for FNAL to Homestake) and 2540 km (for BNL to Homestake) assuming that the detector is located at Homestake.

Lastly, we note that for this analysis the far detector could be at several comparable sites in the western US, notably WIPP or the Henderson mine in Colorado. While the detailed calculations change, the qualitative results are easily deduced from this work for other locations.

The ν_e signal will consist of clean, single electron events (single showering rings in a water Cherenkov detector) that result mostly from the quasi-elastic reaction $\nu_e + n \rightarrow e^- + p$. The main backgrounds will be from the electron neutrino contamination in the beam and reactions that have a π^0 in the final state. The π^0 background will depend on how well the detector can distinguish events with single electron induced and two photon induced electromagnetic showers. Assuming the same detector performance as in [176] we calculate the expected electron neutrino and anti-neutrino spectra shown in Figure A.4. These spectra were calculated for the parameters indicated in the

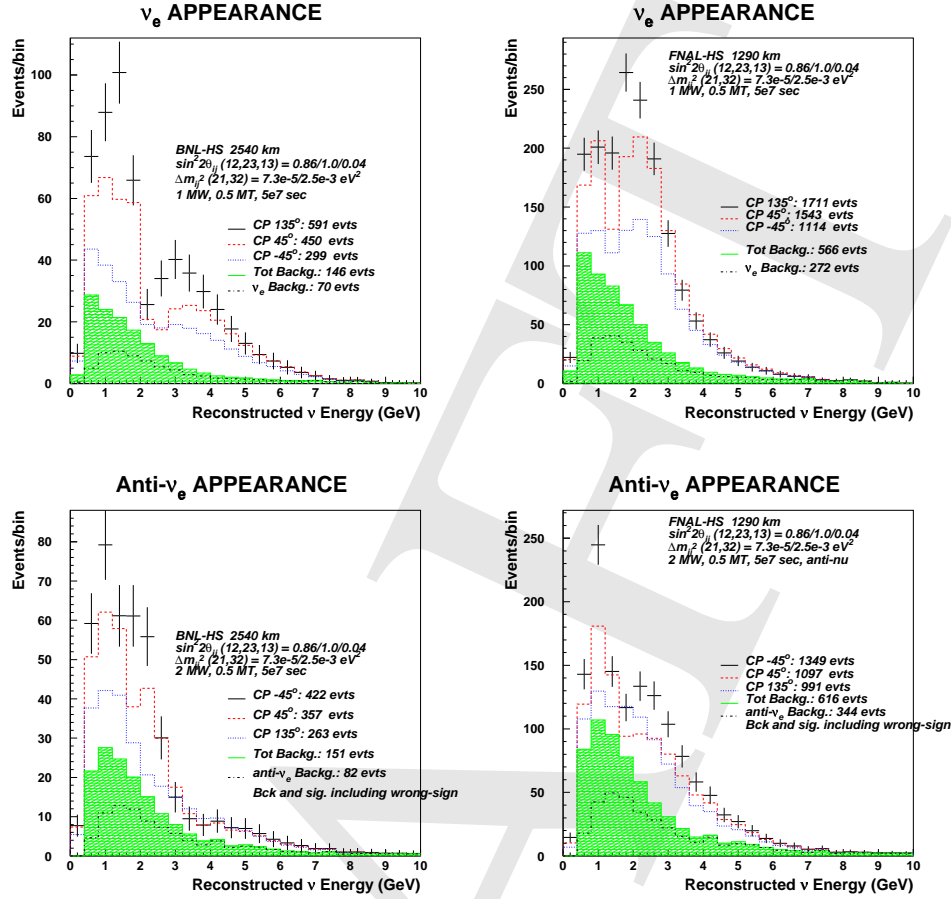


Figure A.4: Simulation of detected electron neutrino (top plots) and anti-neutrino (bottom plots) spectrum (left for BNL-HS 2540km, right for FNAL-HS 1290 km) for 3 values of the CP parameter δ_{CP} , 135° , 45° , and -45° , including background contamination. Obviously, the dependence of event rate on the CP phase has the opposite order for neutrinos and anti-neutrinos. The hatched histogram shows the total background. The ν_e beam background is also shown. The other assumed mixing parameters and running conditions are shown in the figure. These spectra are for the regular mass hierarchy (RO). Figure taken from Ref. [158].

figures for the regular mass ordering (RO). For the reversed mass ordering (UO) the anti-neutrino (neutrino) spectrum will (not) have the large matter enhancement at higher energies. The dependence of the total event rate on the CP phase parameter is the same for RO and UO in either running mode.

A.3 Several Narrow Band Beams to Homestake

As part of the APS study, the physics sensitivity of a new beamline aimed from Fermilab to Homestake has been investigated. The new beamline would utilize both 120 GeV and 8 GeV protons from a proton driver capable of supplying 2 MW at both energies (a total of 4 MW). The beamline would permit both on and off-axis beams

to be generated in order to optimally cover the energy region of the first and second oscillation maxima. Figure A.5 shows a schematic idea for the beamline design. There would be two nearly parallel target/focus stations, one for 120 GeV protons and one for 8 GeV protons. If nothing else, the two stations will make it possible to handle the 4 MW of average proton power. However, it will also permit different beam focus conditions for the two proton energies at the same time. The decay region will be wider but shorter than for the NuMI beamline. Roughly, the decay region will be 4 m wide and tall at the upstream end and 8 m tall by 10 m wide at the downstream end. The extra width at the upstream end is of special importance to the acceptance of lower energy pions which are responsible for producing neutrinos with energies less than a GeV. The 2m diameter of the NuMI beamline is actually a limiting aperture on the production of such neutrinos. Due to the focus on relatively low energy neutrinos, the length of the decay region will be only 250 m, rather than 700 m for NuMI.

Figure A.6 shows the spectrum of neutrino events which would be observed at Homestake with no oscillations. The black line shows the envelope of all neutrino events while the various colored lines show the individual contributions from different proton energies and aiming conditions. The beams shown here were actually those calculated/measured for the NuMI and Mini-BooNE beamlines, so in fact there may be tens of percent corrections compared to these fluxes. However, from this it is possible to extract all the essential features and good estimate of the physics sensitivity.

The sensitivity to measurements based on ν_e appearance depends on the features of both the beam and the detector. Two different detector models which should roughly bound the sensitivity of a fully realistic detector have been used in the calculation. The first model is to assume a 500 kT water Cerenkov detector with performance identical to that currently possible from Super-Kamiokande. (Parameterized response functions from actual Super-K measured performance were used.) For this detector, it is assumed that only quasi-elastic events are useful for the physics analysis (this is probably too severe). The second model assumes a 125 kT detector which for 50% efficiency for selection of ν_e CC events will have negligible background from NC events compared to the intrinsic ν_e events without oscillations. This is perhaps not too far off of the performance that might be expected from a liquid argon detector.

A.4 Beta Beams using the TeVatron

Even if the Tevatron would become available, one big uncertainty is if the Tevatron magnets would be able to handle the losses from the decay products. A simulation study, expected to conclude early next year, will address the issue of how many radioactive ions the Tevatron can accelerate to top energy on a regular basis.

Another issue is the decay ring, which would have to be built from scratch. A 1 Tev (proton equivalent) decay ring could fit on the Fermilab site (Figure A.7). If the Tevatron radius is used for the arcs, the efficiency would be about 20-25%. A higher efficiency could be obtained with stronger magnets. However, the losses in the storage ring are expected to be an order of magnitude larger than those in the Tevatron, so specially designed superconducting magnets with no coils in the midplane are required

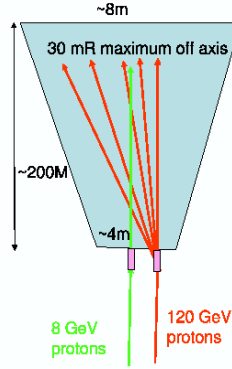


Figure A.5: Schematic of a possible beamline layout for a Fermilab to Homestake beamline which uses both 2 MW of 120 GeV protons and 2 MW of 8 GeV protons. Separate target/focussing stations are used for the 120 and 8 GeV protons in order to make those stations technically feasible as well as allow different aiming and focussing conditions. The 8 GeV beam will be on axis while the 120 GeV beams will be off axis.

to avoid quenches. Such magnets would have to be prototyped and tested for field quality and quench resistance.

Many other issues, such as the acceleration scheme, and decay losses in the injectors (Main Injector, possibly Booster, and any new low energy machines) would have to be addressed.

However, no matter where a Beta Beam facility is built, there are several significant challenges in providing the required intensity, and R&D is required to validate the concepts proposed to deal with them. These issues include:

- **Target:** To provide the required ion intensities, the target must be able to handle the Proton Driver beam intensity for a reasonable lifetime. While the production of ${}^6\text{He}$ looks fairly straightforward, the production of ${}^{18}\text{Ne}$ is less so. The baseline production method for ${}^{18}\text{Ne}$ relies on direct bombardment of the target material with the proton beam. Determining what intensity is acceptable to maintain a reasonable target lifetime must be done.
- **Ion Source:** With an ISOL-type production system, the ions are produced continuously. To prepare the beam for acceleration, it must then be bunched considerably, to below $20\,\mu\text{s}$. It is proposed to get the required intensity and bunch structure by using a new ion source concept, with state-of-the-art specifications. The source is an ECR source operating at high frequency (60 GHz) with a high magnetic field (2–3 T) and high plasma density ($n_e \sim 10^{14}\text{cm}^{-3}$). Such a source has never been built, though a development effort is now under way at Grenoble [198].
- **Storage Ring Issues:** Since the storage ring must be frequently topped off, injection requires the use of bunch-merging techniques. A concept has been worked out for this, and an initial test by the EU Beta Beam collaboration was encouraging. Since many of the problems with rf manipulation techniques are

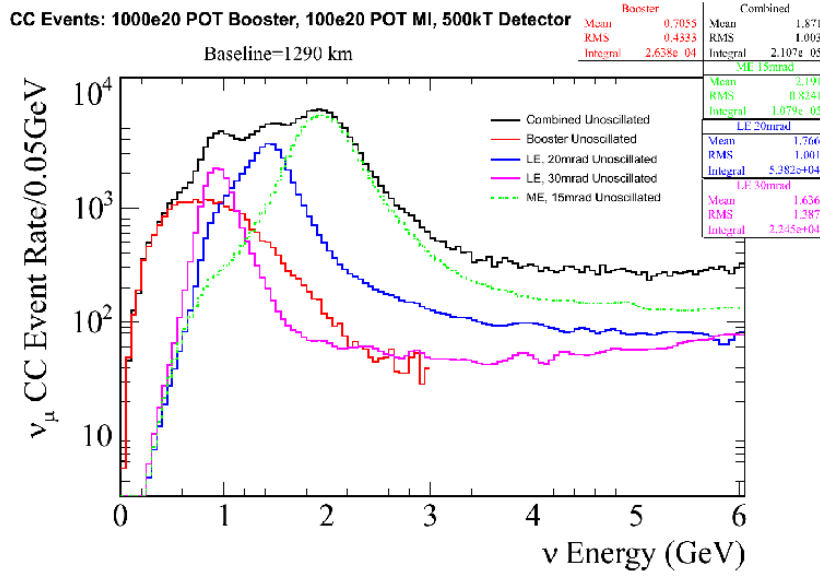


Figure A.6: The spectrum of observed neutrino events in the absence of oscillations expected at Homestake using a new beamline from Fermilab. 2 MW of 8 GeV protons are used to create an on-axis beam and another 2 MW of 120 GeV protons is used to produce three different off-axis beams. The statistics for this plot is for 5 years of running with the time evenly split for the three off axis configurations and with a 500 kT detector at Homestake. Note that the combination of these beams effectively forms a broad-band neutrino beam which will permit precise measurement of energy-dependent oscillation effects at both the first and second oscillation maxima (2 GeV and 700 MeV assuming $\Delta m^2 = 0.002 \text{ eV}^2$). At the same time, each beam can be analyzed independently, providing a relatively narrow-band beam which is helpful for dealing with backgrounds.

intensity dependent, it will probably still be necessary to validate the proposed scheme under fully realistic conditions. Another issue that needs to be evaluated in detail is the influence of the beam parameters (orbits, emittance, beta functions) on the neutrino spectrum at the detector.

A.5 Neutrino Factory at Fermilab

A.5.1 Evolution towards a Neutrino Factory

An impressive Neutrino Factory R&D effort has been ongoing in the U.S. and elsewhere over the last few years. Two design studies [199–201], each involving about 1M\$ of engineering, have established the feasibility of the Neutrino Factory concept, the achievable performance, and the R&D required before a Neutrino Factory could be built. Since the completion of these studies this R&D has been proceeding, and significant progress has been made towards optimizing the design, developing and testing the required accelerator components, and significantly reducing the cost. The baseline Neutrino Factory design has recently been updated [202] to incorporate ideas that have been developed over the last couple of years. The resulting progress on cost reduction is shown in Table A.1.



Figure A.7: (Color) Example layout of decay ring on Fermilab site, pointed at Sudan.

The present Neutrino Factory design consists of the following subsystems:

Proton Driver. Provides 1-4 MW of protons on a pion production target.

Target , Capture and Decay. A high-power target sits within a 20 T superconducting solenoid, which captures the pions. The high magnetic field smoothly decreases to 1.75 T downstream of the target, matching into a long solenoid decay channel.

Bunching and Phase Rotation. The muons from the decaying pions are bunched using a system of rf cavities with frequencies that vary along the channel. A second series of rf cavities with higher gradients is used to rotate the beam in longitudinal phase-space, reducing the energy spread of the muons.

Cooling. A solenoid focusing channel with high-gradient 201 MHz rf cavities and either liquid-hydrogen or LiH absorbers is used to reduce the transverse phase-space occupied by the beam. The muons lose, by dE/dx losses, both

	ALL	No PD
FS2 (\$M)	1832	1538
FS2a/FS2	0.67	0.60

Table A.1: Comparison of the estimated (unloaded) cost of the previous Neutrino Factory baseline design from “Feasibility Study 2” (FS2) with the estimated cost for the updated design (FS2a). The first column shows the total facility cost, and the second column the incremental cost if the Proton Driver and Target Hall already exist for a Neutrino Superbeam.

longitudinal- and transverse-momentum as they pass through the absorbers. The longitudinal momentum is replaced by re-acceleration in the rf cavities.

Acceleration. The central momentum of the muons exiting the cooling channel is 220 MeV/c. A superconducting linac with solenoid focusing is used to raise the energy to 1.5 GeV. Thereafter, a Recirculating Linear Accelerator raises the energy to 5 GeV, and a pair of Fixed-Field Alternating Gradient rings using quadrupole triplet focusing accelerate the beam to 20 GeV.

Storage Ring. A compact racetrack geometry ring is used in which 35% of the muons decay in the neutrino beam-forming straight section.

Bibliography

- [1] Y. Fukuda *et al.* (Kamiokande), Phys. Lett. **B335**, 237 (1994).
- [2] Y. Fukuda *et al.* (Super-Kamiokande), Phys. Rev. Lett. **81**, 1562 (1998), [hep-ex/9807003](#).
- [3] S. Fukuda *et al.* (Super-Kamiokande), Phys. Rev. Lett. **85**, 3999 (2000), [hep-ex/0009001](#).
- [4] S. H. Ahn *et al.* (K2K), Phys. Lett. **B511**, 178 (2001), [hep-ex/0103001](#).
- [5] M. H. Ahn *et al.* (K2K), Phys. Rev. Lett. **90**, 041801 (2003), [hep-ex/0212007](#).
- [6] M. Apollonio *et al.* (CHOOZ), Phys. Lett. **B466**, 415 (1999), [hep-ex/9907037](#).
- [7] Q. R. Ahmad *et al.* (SNO), Phys. Rev. Lett. **87**, 071301 (2001), [nucl-ex/0106015](#).
- [8] S. N. Ahmed *et al.* (SNO), Phys. Rev. Lett. **92**, 181301 (2004), [nucl-ex/0309004](#).
- [9] S. Fukuda *et al.* (Super-Kamiokande), Phys. Lett. **B539**, 179 (2002), [hep-ex/0205075](#).
- [10] K. Eguchi *et al.* (KamLAND), Phys. Rev. Lett. **90**, 021802 (2003), [hep-ex/0212021](#).
- [11] A. Aguilar *et al.* (LSND), Phys. Rev. **D64**, 112007 (2001), [hep-ex/0104049](#).
- [12] E. Church *et al.* (BooNe) FERMILAB-PROPOSAL-0898.
- [13] P. Minkowski, Phys. Lett. **B67**, 421 (1977).
- [14] T. Yanagida, in *Proceedings of the Workshop on the Unified Theory and the Baryon Number in the Universe*, edited by O. Sawada and A. Sugamoto (KEK, Tsukuba, Japan, 1979), p. 95.
- [15] S. L. Glashow, in *Proceedings of the 1979 Cargèse Summer Institute on Quarks and Leptons*, edited by M. Lévy, J.-L. Basdevant, D. Speiser, J. Weyers, R. Gastmans, and M. Jacob (Plenum Press, New York, 1980), pp. 687–713.
- [16] M. Gell-Mann, P. Ramond, and R. Slansky, in *Supergravity*, edited by P. van Nieuwenhuizen and D. Z. Freedman (North Holland, Amsterdam, 1979), p. 315.
- [17] R. N. Mohapatra and G. Senjanović, Phys. Rev. Lett. **44**, 912 (1980).
- [18] J. N. Bahcall, M. C. Gonzalez-Garcia, and C. Pena-Garay, JHEP **08**, 016 (2004), [hep-ph/0406294](#).
- [19] A. Bandyopadhyay, S. Choubey, S. Goswami, S. T. Petcov, and D. P. Roy (2004), [hep-ph/0406328](#).
- [20] M. Maltoni, T. Schwetz, M. A. Tortola, and J. W. F. Valle (2004), [hep-ph/0405172](#).
- [21] E. Ables *et al.* (MINOS) FERMILAB-PROPOSAL-0875.
- [22] H. Minakata, H. Sugiyama, O. Yasuda, K. Inoue, and F. Suekane, Phys. Rev. **D68**, 033017 (2003), [hep-ph/0211111](#).
- [23] P. Huber, M. Lindner, T. Schwetz, and W. Winter, Nucl. Phys. **B665**, 487 (2003), [hep-ph/0303232](#).

- [24] E. K. Akhmedov, R. Johansson, M. Lindner, T. Ohlsson, and T. Schwetz, JHEP **04**, 078 (2004), [hep-ph/0402175](#).
- [25] V. Barger, D. Marfatia, and K. Whisnant, Phys. Lett. **B560**, 75 (2003), [hep-ph/0210428](#).
- [26] P. Huber, M. Lindner, and W. Winter, Nucl. Phys. **B654**, 3 (2003), [hep-ph/0211300](#).
- [27] H. Minakata, H. Nunokawa, and S. J. Parke, Phys. Rev. **D68**, 013010 (2003), [hep-ph/0301210](#).
- [28] Y. Itow *et al.* (2001), [hep-ex/0106019](#).
- [29] A. Cervera *et al.*, Nucl. Phys. **B579**, 17 (2000), [hep-ph/0002108](#).
- [30] V. D. Barger, S. Geer, R. Raja, and K. Whisnant, Phys. Rev. **D63**, 113011 (2001), [hep-ph/0012017](#).
- [31] M. Freund, P. Huber, and M. Lindner, Nucl. Phys. **B615**, 331 (2001), [hep-ph/0105071](#).
- [32] M. Freund, Phys. Rev. **D64**, 053003 (2001), [hep-ph/0103300](#).
- [33] I. Mocioiu and R. Shrock, JHEP **11**, 050 (2001), [hep-ph/0106139](#).
- [34] H. Minakata and H. Nunokawa, JHEP **10**, 001 (2001), [hep-ph/0108085](#).
- [35] A. A. Aguilar-Arevalo (MiniBooNE) (2004), [hep-ex/0408074](#).
- [36] B. Armbruster *et al.* (KARMEN), Phys. Rev. **D65**, 112001 (2002), [hep-ex/0203021](#).
- [37] D. Abbaneo *et al.* (LEP) (2003), [hep-ex/0312023](#).
- [38] A. Strumia, Phys. Lett. **B539**, 91 (2002), [hep-ph/0201134](#).
- [39] H. Paes, L.-g. Song, and T. J. Weiler, Phys. Rev. **D67**, 073019 (2003), [hep-ph/0209373](#).
- [40] O. L. G. Peres and A. Y. Smirnov, Nucl. Phys. **B599**, 3 (2001), [hep-ph/0011054](#).
- [41] V. D. Barger, B. Kayser, J. Learned, T. J. Weiler, and K. Whisnant, Phys. Lett. **B489**, 345 (2000), [hep-ph/0008019](#).
- [42] M. Sorel, J. M. Conrad, and M. Shaevitz (2003), [hep-ph/0305255](#).
- [43] K. S. Babu and S. Pakvasa (2002), [hep-ph/0204236](#).
- [44] B. Armbruster *et al.*, Phys. Rev. Lett. **90**, 181804 (2003), [hep-ex/0302017](#).
- [45] J. R. Musser (TWIST) (2004), [hep-ex/0409063](#).
- [46] H. Murayama and T. Yanagida, Phys. Lett. **B520**, 263 (2001), [hep-ph/0010178](#).
- [47] G. Barenboim, L. Borissov, J. Lykken, and A. Y. Smirnov, JHEP **10**, 001 (2002), [hep-ph/0108199](#).
- [48] G. Barenboim, L. Borissov, and J. Lykken, Phys. Lett. **B534**, 106 (2002), [hep-ph/0201080](#).
- [49] M. C. Gonzalez-Garcia, M. Maltoni, and T. Schwetz, Phys. Rev. **D68**, 053007 (2003), [hep-ph/0306226](#).
- [50] V. Barger, D. Marfatia, and K. Whisnant, Phys. Lett. **B576**, 303 (2003), [hep-ph/0308299](#).
- [51] D. B. Kaplan, A. E. Nelson, and N. Weiner, Phys. Rev. Lett. **93**, 091801 (2004), [hep-ph/0401099](#).
- [52] G. Barenboim and N. E. Mavromatos (2004), [hep-ph/0404014](#).
- [53] V. A. Kostelecky and M. Mewes (2004), [hep-ph/0406255](#).
- [54] A. Donini and D. Meloni, Eur. Phys. J. **C22**, 179 (2001), [hep-ph/0105089](#).
- [55] A. Donini, M. Lusignoli, and D. Meloni, Nucl. Phys. **B624**, 405 (2002), [hep-ph/0107231](#).

- [56] N. Arkani-Hamed, L. J. Hall, H. Murayama, D. R. Smith, and N. Weiner, Phys. Rev. **D64**, 115011 (2001), hep-ph/0006312.
- [57] F. Borzumati and Y. Nomura, Phys. Rev. **D64**, 053005 (2001), hep-ph/0007018.
- [58] R. Kitano, Phys. Lett. **B539**, 102 (2002), hep-ph/0204164.
- [59] R. Arnowitt, B. Dutta, and B. Hu, Nucl. Phys. **B682**, 347 (2004), hep-th/0309033.
- [60] S. Abel, A. Dedes, and K. Tamvakis (2004), hep-ph/0402287.
- [61] L. J. Hall, H. Murayama, and N. Weiner, Phys. Rev. Lett. **84**, 2572 (2000), hep-ph/9911341.
- [62] N. Haba and H. Murayama, Phys. Rev. **D63**, 053010 (2001), hep-ph/0009174.
- [63] A. de Gouvea and H. Murayama, Phys. Lett. **B573**, 94 (2003), hep-ph/0301050.
- [64] A. de Gouvêa, Phys. Rev. **D69**, 093007 (2004), hep-ph/0401220.
- [65] S. M. Barr and I. Dorsner, Nucl. Phys. **B585**, 79 (2000), hep-ph/0003058.
- [66] R. Barbieri, T. Hambye, and A. Romanino, JHEP **03**, 017 (2003), hep-ph/0302118.
- [67] M.-C. Chen and K. T. Mahanthappa, Int. J. Mod. Phys. **A18**, 5819 (2003), hep-ph/0305088.
- [68] G. Altarelli and F. Feruglio (2004), hep-ph/0405048.
- [69] A. S. Joshipura (2004), hep-ph/0411154.
- [70] H. S. Goh, R. N. Mohapatra, and S.-P. Ng, Phys. Rev. **D68**, 115008 (2003), hep-ph/0308197.
- [71] T. Asaka, W. Buchmüller, and L. Covi, Phys. Lett. **B563**, 209 (2003), hep-ph/0304142.
- [72] K. S. Babu, J. C. Pati, and F. Wilczek, Nucl. Phys. **B566**, 33 (2000), hep-ph/9812538.
- [73] C. H. Albright and S. M. Barr, Phys. Rev. **D64**, 073010 (2001), hep-ph/0104294.
- [74] T. Blazek, S. Raby, and K. Tobe, Phys. Rev. **D62**, 055001 (2000), hep-ph/9912482.
- [75] G. G. Ross and L. Velasco-Sevilla, Nucl. Phys. **B653**, 3 (2003), hep-ph/0208218.
- [76] S. Raby, Phys. Lett. **B561**, 119 (2003), hep-ph/0302027.
- [77] R. Kitano and Y. Mimura, Phys. Rev. **D63**, 016008 (2001), hep-ph/0008269.
- [78] N. Maekawa, Prog. Theor. Phys. **106**, 401 (2001), hep-ph/0104200.
- [79] M.-C. Chen and K. T. Mahanthappa, Phys. Rev. **D68**, 017301 (2003), hep-ph/0212375.
- [80] M. Bando and M. Obara, Prog. Theor. Phys. **109**, 995 (2003), hep-ph/0302034.
- [81] W. Buchmüller and D. Wyler, Phys. Lett. **B521**, 291 (2001), hep-ph/0108216.
- [82] P. H. Frampton and R. N. Mohapatra (2004), hep-ph/0407139.
- [83] W. Grimus and L. Lavoura, JHEP **07**, 045 (2001), hep-ph/0105212.
- [84] W. Grimus and L. Lavoura, Phys. Lett. **B572**, 189 (2003), hep-ph/0305046.
- [85] W. Grimus, A. S. Joshipura, S. Kaneko, L. Lavoura, and M. Tanimoto, JHEP **07**, 078 (2004), hep-ph/0407112.
- [86] S.-L. Chen, M. Frigerio, and E. Ma (2004), hep-ph/0404084.
- [87] I. Aizawa, M. Ishiguro, T. Kitabayashi, and M. Yasue, Phys. Rev. **D70**, 015011 (2004), hep-ph/0405201.
- [88] R. N. Mohapatra, JHEP **10**, 027 (2004), hep-ph/0408187.
- [89] S. Antusch and S. F. King (2004), hep-ph/0402121.
- [90] S. Antusch and S. F. King, Phys. Lett. **B591**, 104 (2004), hep-ph/0403053.

- [91] W. Rodejohann and Z.-z. Xing (2004), [hep-ph/0408195](#).
- [92] K. S. Babu, E. Ma, and J. W. F. Valle, *Phys. Lett.* **B552**, 207 (2003), [hep-ph/0206292](#).
- [93] T. Ohlsson and G. Seidl, *Nucl. Phys.* **B643**, 247 (2002), [hep-ph/0206087](#).
- [94] S. F. King and G. G. Ross, *Phys. Lett.* **B574**, 239 (2003), [hep-ph/0307190](#).
- [95] Q. Shafi and Z. Tavartkiladze, *Phys. Lett.* **B594**, 177 (2004), [hep-ph/0401235](#).
- [96] M. Bando, S. Kaneko, M. Obara, and M. Tanimoto, *Phys. Lett.* **B580**, 229 (2004), [hep-ph/0309310](#).
- [97] M. Honda, S. Kaneko, and M. Tanimoto, *JHEP* **09**, 028 (2003), [hep-ph/0303227](#).
- [98] R. F. Lebed and D. R. Martin, *Phys. Rev.* **D70**, 013004 (2004), [hep-ph/0312219](#).
- [99] A. Ibarra and G. G. Ross, *Phys. Lett.* **B575**, 279 (2003), [hep-ph/0307051](#).
- [100] P. F. Harrison and W. G. Scott, *Phys. Lett.* **B594**, 324 (2004), [hep-ph/0403278](#).
- [101] P. H. Frampton, S. L. Glashow, and T. Yanagida, *Phys. Lett.* **B548**, 119 (2002), [hep-ph/0208157](#).
- [102] J.-w. Mei and Z.-z. Xing, *Phys. Rev.* **D69**, 073003 (2004), [hep-ph/0312167](#).
- [103] R. N. Mohapatra, M. K. Parida, and G. Rajasekaran, *Phys. Rev.* **D69**, 053007 (2004), [hep-ph/0301234](#).
- [104] J. C. Pati (2002), [hep-ph/0209160](#).
- [105] P. F. Harrison and W. G. Scott, *Phys. Lett.* **B557**, 76 (2003), [hep-ph/0302025](#).
- [106] J. Kubo, *Phys. Lett.* **B578**, 156 (2004), [hep-ph/0309167](#).
- [107] E. Ma, *Mod. Phys. Lett.* **A19**, 577 (2004), [hep-ph/0401025](#).
- [108] M. Raidal (2004), [hep-ph/0404046](#).
- [109] S. F. King, *Nucl. Phys.* **B576**, 85 (2000), [hep-ph/9912492](#).
- [110] S. F. King, *JHEP* **09**, 011 (2002), [hep-ph/0204360](#).
- [111] S. Antusch and S. F. King (2004), [hep-ph/0405272](#).
- [112] G. G. Ross, L. Velasco-Sevilla, and O. Vives, *Nucl. Phys.* **B692**, 50 (2004), [hep-ph/0401064](#).
- [113] S. Zhou and Z.-z. Xing (2004), [hep-ph/0404188](#).
- [114] P. H. Frampton, S. T. Petcov, and W. Rodejohann, *Nucl. Phys.* **B687**, 31 (2004), [hep-ph/0401206](#).
- [115] W. Rodejohann (2004), [hep-ph/0403236](#).
- [116] T. Appelquist and R. Shrock, *Phys. Lett.* **B548**, 204 (2002), [hep-ph/0204141](#).
- [117] J. A. Casas, J. R. Espinosa, and I. Navarro, *JHEP* **09**, 048 (2003), [hep-ph/0306243](#).
- [118] I. Dorsner and A. Y. Smirnov, *Nucl. Phys.* **B698**, 386 (2004), [hep-ph/0403305](#).
- [119] S. T. Petcov, *Phys. Lett.* **B110**, 245 (1982).
- [120] C. N. Leung and S. T. Petcov, *Phys. Lett.* **B125**, 461 (1983).
- [121] M. Magg and C. Wetterich, *Phys. Lett.* **B94**, 61 (1980).
- [122] G. Lazarides, Q. Shafi, and C. Wetterich, *Nucl. Phys.* **B181**, 287 (1981).
- [123] R. N. Mohapatra and G. Senjanović, *Phys. Rev.* **D23**, 165 (1981).
- [124] M. Fukugita and T. Yanagida, *Phys. Lett.* **174B**, 45 (1986).

- [125] G. C. Branco, T. Morozumi, B. M. Nobre, and M. N. Rebelo, Nucl. Phys. **B617**, 475 (2001), hep-ph/0107164.
- [126] S. Pascoli, S. T. Petcov, and W. Rodejohann, Phys. Rev. **D68**, 093007 (2003), hep-ph/0302054.
- [127] S. F. King, Phys. Rev. **D67**, 113010 (2003), hep-ph/0211228.
- [128] S. Antusch, J. Kersten, M. Lindner, and M. Ratz, Nucl. Phys. **B674**, 401 (2003), hep-ph/0305273.
- [129] P. H. Chankowski, W. Krolkowski, and S. Pokorski, Phys. Lett. **B473**, 109 (2000), hep-ph/9910231.
- [130] J. A. Casas, J. R. Espinosa, A. Ibarra, and I. Navarro, Nucl. Phys. **B573**, 652 (2000), hep-ph/9910420.
- [131] S. Antusch, P. Huber, J. Kersten, T. Schwetz, and W. Winter (2004), hep-ph/0404268.
- [132] J. A. Casas, J. R. Espinosa, A. Ibarra, and I. Navarro, Nucl. Phys. **B556**, 3 (1999), hep-ph/9904395.
- [133] J. A. Casas, J. R. Espinosa, A. Ibarra, and I. Navarro, Nucl. Phys. **B569**, 82 (2000), hep-ph/9905381.
- [134] S. F. King and N. N. Singh, Nucl. Phys. **B591**, 3 (2000), hep-ph/0006229.
- [135] S. Antusch, J. Kersten, M. Lindner, and M. Ratz, Phys. Lett. **B538**, 87 (2002), hep-ph/0203233.
- [136] S. Antusch, J. Kersten, M. Lindner, and M. Ratz, Phys. Lett. **B544**, 1 (2002), hep-ph/0206078.
- [137] S. Antusch and M. Ratz, JHEP **11**, 010 (2002), hep-ph/0208136.
- [138] J.-w. Mei and Z.-z. Xing (2004), hep-ph/0404081.
- [139] F. Vissani, M. Narayan, and V. Berezinsky, Phys. Lett. **B571**, 209 (2003), hep-ph/0305233.
- [140] P. Huber, M. Lindner, M. Rolinec, T. Schwetz, and W. Winter (2004), hep-ph/0403068.
- [141] K. B. McConnell and M. H. Shaevitz (2004), hep-ex/0409028.
- [142] P. Aprili *et al.* (ICARUS) CERN-SPSC-2002-027.
- [143] D. Duchesneau (OPERA), eConf **C0209101**, TH09 (2002), hep-ex/0209082.
- [144] E. Collaboration, *Physics design report* (1995), bNL No. 52459, URL <http://minos.phy.bnl.gov/nwg/papers/E889>.
- [145] D. Ayres *et al.* (Nova) (2002), hep-ex/0210005.
- [146] *Numi off-axis proposal*, in preparation. See <http://www-off-axis.fnal.gov/>.
- [147] M. Apollonio *et al.*, Eur. Phys. J. **C27**, 331 (2003), hep-ex/0301017.
- [148] F. Boehm *et al.*, Phys. Rev. **D64**, 112001 (2001), hep-ex/0107009.
- [149] *Double-chooz letter of intent*, in preparation.
- [150] H. Minakata and H. Sugiyama, Phys. Lett. **B580**, 216 (2004), hep-ph/0309323.
- [151] K. Heeger, *Measuring theta13 with reactor neutrinos: Initiatives in the us*, talk given at NOON 2004, available at <http://www-sk.icrr.u-tokyo.ac.jp/noon2004/>.
- [152] M. Shaevitz, talk given at the APS Neutrino Study, working group meeting, Feb. (2004), <http://apsreactor.uchicago.edu/meetings/chicago/shaevitz.pdf>.

- [153] G. L. Fogli, E. Lisi, A. Marrone, and D. Montanino, Phys. Rev. **D67**, 093006 (2003), hep-ph/0303064.
- [154] M. Maltoni, T. Schwetz, M. A. Tortola, and J. W. F. Valle, Phys. Rev. **D68**, 113010 (2003), hep-ph/0309130.
- [155] Y. f. t. S.-K. C. Hayato, talk given at the HEP2003 conference (Aachen, Germany, 2003), <http://eps2003.physik.rwth-aachen.de>.
- [156] W. Winter, Phys. Rev. **D70**, 033006 (2004), hep-ph/0310307.
- [157] M. Apollonio *et al.* (2002), hep-ph/0210192.
- [158] M. V. Diwan (2004), hep-ex/0407047.
- [159] V. D. Barger *et al.* (2001), hep-ph/0103052.
- [160] C. Ankenbrandt *et al.*, *Proton driver physics study (fermilab)*, <http://projects.fnal.gov/protondriver/>.
- [161] I. Mocioiu and R. Shrock, AIP Conf. Proc. **533**, 74 (2000), hep-ph/9910554.
- [162] I. Mocioiu and R. Shrock, Phys. Rev. **D62**, 053017 (2000), hep-ph/0002149.
- [163] M. Freund, M. Lindner, S. T. Petcov, and A. Romanino, Nucl. Phys. **B578**, 27 (2000), hep-ph/9912457.
- [164] P. Huber and W. Winter, Phys. Rev. **D68**, 037301 (2003), hep-ph/0301257.
- [165] A. Asratyan *et al.* (2003), hep-ex/0303023.
- [166] F. DeJongh (2002), hep-ex/0203005.
- [167] H.-s. Chen *et al.* (VLBL Study Group H2B-1) (2001), hep-ph/0104266.
- [168] S. Geer, Phys. Rev. **D57**, 6989 (1998), hep-ph/9712290.
- [169] C. Albright *et al.* (2000), hep-ex/0008064.
- [170] P. Huber, M. Lindner, and W. Winter, Nucl. Phys. **B645**, 3 (2002), hep-ph/0204352.
- [171] P. Zucchelli, Phys.Lett. **B532**, 166 (2002).
- [172] H. R. *et al.*, *Feasibility study for a european isotope-separation on-line radioactive ion beam facility: Appendix c*, http://www.ganil.fr/eurisol/Final_Report/APPENDIX-C.pdf (2003).
- [173] J. Burguet-Castell, D. Casper, J. J. Gomez-Cadenas, P. Hernandez, and F. Sanchez, Nucl. Phys. **B695**, 217 (2004), hep-ph/0312068.
- [174] M. Ishitsuka (Super-Kamiokande) (2004), hep-ex/0406076.
- [175] T. Yang and S. Wojcicki NOvA-NOTE-30, <http://www-nova.fnal.gov/notes/notes.html>.
- [176] M. V. Diwan *et al.*, Phys. Rev. **D68**, 012002 (2003), hep-ph/0303081.
- [177] Y. Fukuda *et al.*, Nucl. Instrum. Meth. **A501**, 418 (2003).
- [178] V. Barger, M. Sorel, and K. Whisnant, in preparation.
- [179] G. Barenboim, L. Borissov, and J. Lykken (2002), hep-ph/0212116.
- [180] The Spallation Neutron Source (SNS) is an accelerator-based source being built in Oak Ridge, Tennessee, by the U.S. DOE. Also see <http://www.phy.ornl.gov/workshops/sns2/> for details on the neutrino source., URL <http://sns.gov/>.
- [181] S. J. Brice, S. Geer, K. Paul, and R. Tayloe (2004), hep-ex/0408135.
- [182] C. Athanassopoulos *et al.* (LSND), Phys. Rev. **C54**, 2685 (1996), nucl-ex/9605001.
- [183] G. J. VanDalen (2003), nucl-ex/0309014.

- [184] G. Garvey *et al.*, *Measuring active-sterile neutrino oscillations with a stopped pion beam*, in preparation.
- [185] K. Kodama *et al.* (DONUT), Phys. Lett. **B504**, 218 (2001), hep-ex/0012035.
- [186] E. Eskut *et al.* (CHORUS), Phys. Lett. **B497**, 8 (2001).
- [187] P. Astier *et al.* (NOMAD), Nucl. Phys. **B611**, 3 (2001), hep-ex/0106102.
- [188] D. OPERA Collaboration *et al.*, proceedings of Neutrino 2004.
- [189] A. ICARUS Collaboration *et al.*, proceedings of Neutrino 2004.
- [190] D. A. Petyt Off-Axis-NOTE-SIM-32.
- [191] I. Ambats *et al.* (NOvA) FERMILAB-PROPOSAL-0929.
- [192] F. N. Group, *Numi facility technical design report*, fermilab Report NuMI-346.
- [193] M. Collaboration, megaton Modular Multi-Purpose Neutrino Detector, URL <http://www.hep.upenn.edu/Homestake>.
- [194] U. Collaboration (2001), physics Potential and Feasibility of UNO, SBHEP01-03.
- [195] F. Arneodo *et al.* (ICARUS), Nucl. Instrum. Meth. **A471**, 272 (2000).
- [196] J. A. *et al.*, *Ags super neutrino beam facility, accelerator and target system design* (2003), bNL-71228-2003-IR, URL <http://nwg.phy.bnl.gov/>.
- [197] P. Antonioli *et al.*, Nucl. Instrum. Meth. **A433**, 104 (1999).
- [198] http://moriond.in2p3.fr/radio/Moriond-Sortais_1.ppt.
- [199] N. Holtkamp and S. Geer, ICFA Beam Dyn. Newslett. **21**, 37 (2000).
- [200] A. T. *et al.*, *A feasibility study of a neutrino source based on a muon storage ring*, fERMILAB-Pub-00/108-E.
- [201] G. M. *et al.*, *Feasibility study ii*, bNL-52623.
- [202] A. C. *et al.*, *Neutrino factory and beta beams experiments and development*, fNAL-TM-2259.